Author/s:
Zhou, Jie

Title:
Intracellular competition regulates B lymphocyte differentiation

Date:
2019

Persistent Link:
https://hdl.handle.net/11343/237435

Intracellular competition regulates B lymphocyte differentiation

Jie H S Zhou

ORCID 0000-0002-9113-800X

Submitted in total fulfilment for the degree of
Doctor of Philosophy

December 2019

The Walter and Eliza Hall Institute of Medical Research
Department of Medical Biology
The University of Melbourne

Abstract

The production of antibodies, with their potential to recognise unique targets and prevent repeat infections, is an important aspect of immune health. In order to generate free antibodies, the cells responsible, B cells, must undergo a differentiation step to transform from lymphoblast to antibody secreting cell (ASC). This differentiation step prevents further antibody modifications and hence the timing for optimal immunity requires a delicate balance between expanding useful clones and providing early protection. How differentiation is controlled to achieve this balance for an effective immune response is of great interest.

In this study, the progression from naïve B cells to ASC was investigated in the context of an emerging model for competing cell fates. By this model, alternate cell fates, such as division, death and differentiation, are pursued independently in individual cells but are in competition such that events which occur earlier prevent those that require more time from being observed. Evaluation and testing of this model requires careful measurement of distributions of times to fates which is only possible with single cell fate tracking. Here I have developed and applied methods for live cell imaging and analysis for assessing and evaluating cell fate changes over time.

Using these methods, several modes of regulating differentiation times were revealed. Low levels of stimulation through CD40 produced a greater proportion of antibody secreting cells per generation as division is slowed and more time is allowed for differentiation, consistent with competing cell fates. A second mechanism was found where increasing division numbers directly reduced the amount of time required for cells to differentiate, without modulating division times, ensuring the natural development of ASC during the ongoing immune response.

A direct method of uncensoring was explored where cell cycle inhibitors were used to prevent division, with the hypothesis that more cells would go on to differentiate in the absence of competition. Various inhibitors were assessed for their suitability to this task, and a panel of compounds were found to be suitable for uncensoring underlying differentiation and cell death times.

Findings from this study are consistent with the model of independent and competing cell fates, and significantly advance our understanding of how antibody responses are controlled and can be modelled at the cell population level.

Declaration

This is to certify that:

i) this thesis comprises only my original work towards the Doctor of Philosophy except where indicated in the Preface;

ii) due acknowledgement has been made in the text to all other material used; and

iii) this thesis is fewer than 100,000 words in length, exclusive of tables, bibliographies and appendices.

Jie Zhou

Preface:

In accordance with the regulations of The University of Melbourne, I acknowledge that some of the work presented in chapters 3, 4, and 5 was collaborative, specifically:

- Imaging in Chapter 3 was performed with the assistance of John Markham. Image processing was performed by John Markham.
- Statistical analyses and model fitting in Chapter 3 was performed in collaboration with Ken Duffy.
- Image processing in Chapters 4 and 5 were performed by Andrey Kan

The remainder of this thesis comprises only my original work. I assess my contribution to this thesis as being:

- Chapter 3: 75%
- Chapter 4: 95%
- Chapter 5: 98%

Overall, I assess my contribution to this thesis as being more than 90%.

I acknowledge that cell imaging described in Chapter 3 was conducted by me prior to my enrolment in the degree, however >60% of the data extraction for analysis and 100% of the subsequent statistical and theoretical analyses presented in the chapter were performed during my PhD candidature.

The article in Chapter 3 was published by Frontiers in Immunology on the 10th September 2018, in collaboration with Philip Hodgkin, Ken Duffy, and John Markham.

This project was supported by the Australian Postgraduate Award, Edith Moffat Scholarship, and the NHMRC.

List of Publications

Zhou, J. H. S., Markham, J. F., Duffy, K. R. and Hodgkin, P. D. (2018) 'Stochastically Timed Competition Between Division and Differentiation Fates Regulates the Transition From B Lymphoblast to Plasma Cell', *Frontiers in Immunology,* 9(2053).

https://doi.org/10.3389/fimmu.2018.02053

Tempany, J. C.*, **Zhou, J. H. S.***, Hodgkin, P. D. and Bryant, V. L. (2018) 'Superior properties of CellTrace Yellow™ as a division tracking dye for human and murine lymphocytes', *Immunology & Cell Biology,* 96(2), pp. 149-159.

***equal first authors**

https://doi.org/10.1111/imcb.1020

Horton, M. B., Prevedello, G., Marchingo, J. M., **Zhou, J. H. S.**, Duffy, K. R., Heinzel, S. and Hodgkin, P. D. (2018) 'Multiplexed Division Tracking Dyes for Proliferation-Based Clonal Lineage Tracing', *The Journal of Immunology,* 201(3), pp. 1097-1103.

https://doi.org/10.4049/jimmunol.1800481

Kan, A., Pavlyshyn, D., Markham, J. F., Dowling, M. R., Heinzel, S., **Zhou, J. H. S.**, Marchingo, J. M. and Hodgkin, P. D. (2016) 'Stochastic Measurement Models for Quantifying Lymphocyte Responses Using Flow Cytometry', *PLOS ONE,* 11(1), pp. e0146227.
https://doi.org/10.1371/journal.pone.0146227

Dowling, M. R., Kan, A., Heinzel, S., **Zhou, J. H. S.**, Marchingo, J. M., Wellard, C. J., Markham, J. F. and Hodgkin, P. D. (2014) 'Stretched cell cycle model for proliferating lymphocytes', *Proc Natl Acad Sci U S A,* 111(17), pp. 6377-82.

https://doi.org/10.1073/pnas.1322420111

Chakravorty, R., Rawlinson, D., Zhang, A., Markham, J., Dowling, M. R., Wellard, C., **Zhou, J. H. S.** and Hodgkin, P. D. (2014) 'Labour-efficient in vitro lymphocyte population tracking and fate prediction using automation and manual review', *PLoS One,* 9(1), pp. e83251.

https://doi.org/10.1371/journal.pone.0083251

Hawkins, E. D., Turner, M. L., Wellard, C. J., **Zhou, J. H. S.**, Dowling, M. R. and Hodgkin, P. D. (2013) 'Quantal and graded stimulation of B lymphocytes as alternative strategies for regulating adaptive immune responses', *Nat Commun,* 4, pp. 2406.

https://doi.org/10.1038/ncomms3406

Chan, W. F., Coughlan, H. D., **Zhou, J. H. S.**, Keenan, C. R., Bediaga, N. G., Hodgkin, P. D., Smyth, G. K., Johanson, T. M. and Allan, R. S. (2019) 'Genome reconfiguration prior to mitosis shapes the generation of adaptive immunity', *bioRxiv*, pp. 762757.
[submitted for publication]

Acknowledgements

First and foremost, I would like to thank Phil for giving me the opportunity to work on this project. Bridging my love for biology and comfort with mathematics was not something I had given much thought to as a naïve graduate, but upon meeting the lab, was overwhelmed with a sense of belonging. I may not have been the perfect student, but your support, patience, kindness and guidance were exactly what I needed to grow, and I am forever grateful.

Lynn – for always looking out for me, showing me how to be strong and sometimes asking the hard questions. Between you and Phil, I could not have asked for better role models. DT - for your pespective, wit, and down-to-earth nature. Steve - for your insights, but also for sharing your love of the wilderness and artisan food. Edwin - for all your help and constructive conversations. I feel extremely privileged to have been watched over by you all, and even if a little of your brilliance, wisdom, generosity, and scientific integrity rubs off on me, I'd be happy.

Su – for your care, kindness, patience, and advice. Julia – for being my student buddy. The two of you were there for celebrations, commiserations, tears of grief, fear, joy and frustrations; with lots of delicious cake, many, many biscuits, cups of tea, and drinks at the pub in between. Thank you both for joining me on the ride (and for the scientific advice, of course).

Kim, Andrey, Mark, John, Cam – it was delightful working with you, and I have learned so much from each and every one of you.

Ken – for the insight, fresh perspectives, laughs, and overnight turnarounds when required!

Kim – for keeping everything running, and for always looking out for me.

Mel, Amy, Milon, Shirley, Chin, Patrick, Matt, Felix, Felix, Suzie, Tom – for always being up for dinner and Melbourne/Singapore/Germany shenanigans! Ang – for being my guardian angel. Libby, Ness, Jo, Charlotte – your moral and scientific support have all been invaluable. Jessica, Miles, Michelle, Melissa, Ilariya – you are each incredible in your own way, and I continue to learn from you. Jacques – for being an inspiration, and for rekindling my passion for art; thank you for your stories, friendship, and guidance.

There are so many more people to thank – Melissa, David, Amanda, Manny, Kristy, Dimmy, Brigette, Tobias, Simon, Kelly, Lachie – you are my go-to peeps for experimental, flow cytometry, and microscopy issues, thank you for keeping me sane. And everyone else on 3 West – lab heads, post-docs, RAs and students alike – thank you for the reagents, advice, and sometimes philosophical lunchtime discussions.

Sue and Keely – for your patience and support.

Our lovely animal technicians: Bec, Lisa, Shannon, Melinda, Teisha, Lauren, Merle, and Kristy, and many more in the Bioservices department – for caring for our mice and dealing with all my requests. The mice themselves – for furthering our understanding of the world.

Media, Purchasing, Engineering, ITS, Graphics & Comm departments – for all your hard work in the shadows. And thanks especially to those who let me nerd out over RasPi, tech, bookmaking, design, guerrilla artwork, skateboarding, electronics, animation… the list goes on.

MUKC – Alex, Sean, Kit and Joachim, who welcomed me back from my hiatus. Karate-do continues to teach me to be brave, patient, and to persevere.

Old friends, new friends, a big thank you for sticking with me through it all.

Will, Lisa – I am so proud to be your sis. Mum and dad – thank you for all your support and encouragement over the years.

And Mr. Simpson – thank you for nurturing my curiosity all those years ago. Your legacy of courage, determination, and compassion give me strength when I need it most.

Thank you all from the bottom of my heart.

Table of Contents

List of Figures and Tables

List of Abbreviations

2-ME	2-mercaptoethanol
Ab	antibody
AdvBCM	advanced B cell medium
AdvBCM-F	advanced B cell medium for filming
Ag	antigen
ANOVA	analysis of variance
APC	allophycocyanin
ASC	antibody secreting cell
BCIP/NBT	5-bromo-4-chloro-3-indolyl phosphate/nitro blue tetrazolium
Bcl-2 (*BCL2* gene)	B cell lymphoma 2
BCR	B cell receptor
BD	Becton Dickinson
Blimp-1 (*PRDM1* gene)	B lymphocyte induced maturation protein 1
BSA	bovine serum albumin
cat#	catalogue number
CD	cluster of differentiation marker
CD40L	CD40-ligand
CFSE	5(6)-carboxyfluorescein diacetate succinimidyl ester
CI	confidence interval
CLP	common lymphoid progenitor
CSV	comma separated value
CTV	CellTrace Violet
DMSO	dimethyl sulfoxide
DNA	deoxyribonucleic acid
DPBS	Dulbecco's phosphate-buffered saline
EDTA	ethylenediaminetetraacetic acid
ELISA	enzyme-linked immunosorbent assay
ELISpot	enzyme-linked immunospot assay

FACS	fluorescence activated cell sorting
FCS	foetal calf serum / foetal bovine serum
FITC	fluorescein isothiocyanate
FSC	forward scatter
Fucci	fluorescent, ubiquitination-based cell cycle indicator
GFP	green fluorescent protein
HEPES	4-(2-Hydroxyethyl)piperazine-1-ethanesulfonic acid
Ig	immunoglobulin
IL	interleukin
KM	Kaplan-Meier (survival estimates)
LED	light emitting diode
MACS	magnetic activated cell sorting
mAG	monomeric Azami Green
MHC	major histocompatibility complex
mKO2	monomeric Kusabira Orange 2
MTPBS	mouse tenacity phosphate buffered saline
MZ	marginal zone
PAMP	pathogen-associated molecular pattern
PBS	phosphate-buffered saline
PCR	polymerase chain reaction
PE	phycoerythrin
PI	propidium iodide
PRDM1	PR domain zinc finger protein 1 (alternatively, Blimp-1)
PRR	pattern recognition receptor
RPMI	Roswell Park Memorial Institute medium
SSC	side scatter
TCR	T cell receptor
Tg	transgenic
WEHI	The Walter and Eliza Hall Institute of Medical Research

CHAPTER 1

Introduction

1.1 The multi-level immune system

As vertebrates, we are complex organisms co-habiting our planet with a multitude of other species, often competing for resources. For the range of competitors visible to us, we may take evasive measures, set traps, actively eliminate, or build barricades to maximise our chances of survival. For dangerous microorganisms invisible to the naked eye, our body is equipped with its own armoury more suited to that scale: skin and mucosal surfaces as barrier protection, innate immune cells to remove common pathogens or foreign bodies, and lymphocytes, each with their own unique receptors for recognising specific pathogens. Identifying how lymphocytes develop and fulfil their roles is therefore fundamental to our complete understanding of immune system function, and a pre-requisite to many potential immunotherapies.

1.2 Adaptive immunity

The adaptive immune system plays a pivotal role in protection from infectious diseases for vertebrate species, utilising unique pathogen-specific receptors formed by somatic recombination. This generation of randomised receptors is a feature of the adaptive immune system implemented by lymphocytes, and distinguishes this cell type from other leukocytes, known as 'innate' immune cells, which utilise germline coded receptors to identify common invaders. As a result of the stochastic processes producing their receptor's 'variable region', each lymphocyte specifies a unique receptor structure, and collectively they can recognise virtually any shape (epitope) of a foreign particle (antigen). Occupied receptors typically trigger activation pathways, causing selected cells to expand exponentially in numbers for several days while simultaneously differentiating into specialised cell types, thus producing a large cell population to combat an infection. The majority of clones then die, leaving a small population of antigen-cognisant memory cells that respond more rapidly upon repeat exposure to the same antigen. This 'Clonal selection' paradigm was first postulated by Burnet in 1957 [1],

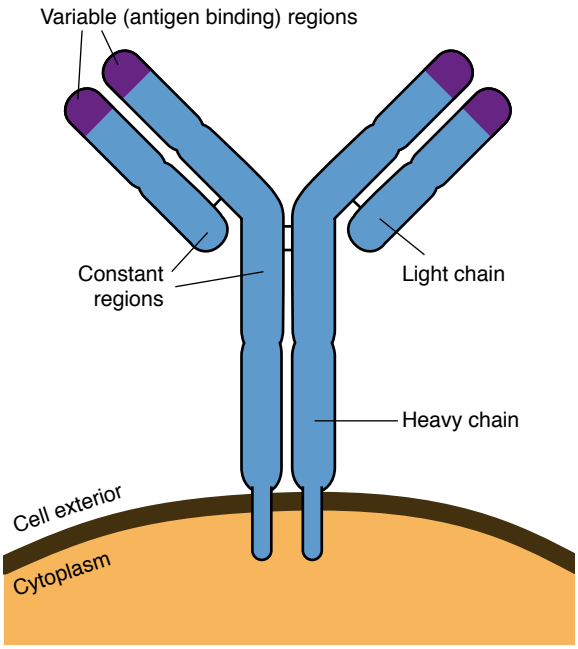

Figure 1.1: Schematic of the B cell receptor complex.
B cell receptors, also known as immunoglobulins, are constructed from two identical heavy chains and two identical light chains, covalently bonded with disulphide bridges. Each chain contains a variable and a constant region. The constant region of the heavy chains determines the antibody isotype, while the variable regions determine antigen specificity.

and remains a central dogma in the field of immunology (reviewed in [2]). The ability to target diverse, novel structures and retain immunological memory is so effective that the development of lymphocytes has been evolutionarily conserved across all known jawed vertebrates (gnathostomes), with analogous structures in jawless fish (agnathans) [3].

Lymphocytes fall into two major categories: B and T cells [4, 5], named after the organs which, when removed, prevented the development of specific cell types: the Bursa of Fabricius in chickens [6], and the Thymus [7]. T cells typically effect cell-mediated immunity, either by orchestrating the action of other cells (helper T cells), or by directly killing virally-infected cells or even potential tumour cells (cytotoxic T cells) (reviewed in [8]).

In contrast, B cells are the principle mediators of humoral (ie. fluid associated) immunity. After selection and activation, cells can modify their unique B cell receptors (BCR, also known as 'membrane-bound immunoglobulin', mIg, **Figure 1.1**), to be secreted as soluble immunoglobulin (sIg, commonly known as antibodies). This differentiation step to antibody secreting cells (ASCs) allows B cells to fulfil their role as producers of serum immunoglobulin, offering systemic protection against target antigens. ASCs can further be distinguished into plasmablasts if the B cell is still dividing, or plasma cells if terminally differentiated [9-11].

Prior to becoming ASC, B lymphoblasts may also 'switch' their antibody between different Ig isotypes. Each isotype, as defined by the structure of the heavy chain component of the antibody, harbours different properties, particularly when secreted (outlined in **Table 1.1** [12]). Naïve cells, for example, first produce IgM, typically of low affinity, but when secreted, these antibodies form multivalent pentamers, large structures that excel at cross-linking and agglutination of their targets. IgG, on the other hand, remain as bivalent molecules when secreted, may cross membranes such as the placenta, and are typically of higher affinity (reviewed in [13]).

Secreted antibodies of different isotypes have numerous ways of conferring protection. Simply binding to the surface of a pathogen can neutralise its ability to infect other cells, while toxins bound by antibody can be prevented from accessing their target. Binding a pathogen can also 'flag' the particle (opsonise) for phagocytosis, and/or initiate further damage by activating a series of complement proteins that ultimately destroy bacterial membranes [14]. Thus, readily available antibodies hasten pathogen clearance, and will often prevent the onset of illness, or at least reduce the severity of an infection. For the endogenous microbiota, carried on skin, but particularly in the gastrointestinal tract, the immune system also plays a crucial role in maintaining homeostasis between the symbiotic effects of the microorganisms and systemic infection [15]. In patients presenting with low Ig, not only are they more susceptible to common infections, but they are also prone to such opportunistic infections that are otherwise harmless to healthy individuals [16, 17].

Antibody class	Function	Excreted structure	Diagram
IgM (μ)	Expressed early, binding sites usually of low affinity. Large, pentameric molecule unable to cross most barriers. Effective at agglutination, activating complement.	Pentamer	
IgD (δ)	Expressed early, most often with IgM. Function uncertain.	Monomer	
IgG (γ)	The most abundant circulating antibody, can cross capillary endothelium, access intercellular spaces, and confer antibody protection to newborn. Effective binding to Fc receptors on phagocytes. Can activate complement.	Monomer	
IgA (α)	Secreted across mucosal membranes, controls antigen, such as in the gastrointestinal tract and on skin. Can activate complement.	Dimer	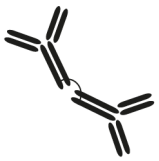
IgE (ε)	Primarily bound to mast cells and eosinophils, induces inflammatory response in area of infection. Thought to have increased effectiveness against parasitic worms and bee venom, but also responsible for atopic allergic reactions.	Monomer	

Table 1.1*: Antibody classes and their functions*

Since the structure of antibodies affect their function, and the transition from activated B cell (or 'lymphoblast') into a plasmablast or plasma cell is irreversible [18], the timing of these two outcomes is important. The resulting effector cells, unable to further modify their immunoglobulin structures or specificity, secrete antibody which circulates in serum and mucosal fluids, providing important immune protection. How the many different B cell activation signals influence and control B cell responses, and manipulate their proliferation, switching and differentiation outcomes to produce an optimal humoral response is the subject of intense ongoing research.

1.3 Making B and T cells

The life of B cells is conveniently viewed as proceeding through three distinct phases. First is the development and creation of the 'naïve cell', antigen-inexperienced B cells expressing intact BCRs. Once made, mature naïve B cells enter their second phase and circulate

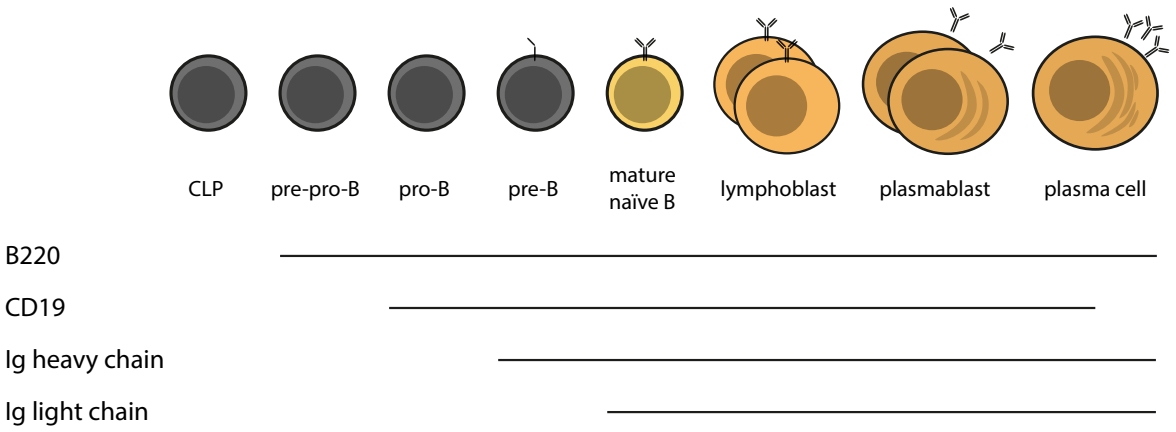

Figure 1.2: Life of a B cell.
Diagram of B cell development from common lymphoid progenitors (CLP) to plasma cells. Lines indicate expression of surface markers B220 and CD19, as well as timing of immunoglobulin (Ig) chain expression. Adapted from [23].

continuously between blood and lymphatic vessels, behaving as sentinels and monitoring for foreign material and suitable activation conditions. Upon activation, B cells are drawn into a new phase and proceed with their immune reaction, proliferating and modifying their immunoglobulin structures until they differentiate into either ASCs or long-lived memory cells. Fully differentiated ASCs must then find a niche providing the correct survival signals, and settle as plasma cells for lifelong antibody production [19-22].

The first phase, the generation of naïve B cells, is initiated in the bone marrow for mammals. Steps in progressive development are illustrated in **Figure 1.2**. Surface expression of the CD45 isoform B220 on common lymphoid progenitors (CLP) signifies differentiation to pre-pro B cells, and commitment to the B cell lineage. Subsequently, pro-B cells upregulate CD19, and both B220 and CD19 are maintained throughout the B cell lineage until the downregulation of CD19 on late plasma cells (reviewed in [23]) [24]. Hence, the B220+ CD19+ compartment is commonly used to distinguish the B cell lineage from other lymphocytes.

The pro-B cell stage initiates a program vital to receptor diversity – gene rearrangements that produce BCRs unique to each cell. Each BCR is assembled from duplicate Ig heavy chains and duplicate Ig light chains, with each chain containing a variable region susceptible to randomisation. Pro-B cells first attempt to produce an immunoglobulin heavy chain from one chromosome by concatenating a single diversity (D) region (of 25 known active regions in humans) [25] and a junction (J) region (of 6 known active regions) [26], and subsequently an additional variable (V) region (of around 51 known active regions) [27] (**Figure 1.3**). The combinatorics with which these gene segments can be ligated, together with additional nucleotide insertions at the joins between the segments [28] is a major source of receptor

diversity. The potential antibody repertoire is estimated to far exceed the B cell portion of approximately 10^{11} lymphocytes in a healthy human [29, 30]. Often no viable heavy chain is produced by the first chromosome however, and a second opportunity is afforded by the other chromosome, while the unproductive gene is silenced by allelic exclusion [31]. Cells producing successful Ig Heavy chains are re-classed as pre-B cells, and proceed to assemble Ig light chains.

In a process similar to the formation of Ig heavy chains, V and J gene segments must be combined to construct a functional light chain. Four opportunities are provided for doing this – two from the kappa (κ) locus (35 V_κ domains, 5 J_κ domains), followed by two from the lambda (λ) light chain locus (33 V_λ domains, 7 J_λ domains) [31-33]. Failure to assemble either heavy or light chains results in apoptosis of the immature cell. Those cells that successfully bring together two units each of the Ig heavy and light chains to form complete Ig progress to become 'immature B cells', which are subject to stringent negative selection against self-reacting receptors to prevent autoimmunity [34, 35]. In this immature state, Ig recognition leads to cell apoptosis and deletion [36-38]. The remaining cells, now classed as mature, naïve B cells, migrate and circulate around to peripheral lymphoid organs and remain quiescent until subjected to activating signals.

The maturation of T cells follows a similar course to B cells, using VDJ recombination to produce the variable regions of T cell receptors (TCRs); hence TCRs are homologous to BCRs, but are never secreted. T cell progenitors, also known as thymocytes, mature in the thymus and must successfully assemble TCR-α and TCR-β chains (or γ and δ chains), then undergo extensive positive and negative selection in order to preserve self-tolerance (reviewed in [39-41].

T and B cell receptors are homologous and share many similar attributes, but differ in an important way. Whereas BCRs can bind free antigen, TCR specificity is always limited

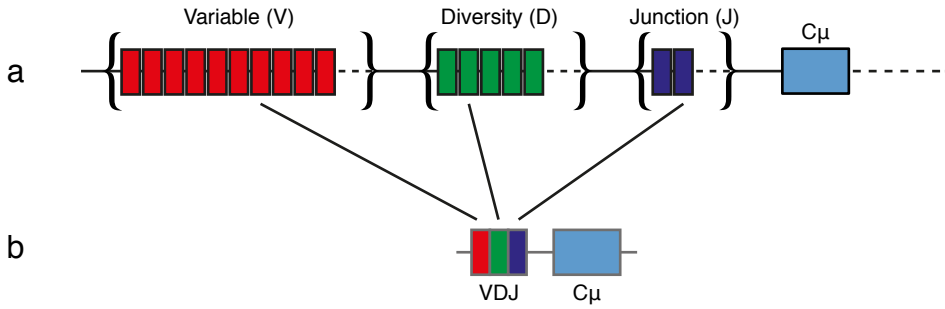

Figure 1.3: VDJ recombination in the immunoglobulin heavy chain locus.

a) Germline sequence representing the multitude of variable, diversity, and junction compartments from which the antigen binding region of an immunoglobulin heavy chain can be assembled. **b)** Introns and excess exons are excised, leaving one segment from each compartment. The reassembled gene locus must then be transcribed and successfully produce heavy chain proteins for the cell to continue development.

to intracellular peptides presented by, and in combination with, major histocompatability complex (MHC) molecules on the cell surface [42]. This level of specificity is achieved during T cell development in the thymus, where newly formed cells with TCRs that recognise self MHC are given survival signals and undergo positive selection, while the rest die by neglect. A second round of negative selection occurs, where cells with TCRs possessing excessive affinity to MHC alone or in association with self-peptides are eliminated, to prevent auto-reactive binding and maintain self-tolerance (reviewed in [43]). As a result of such stringent selective pressures on the T cell repertoire, the surviving T cells are 'MHC restricted'; conversely, the body's tissues must also be compatible with the available T cells to maintain tolerance, hence 'histo (tissue) – compatible'.

Two T cell co-receptors, CD8 and CD4, assist with directing specificity towards either MHC class I or MHC class II, respectively. All nucleated cells express class I MHC, and can present cytoplasmic antigens to CD8+ T cells, as in the case of a viral infection [44]. Expression of class II MHC is limited to professional antigen presenting cells (APC), such as dendritic cells and macrophages, that can capture foreign material, process it in lysosomes, and present derivative peptides at the cell surface in association with class II MHC [45]. The affinity of each cell's TCRs for either class of MHC molecule is tested for at the conclusion of the 'double positive' (CD4+ CD8+) stage of thymocyte development. At this time, one of the two types of receptors are stochastically downregulated, and the remainder used to test for positive TCR engagement with the corresponding MHC [46, 47]. Subsequently, conventional T cells are allocated as either CD8+ 'cytotoxic T cells' or CD4+ 'helper T cells', named after their MHC class restriction and ultimately the course of their development and function.

As a class of APC, B cells constitutively express class II MHC. This expression is an important mode of activation by T cells, and essential for T cell dependent (TD) activation of B cells *in vivo*. Antigens captured by the BCR are internalised, processed into peptide components, and loaded onto suitable MHC class II molecules for detection by helper T cells [48]. Here, the evolution of two parallel classes of lymphocytes converge and together promote a seemingly complex and sophisticated immune reaction.

1.4 The B cell response

Immune responses, whether T or B, typically follow a canonical pattern over time, illustrated in **Figure 1.4**. In general, a small number of specific cells are selected following antigen detection to undergo intense proliferation. One to two days after activation, those lymphocytes begin dividing, expand in numbers, eventually cease proliferation, and the majority of the newly formed population dies, leaving a small number of antigen-experienced cells in

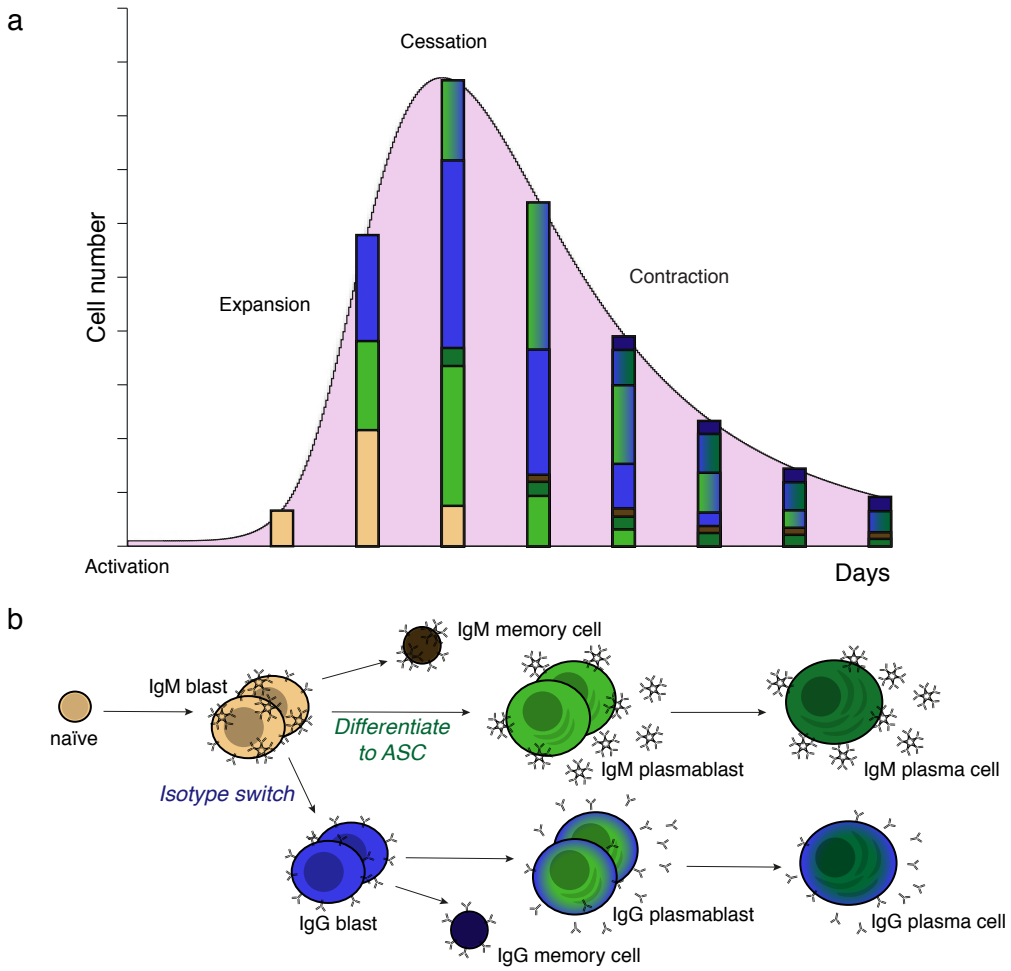

Figure 1.4: The heterogeneous immune response.

a) The immune response is consistently heterogenous. A few days after stimulation, lymphocytes go through expansion, cessation of proliferation, and contraction phases, producing suitable cell numbers for the corresponding stage of response. Coloured bars represent the combinations of fate outcomes shown in b. **b)** Examples of possible cell fates, produced by a combination of immunoglobulin isotype switching, differentiation to antibody secreting cell (ASC), and becoming long-lived memory cells. (Figure adapted from [125])

preparation for a repeated exposure to the same antigen. This proliferation is accompanied by differentiation to a range of new cell types, including short-lived effector and long-lived memory cells [49-53].

The activation requirements for B cells to be drawn into an immune response after exposure to antigen are complex and requires numerous other regulating signals. These activation paths are commonly categorised into two classes. In one, mentioned above, the B cell is assisted by T cells leading to 'T-dependent' (TD) activation [54, 55]; in the second, activation signals are provided from other sources and can occur in the absence of T cells, and hence are referred to as being T-independent (TI) [56, 57].

Both TD and TI modes of stimulation (explored further in the next sections) can lead to development of ASC, although they differ in the range of isotypes produced, in the formation

of long-lived memory, and in the development of high affinity plasma cells. They each produce an initial 'extrafollicular' response that leads to efficient early antibody production [49]. This process, however, does not evoke strong memory or cells of particularly high affinity. In order to generate high affinity memory and long-lived plasma cells, a second phase of immune response follows the initial proliferation and takes place in a specialised niche in lymphoid tissue: the germinal centre (GC) within B cell follicles [58].

GC formation is a prominent feature of TD responses and can proceed for a number of weeks after antigen exposure (reviewed in [59]). It is formed within lymphoid tissue when a primary follicle is seeded with cells from the extrafollicular response, and multiple rounds of selection proceed. During this phase, the BCR is further mutated, enabling improvements in antibody affinity over time [60]. Immunoglobulin isotype switching, a feature of the extrafollicular response, occurs prior to GC formation [61]. As a result of intense selection in the GC and the deliberate introduction of point mutations (somatic hypermutation) to receptor variable regions [62], high affinity memory cells and plasma cells eventually emerge. The former typically behave like naïve B cells, and do not proliferate, but circulate with the naïve group and are rapidly activated upon recognising antigen. Plasma cells migrate to the bone marrow, where given the right environment, they may survive for the lifetime of their host, conferring sustained antibody production and hence protection (reviewed in [22, 63, 64]), [65].

As the methods required for monitoring cell proliferation and differentiation events *in vivo* remain labour intensive and technologically challenging, data acquired by other experimental strategies is advantageous for extending our current knowledge. Since the production of switched plasmablasts from naïve B cells can be recreated *in vitro* [66, 67], such experiments facilitate a controlled setting where the effects of variables on B cell fate can be followed in great detail.

1.5 T-independent activation

Like other professional APCs, B cells also express pattern recognition receptors (PRRs) which are sensitive to pathogen-associated molecular patterns (PAMPs), and can respond to common infection cues such as bacterial cell wall components or unmethylated DNA (reviewed in [68, 69]). Binding of these receptors initiates TI responses, likely an ancient and evolutionarily conserved response which allows the host to respond rapidly to a broad range of antigens commonly associated with infections. As such, the B cells activate and proliferate with little delay, although the response to PRRs alone is short-lived and has limited potential for isotype switching and affinity maturation [70].

PRRs expressed by B cells include a number of toll-like receptors (TLRs), and in mice, the

responses of intracellular TLR-9 to CpG and surface TLR-4 to LPS are well-characterised as stimuli for proliferation [71, 72]. CpG-activated B cells begin proliferation around 30 hours after stimulation, and will cease dividing approximately 3 days later. Cells are not observed to change their antibody isotype, nor differentiate to ASC. In comparison, LPS-activated B cells also respond rapidly and follow a similar proliferation pattern to CpG; however, cells will isotype switch from IgM to IgG_3, and can differentiate at high frequency into short-lived antibody secreting plasmablast cells [70, 73]. Thus, differentiation to ASC and the early production of antibodies appears to be a primitive, autonomous program that does not require T cell cooperation [74].

BCRs are not entirely excluded from the TI response, however. Captured antigen from BCRs may be attached to, bring to the surface, and activate corresponding PAMPs. Thus, the cell can receive signals from both the BCR and the PAMP, resulting in significant synergy for activation [75].

1.6 T-dependent activation.

In contrast to T-independent activation, T-dependent activation relies on TCR recognition of peptides in the context of MHC Class II presented on the B cell surface.

First noted *in vivo* by Mitchell and Miller [7], the presence of both bone-marrow derived lymphocytes and thymus derived lymphocytes synergise to mount an immune response much greater than that observed from challenging either cell type alone. The mechanisms of cooperation have since been the subject of much study, and revealed a system where a B cell and a T cell, both recognising different epitopes of the same antigen, must come together and transmit further reciprocal signals to produce an appropriate antibody response. Upon binding to cognate antigen, previously circulating B cells localise to the outer part of the T cell zone of lymphoid organs [76, 77], while T cells continue to circulate, such that every T cell should have come in close proximity to an antigen-presenting B cell within approximately two days [78].

When engaged by antigen, B cells internalise their BCRs and process bound proteins into smaller components. As endosomes containing peptide fragments fuse with exocytic vesicles transporting MHC Class II molecules, compatible peptides are loaded to form peptide-MHC complexes, and the structures exported for surface expression and antigen presentation [79, 80]. With appropriate binding between a B cell's peptide-MHC Class-II complex and TCR on a CD4+ helper T cell, an immunological synapse is established between the two lymphocytes [48, 81]. CD40L induced on activated T cells engages with CD40 (constitutively expressed on mature B cells) as a primary activation signal, and may be supported by the transmission of soluble immune mediators – cytokines such as interleukin (IL)-4, IL-10, or IL-21 [82-86].

Remarkably, many of the major events associated with TD activation can be recreated *in vitro* and naïve cells can be induced to proliferate, class switch and become plasmablasts in minimal tissue culture conditions [87, 88]. Although BCR engagement induces signalling in the cytoplasmic domain of the receptor [89, 90] and affects the amount of antigen internalised by an individual cell, stimulatory methods that bypass the need for antigen can recapitulate T cell-derived signalling. For example, CD40 engagement in combination with cytokines are sufficient to induce similar proliferation, death, and differentiation patterns as seen in the extrafollicular B cell response [67, 91-94].

There are many methods of engaging CD40 for stimulation including the use of agonistic anti-CD40 antibody 1C10 [95]. This monoclonal antibody removes the need for co-culture with T cells, and activates all B cells present in a highly consistent and controlled way. By regulating the availability of stimuli, and providing all cells with equal access to activation signals, the effects of individual factors may be carefully interrogated with limited other variables.

1.7 Immunoglobulin class switching and division-linked changes

For both TD and TI activation pathways, the BCR plays an essential role in attracting antigen and initiating activation responses. Its mutable structure, even after initial formation, is unique to B cells, and vital to the function of not just the individual cell, but the function of the B cell population as a whole, which relies on probabilities to recognise even completely unknown antigens.

Selecting and regulating the various heavy chain isotypes of B cell receptors is a critical feature of B cell activation, as it ultimately affects the effectiveness of antibody mediated defences. The decision to antibody isotype switch can be swayed by the cytokines B cells are exposed to during activation. For instance, in murine B cells IL-4 induces switching to IgG_1 and IgE [96], and interferon-γ (IFN-γ) induces IgG2a [97].

Curiously, despite clear evidence that stimulatory signals can induce antibody isotype switching, not all cells exposed to the same stimuli will switch and undergo the same fate. An explanation for this came about with the discovery of carboxyfluorescein diacetate succinimidyl ester (CFSE) as a division-tracking dye [98, 99], which paved the way for use of subsequent cell division tracking dyes such as CellTrace Violet [100, 101]. Using this technology to instantly identify the number of times cells have divided by flow cytometry [94], antibody isotype switching to IgG_1 was observed to follow a distinct division-linked pattern. The propensity for isotype switching corresponded directly with the number of divisions cells had cycled through, regardless of time from stimulation and variation in division times; and the degree of switching could be modulated by modifying strength of stimuli [102].

Similar patterns of division-linked behaviour were found for other antibody isotypes – in mice: IgE and IgG_{2a} [92], IgG_3, IgG_{2b}, and IgA [103] – and in humans [104]. These findings indicate a method of regulation common to the different immunoglobulin heavy chains, which could be modulated by stimulation type and strength, and division number, but not time. Further, when stimuli that promote switching to different antibody isotypes were used together, the probability of switching remained independent for each isotype. Although dominance effects could be observed, for instance when the addition of TGF-b to LPS cultures favoured switching to IgG2b over IgG3, this phenomena could be explained by sequential switching, where B cells may only switch to immunoglobulin heavy chains downstream of the existing isotype [103, 105].

1.8 Regulation of the ASC

The transition of a B cell to an ASC has been well studied at the molecular level. Key transcription factors maintain the proliferative and immunoglobulin modulating aspects of lymphoblasts, while suppressing differentiation to ASC. Among these, and critical for B cell identity, is paired box protein 5 (Pax5) [106, 107]. This transcription factor is required for initial lineage commitment from lymphoid progenitors, and regulates components of several immune receptors including the BCR, as well as other important transcription factors such as interferon regulatory factor 4 (IRF4), IRF8, BTB and CNC homologue 2 (BACH2), Aiolos, and SPIB [108, 109]. These factors together predominantly maintain the GC, and repress key regulators of ASC development, including B lymphocyte-induced maturation protein 1 (Blimp-1; *Prdm1* gene) [18, 110].

Blimp-1 is a transcriptional repressor that promotes terminal differentiation in both B cells and T cells [111-113]. After B cell activation, and as Pax5 levels drop, IRF8 and Bach 2 are lost, allowing the expression of Blimp-1, which further downregulates B lymphoblast programs in favour of an ASC gene expression profile. As such, Blimp-1 expression is an early indicator of differentiation to ASC, and a reporter construct linked to this gene has been critical for the study of B cell differentiation [114].

The Blimp-1-GFP mouse strain carries a green fluorescence protein (GFP) gene inserted into the Blimp-1 locus, resulting in a truncated Blimp-1 protein and GFP from the same mRNA transcript. This construct makes a reliable reporter, as GFP expression is subject to the same regulatory elements as Blimp-1 protein. Although Blimp-$1^{GFP/+}$ mice only carry one copy of the Blimp-1 gene (known as *Prdm1*) that makes functional protein, these mice appear to be haplosufficient, as heterozygous mice and their cells have not been observed to behave any differently from C57BL/6 wild types [114]. Homozygous mice, however, effectively Blimp-1 knockouts, experience embryonic lethality, although this has been shown to be independent

of haematopoiesis [115]. For the purpose of these studies, heterozygous Blimp-$1^{GFP/+}$ mice were used as an indicator of differentiation to ASC, superseding the need for fluorescent labelling of Syndecan-1 (CD138), a commonly used marker for secreting cells [116].

In studying B cell differentiation to ASC, the transition from lymphoblast to plasmablast was also found to be division-linked [117]. Regardless of generation number or time from stimulation, the proportion of cells expressing Syndecan-1 remained the same for each cell generation [67]. Curiously, when the isotype switching effects and differentiation effects of the T cell derived cytokine IL-5 were quantified, the two cell fate options appeared to operate independently, producing a heterogenous mix of phenotypes resulting from permutations in fate combinations [67].

Being irreversible, the timing of differentiation to ASC is crucial to successful plasma cell production [18, 67, 118]. Cells require multiple divisions to undergo somatic hypermutation of the BCR's variable region, further diversifying the responding clone, and isotype switch to different antibody classes each with their own specialised functions [119]. Thus, it is important to understand how differentiation is balanced with the timing of other cell fates during B cell development.

1.9 Competition between cell death and division assumed for Cyton model

Just as isotype switching and differentiation to ASC were found to operate independently, despite being functionally related outcomes, cell division and death by stimulated B cells were observed to operate independently and in competition with each other up until their first division [120]. For a population of cells, both fates could be described by right-skewed probability distributions, and their features, such as average time and variance, were affected by stimulation strength and type. Once cells divided for their first time, the fates of their progeny could not be directly followed further, however division tracking and BrDU pulsing indicated that the faster dividing cells did not dominate the system, suggesting a resetting and re-randomizing of division times with each generation. On the basis of these principles, Hawkins *et al.* proposed the Cyton model for the cellular mechanics governing lymphocyte proliferation and control. By this model, each cell contained two fate modules governing division and death (the combination was called the cell's 'cyton'). The construction or operation of each timer was assumed to be stochastic, and would conform to log-normal distributions of times, potentially different for each generation, and could be modifiable by signalling inputs. Numerical calculators based on this model produced accurate fits to observed cell division data, and illustrated highly non-linear, but calculable effects of changing times to divide or die on total cell numbers [120].

Thus, the first iteration of the Cyton model was built around lymphocyte division and death,

with the concept that these two mutually exclusive fate outcomes operate independently and in competition [120, 121]. By this model, each activated B or T cell has the potential to undergo either of these fates, but the underlying cellular processes require different lengths of time to become actualised; consequently, the event that occurs earlier prevents the second from being observed, effectively 'censoring' the alternate fate. For cells that continue to divide, these timers appeared to be reset upon mitosis [120].

By harvesting information from division tracking dyes, combined with temporal information and total cell numbers, the proliferation rate, activation time, and survival of lymphocyte populations could be calculated [70, 120, 122-125]. Thus, despite making as yet un-verified implicit assumptions, the Cyton model served as a proof of principle that cell machinery working in competition and subject to signal dependent modification could serve as a foundation for a quantitative framework for lymphocyte control. It remained to test the model in greater detail, and for its potential to accommodate other fates to be established.

1.10 Further insights from single cell time-lapse imaging

The data collected from flow cytometry experiments is limited in that only 'snapshots' of populations can be observed. Identical cell cultures are required to be grown in parallel, and individual plates analysed at different times to capture the proliferation response over time. Times to fates for divided cells of particular phenotypes required sorting for pure cell populations. To overcome these limitations, live cell imaging can be used to track the fates of the same population of cells over time.

Initial imaging experiments were conducted on CpG stimulated (ie. TLR-9) B cells using Terasaki plates containing 60 flat-bottomed microwells [126]. CpG provided the benefit of the cells remaining spherical even after activation, and divided cells would distribute themselves in a sparse monolayer across the base of the small, round concave wells. The division and death times of the progeny from dozens of founder cells were recorded with time-lapse imaging over four days. A high level of correlation was found between the division times of sister cells, and cells from the same founder tended to die after the same number of divisions, suggesting governance by heritable factors controlling these outcomes. Division times from mother to daughter and grand-daughter cells, however, tended to revert back to the level of variation found across the population, indicating a re-randomisation of division times through subsequent cell generations [126, 127].

The CpG system could not be used to track differentiation to ASC, so TD stimulation was studied with the use of CD40 and IL-4 stimulation on Blimp-1-GFP reporter B cells, and an added fluorescent antibody to track Ig isotype switching to IgG_1 [128]. This system brought

the additional problem of homotypic adhesion, and so new culture methods were devised to prevent aggregation and allow imaging of actively dividing cells. Cells from a specific cell generation were sorted into miniature cell paddocks [129], small depressions at the base of filming chambers which segregated cells from each other, and allowed the tracking of two sister cells per paddock until their subsequent divisions.

Using this system, over a thousand sibling pairs were followed, tracking the times to divide, die, differentiate to ASC, or isotype switch, for cells that had undergone different numbers of divisions. The data again illustrated strong sibling concordance for division and death, but also for differentiation and isotype switching. Curiously, striking intracellular correlations were also demonstrated between separate cell fates. At face value, this finding appeared to break the rule of independence established earlier [67, 120, 130], however the observed correlations could also be due to censorship between mutually exclusive cell fates [125].

To test for competition and censorship between individual cell fates, a model was fitted to the data with the assumptions of independence between alternate fate outcomes, and competition between mutually exclusive fates. That is, cells that differentiate can no longer isotype switch, and cells that divide or die can no longer undergo any other fate within the observed generation. Each of the four fate outcomes were assigned three parameters for its 'uncensored' log-normal probability distribution function (PDF) in the absence of competition – mean, variance, and propensity; with the exception of death times, where the sum of all probabilities over time is designated as 1. Values for sibling correlations within each of the four cell fates were included, totalling 15 parameters. The highest likelihood values calculated for these parameters produced a model fit that was able to recapitulate key aspects of the observed data, with observed ('censored') times to fates and proportions undergoing each fate outcome, as well as sibling correlations all falling within the expectations of the constrained model.

Remarkably, the fitted model was also able to predict levels of intracellular and intercellular non-concordant correlations. That is, under the assumptions of independence, competition, and censorship for the four fate outcomes tested, one would expect to see: a correlation between differentiation and division times, due to their overlapping distributions of times to fates; no correlation between isotype switching and division times, due to lack of overlap in times to fates; and a correlation in times for siblings to undergo non-concordant fate outcomes, as the disparate fates would only be observed if their timers were quite similar, due to high levels of sibling correlations. Experimental values closely matched the modelled outcomes, indicating that the rules used to generate this model are sufficient for producing the heterogenous mix of concordant and asymmetric events at the observed frequencies.

1.11 A quantitative Clonal Selection Theory for lymphocyte activation

The above experiments and quantitative modelling demonstrate how simple rules for fate allocation are able to generate the complex array of heterogenous fate outcomes observed in normal immune responses. For individual cells, even in defined cultures, the potential of its progeny to divide, antibody isotype switch, differentiate to ASC, or when they will die is impossible to predict accurately with current technology. Nevertheless, at the population level, lymphocyte responses are highly consistent, both *in vitro* and *in vivo* [131, 132], making statistical methods an effective tool for investigating B cell responses and their emergent properties [133].

The preferential selection and expansion of antigen-experienced B cells is a central aspect of Burnet's Clonal Selection Theory [1]. Elegantly expressed in 1957, Burnet outlines the "randomization of the coding responsible" for immunoglobulins, and how cells that come into contact with cognate antigen are selectively activated and proliferate. Burnet's influential theory, however, does not encompass the sheer heterogeneity of fate choices observable in the immune response known today, nor does it provide any guidance for how to quantify immune responses and predict the effects of changing conditions on immunity.

The Cyton model can be viewed as an attempt to formalise a quantitative adaptation of the Clonal Selection Theory [125, 134], to account for the full spectrum of cells in the responding lymphocyte population, whether strongly or weakly stimulated. Rather than a dichotomous assignment of whether cells undergo clonal selection or not, the Cyton model incorporates probabilities and temporal information to navigate the cell fate choices occurring within the population. Initially governing just cell division and death, this formalisation leaves open the possibility of adding in other cellular fate controlling components, for assigning cells to additional fates and exploring complex and heterogeneous outcomes.

1.12 A model of independent, stochastic, and competing cell fates

Thus far, a quantitative Cyton model has tested the features of B cell responses and supported several aspects of B cell fate regulation. This model is consistent with an Autonomous Competition Hypothesis [125] (**Figure 1.5**), which features independent, stochastic, and competing cell fates, reset upon division:

Alternate cell fates operate independently of each other.

Individual cell fates progress at expected frequencies regardless of a cell's phenotypic history, as long as the different outcomes are not mutually exclusive. For example, isotype switching to IgG_{2b} proceeds regardless of prior switching to IgG_3 [103], and differentiation to ASC

proceeds regardless of immunoglobulin isotype [67]. Division and death also appear to be controlled independently [120, 121, 135]. Further striking evidence for this feature was found from single cell imaging experiments, where such a model was able to reproduce correlations in unrelated fate outcomes at the expected levels [128].

Times to individual fates are stochastically allocated.

Although the molecular properties governing the exact timing for individual cells to undergo a phenotypic change are unmeasurable with current technologies, for a population of cells, the times to fates appear to be stochastically distributed [103, 120]. With a large enough population, a histogram for the times to fates, when observed from last mitosis, closely resemble a log-normal distribution, and this is consistently observed for cell division, death, immunoglobulin isotype switching, and differentiation to ASC [120, 128].

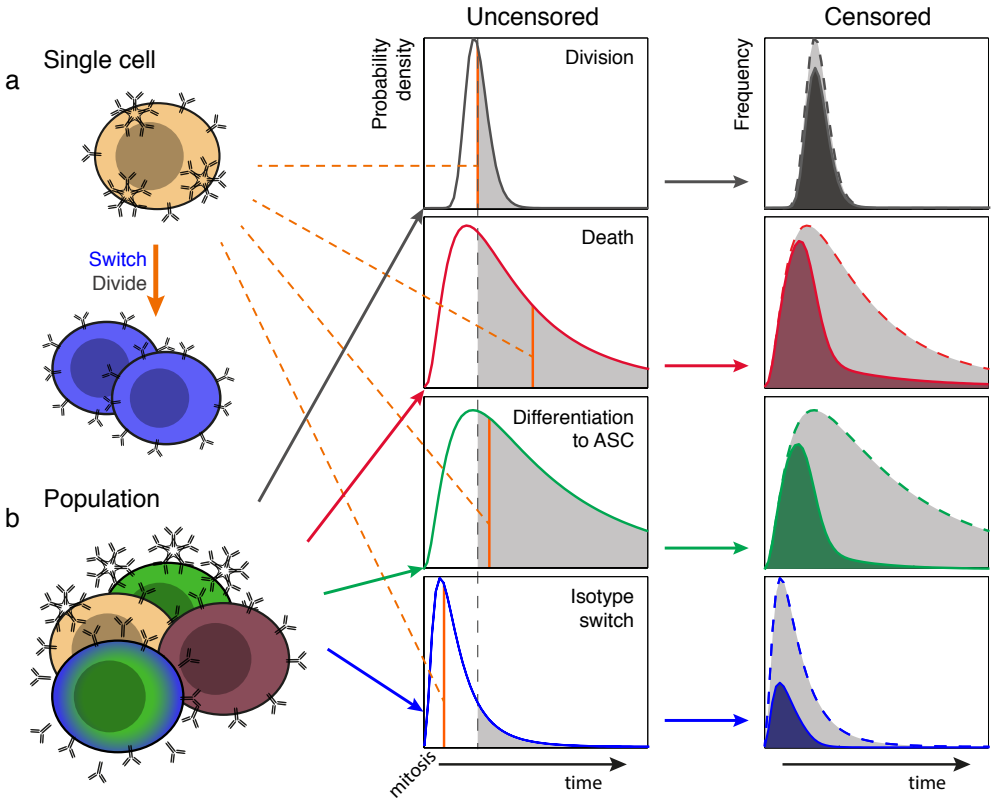

Figure 1.5: A model of independent, stochastic, and competing cell fates.

a) Individual cells simultaneously pursue a number of independent fate possibilities, each requiring a different length of time to be achieved (orange). Events that require less time may prevent others that take longer from being observed; hence, these fates are in competition. In the example here, the cell will first isotype switch, and then divide. The division event prevents the death and differentiation events from being observed. **b)** The times required to any given fate is stochastically assigned, and across a population, the distribution of times to fates conforms with a log-normal probability distribution function, which can be modelled with a mean, variance, and probability. As a result of competition and censorship, the observed times to fates form a signature 'censored' distribution.

Intracellular fate outcomes operate in competition.

Given that the alternative cell fates are motivated independently of each other, and appear to be reset upon mitosis [67, 126, 128], these times to fates would thus operate in competition. By this logic, events requiring less time are observed first, and censor from the observer alternate outcomes that require more time to be achieved. For example, a cell that divides quickly will have died later had there been no division event, and could potentially have differentiated to ASC if given more time to attain that threshold. Modelled outcomes after measuring times to various cell fates remains consistent with this feature [125, 128].

By applying the above principles and investigating lymphocyte behaviour at the population level, emergent properties may arise from the interactions within the system, and contribute to the heterogeneous cell fate trajectories essential to a healthy immune response. These population-level properties may be missed at the molecular or single cell level, and indeed may even be informative as to the molecular mechanisms underpinning the direction of an immune response [135].

1.13 Summary of outstanding questions

The ultimate purpose of any model is its ability to project likely outcomes when changes are applied to the system. In order to make these calculations, it is important to understand how the many components of a model are able to be altered, and under what circumstances. B cell division, death, isotype switching, and differentiation kinetics after one level of stimulation appear to be consistent with the model of independent, stochastic, and competing cell fates.

For generation-linked isotype switching, filming experiments found that generation number did not change the time required after mitosis for cells to switch, only the proportions of cells capable of doing so [128]. There was little competition between switching and differentiation, division, or death, due to the differences in distributions of times from mitosis to achieve these latter fate outcomes. For differentiation to ASC, however, changes with division numbers were unclear due to potential censorship, and hence further work was required to characterise how varying signalling conditions influence the passage to ASC.

The Cyton model of competing cell fates provides a framework for quantifying the likelihood of cells to reach particular fate outcomes, and how the key parameters – time (mean, variance) and propensity – can be modulated under different conditions. Further, we can investigate how these alternative fate options may interact in the presence of intracellular competition and censorship; and how the emergent properties from these interactions influence population outcomes.

Finally, with an understanding of intracellular fate allocation, it would be of interest whether the system can be artificially manipulated in a predictable way to sway population outcomes. This would be highly desirable in a clinical setting where a patient's immunodeficiency can be isolated and allocated to individual parameters, which may then be treated with targeted, precision immunotherapy.

1.14 Major aims of this project:

In this thesis, I set out to rigorously test the hypothesis of competing B cell fates by placing cells under a series of extreme conditions that affect their responses. With these findings, I aim to extend upon the current quantitative principles surrounding B cell fate regulation. In particular, I aim to:

- Investigate conditions which control differentiation to ASC; specifically changing CD40 stimulation strength and generation number.

- Investigate observed data in the context of the hypothesis for independent, stochastic, and competing cell fates.

- Screen cell cycle inhibitors with the goal of removing division as a competing cell fate, and consequently observing cell death and differentiation in the absence of intracellular competition.

I will use quantitative modelling to predict and examine how alternative cell fate outcomes are programmed in response to different conditions, with a focus on the logic of fate decisions affecting ASC formation.

CHAPTER 2

Materials and Methods

2.1 Mice

All mice used were maintained in specific pathogen-free conditions at The Walter and Eliza Hall Institute (WEHI) animal facilities (Kew, Bundoora, and Parkville, Victoria, Australia) in accordance with WEHI Animal Ethics Committee (AEC) regulations. All transgenic mouse strains used were bred on a C57BL/6 background, and maintained through matings with purebred C57BL/6 mice.

Blimp-1-GFP reporter mice (Blimp-$1^{GFP/+}$, also known as *Prdm-1*$^{GFP/+}$) [424 Blimp4F7(BlimpGFP)] were kindly provided by Stephen Nutt (WEHI). Only heterozygous mice were used here, as the green fluorescent protein (GFP) truncates the Blimp-1 transcript, hence Blimp-$1^{GFP/GFP}$ mice are effectively Blimp-1 knockouts. Heterogyzous mice are haplosufficient for the Blimp-1 protein, and function is identical to C57BL/6 wild type [114].

Bcl-2-Tg mice (Bcl-$2^{Tg/+}$) [VavP-BCL2-69] were kindly provided by Philippe Bouillet (WEHI). These mice overexpress human Bcl-2 in haematopoietic cells [136], and were crossed with Blimp-1-GFP reporter mice to produce Blimp-$1^{GFP/+}$/Bcl-$2^{Tg/+}$ mice [VavP-BCL2-69 x 424 Blimp4F7 (Blimp GFP)]. Heterozygosity is sufficient for producing the phenotype associated with overexpressing the survival protein Bcl-2. Age-matched Blimp-$1^{GFP/+}$/Bcl-$2^{+/+}$ mice were used as controls.

Fucci (fluorescent, ubiquitination-based cell cycle indicator) Red$^{Tg/+}$/Green$^{Tg/+}$ mice [137] were used briefly in Chapter 5 [B6.B6D2-Tg(Fucci)639Bsi (RBRC02709) x B6.B6D2-Tg(Fucci)492Bsi (RBRC02705)]. These mice were produced at WEHI by crossing Fucci Red [B6.B6D2-Tg(Fucci)596Bsi] with Fucci Green [B6.B6D2-Tg(Fucci)504Bsi] mice, both obtained from the Brain Science Institute, Riken (Hirosawa, Wako, Saitama, Japan). The Red transgene produces monomeric Kusabira Orange (mKO2) during G_1 and S phases of the cell cycle, while the Green transgene produces monomeric Azami Green (mAG) during the S, G_2, and M phases of the cell cycle. This system provides a visual indicator of cell cycle stage without the need for additional DNA staining, and cells from these mice function identically to C57BL/6 wild type.

2.2 Mouse genotyping

Mouse genotypes were determined with a standard polymerase chain reaction to amplify DNA, and gel electrophoresis to separate DNA by size. The following primers were used for DNA amplification:

Prdm-1 locus (Blimp-1)

loxfltR: 5'GCGGAATTCATTTAATCACCCA3'
BlimpR: 5'GGCAAGATCAAGTATGAGTGC3'
blseq16: 5'TGAGTAGTCACAGAGTACCCA3'

94°C for 2 min, then 35 cycles of [94°C 15 sec, 60°C 20 sec, 72°C 30 sec].

Prdm-1^{+}: 611 base pairs

Prdm-1^{GFP}: 531 base pairs

Bcl-2 locus

CPAU2 5'-GCCGCAGACATGATAAGATACATTGATG-3'
CPAL2 5'AAAACCTCCCACACCTCCCCCTGAA-3'

94°C for 2 min, then 30 cycles of [94°C 15 sec, 58°C 20 sec, 72°C 30 sec].

Bcl-2^{Tg}: 200 base pairs

Bcl-2^{+}: no band

2.3 B cell isolation

Naïve, splenic B lymphocytes were isolated from mice at 6-12 weeks of age. One mouse per genotype was used for each time-series experiment, and two for each filming experiment. Whole spleens were mashed through a 70 μM strainer to form a single cell suspension and centrifuged to remove the supernatant. Cells were treated with 5 mL red blood cell lysis buffer (WEHI media kitchen), layered on top of 1 mL foetal calf serum (FCS), and centrifuged to remove buffer. Remaining leukocytes were rinsed with wash buffer (RPMI 5% FCS), then dispensed on top of a discontinuous percoll density gradient (50%:65%:80%, see Appendix II). Cells were separated across this density gradient with a 20-minute spin at 1400 g, with centrifuge brakes off. Small, dense cells were collected from the 65%:80% interface and washed. B cells were enriched using magnetic activated cell sorting (MACS), following protocol with a negative selection kit (Miltenyi Biotec) with cells suspended in MACS buffer (see Appendix I). B cell purity was verified by fluorescence activated cell sorting (FACS) to be >98% B220+ and CD19+.

2.4 Labelling with division tracking dye

Purified, unstimulated B cells were labelled with division tracking dye immediately prior to culture (**Figure 2.1**). CellTrace Violet (CTV) stock was prepared at 5 mM in dimethyl sulfoxide (DMSO), then diluted 1/10 in PBS with bovine serum albumin (PBS/0.1%BSA) for a 500 µM working concentration. Dye was added at 15 µL to each mL of PBS/0.1%BSA, with cells suspended at 10^7 per mL, for a final CTV concentration of 7.5 µM. The cell suspension was mixed immediately and thoroughly, and incubated in a 37°C water bath for 20 minutes, with agitation at 5-minute intervals. Reaction was stopped with the addition of ice-cold Advanced B cell medium (AdvBCM, see Appendix I) to top up to 10mL (approx. 10x staining volume). CTV labelled cells were washed with AdvBCM once more before being used in assays as described below.

2.5 B cell activation and culture for time-series experiments

Purified naïve resting B cells were stimulated in a T cell dependent manner to induce differentiation to ASC, using an anti-CD40 (αCD40) agonistic monoclonal antibody (1C10) and recombinant mouse IL-4 (see Appendix II). Recombinant mouse IL-5 was included for enhanced differentiation where stated for the relevant experiments.

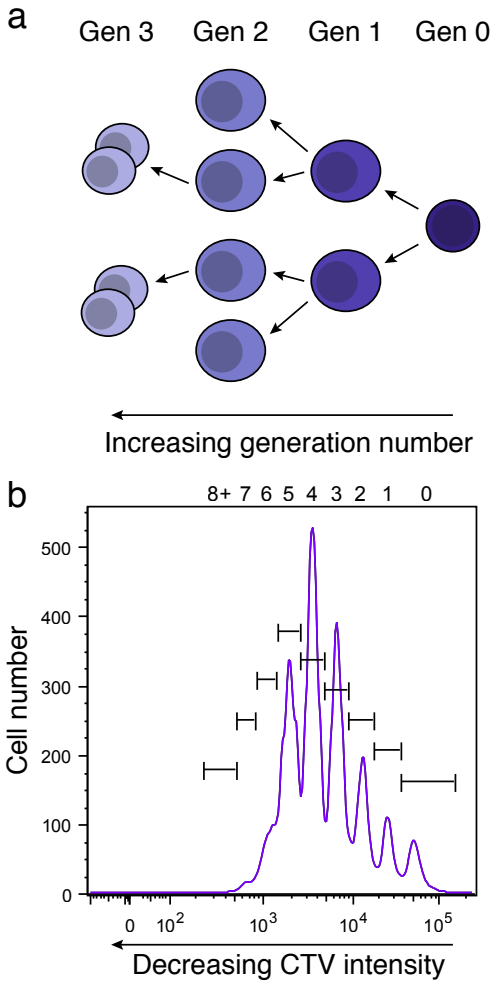

Isolated, CTV labelled B cells were cultured for time-series experiments at 10^4 cells per well in 200 µL AdvBCM using 96 well flat-bottomed plates. Multiple identical plates were prepared on 'day 0' and cells were cultured undisturbed until flow cytometric analysis, where one plate was used for each time point.

For imaging and cell cycle inhibition experiments, cells were cultured at 10^6 cells/mL in 5 mL wells using multiple 6 well plates and the appropriate stimuli. After 3-4 days, cells harvested from the same condition were pooled, washed out of

Figure 2.1: Use of CellTrace Violet as a division tracking dye.

(a) CellTrace Violet (CTV) is a fluorescent labelling dye that separates equally between daughter cells when lymphocytes divide. **(b)** It therefore makes an effective division tracking dye, as labelled cells halve their fluorescence values with every round of mitosis, allowing accurate identification of cell generation number based on fluorescence intensity. [94]

existing media, treated as indicated, then re-cultured in 200 µL wells using fresh media with fresh stimuli.

All cells were incubated at 37°C with 5% CO_2 and humidity control.

2.6 Surface marker labelling for flow cytometry

Immunoglobulin isotype switching was detected by cell surface-labelling for IgG_1, the primary isotype driven by IL-4 stimulation. Some experiments were conducted in the absence of a Blimp-1-GFP reporter mouse, and so Syndecan-1 labelling was used as an indicator of differentiation to ASC.

For phenotyping of time-series experiments, triplicate wells were harvested into 96 well V-bottom plates, and washed twice with FACS buffer (Appendix I). The media was flicked off, then 50 µL of FACS buffer added containing fluorochrome-conjugated antibodies at the appropriate dilutions (see Appendix III). Cells were incubated on ice for 20 minutes, washed twice with 200 µL FACS buffer, then resuspended in 100 µL FACS buffer for flow cytometry. Cells labelled with biotin-conjugated antibodies were labelled again with a secondary streptavidin-fluorochrome conjugate using the same steps.

For checking cell purity after B cell isolation, 20 µL of cells collected after MACS enrichment was added to 50 µL of FACS buffer containing anti-B220, anti-CD19, anti-IgM, and anti-IgD (Appendix III), and processed as above.

For sorting and subsequent re-culture, cells were labelled in 1 mL PBS/0.1%BSA with anti-IgG_1-APC (1/500). Cells were incubated for 20 minutes at 4°C, then washed twice with 10 mL PBS/0.1%BSA.

2.7 Determining cell numbers in proliferation assays

Cell numbers in each well of culture were calculated with the addition of a known number of beads to the 200 µL cultures immediately prior to flow cytometric analysis.

A mix of Flow Check Rhodamine Low-Brite Beads (Polysciences) and propidium iodide (PI) was prepared such that 5,000 beads would be added to each well in 10 µL of FACS buffer, with PI (0.5 µM final) for dead cell exclusion. On the flow cytometer, these beads are lower in forward-scatter (FSC) and higher in side-scatter (SSC) compared with lymphocytes, and fluoresce brightly in the violet (405 nm) 450/50 nm channel. These beads were later replaced with Sphero Rainbow Calibration particles (6 peaks, BD Biosciences), which were used in exactly the same way, although they were fluorescent in every channel.

Total cell numbers in each well was calculated using the following equation:

$$\textit{Total cell number} = \frac{\textit{number of acquired cells}}{\textit{number of acquired beads}} \times \textit{number of beads added}$$

Number of cells in each generation were calculated after determining the proportion (or number) of cells in each peak on a histogram of CTV fluorescence values (**Figure 2.1**).

2.8 Flow cytometry

Flow cytometric data was acquired on a Becton Dickinson (BD) FACS Canto II or BD Fortessa X20 (see Appendix III for detector configurations) using native BD Diva software. Data was exported for further analysis with FlowJo (TreeStar), where populations of interest could be gated for study. Beads were gated on size and fluorescence. Cells were gated on size (FSC vs SSC), live cells (low PI), single cells (FSC height vs FSC area), and then examined using the appropriate fluorescence channels.

For cell cycle inhibitor-treated cells (Chapter 5), autofluorescence tended to increase over time, particularly at around the 500 nm range. This interfered with the standard binary gating of GFP+ and GFP- cells, so an alternative gating strategy was devised using a polygonal gate on GFP vs SSC (**Figure 2.2**). The correlation between signals in the GFP and SSC channels of live, wild-type cells was used to determine the boundary between GFP -positive and -negative cells.

Numbers or proportions of cells in the gates of interest were exported from FlowJo and transferred to Excel (Microsoft) or Prism (GraphPad) for quantitative analyses.

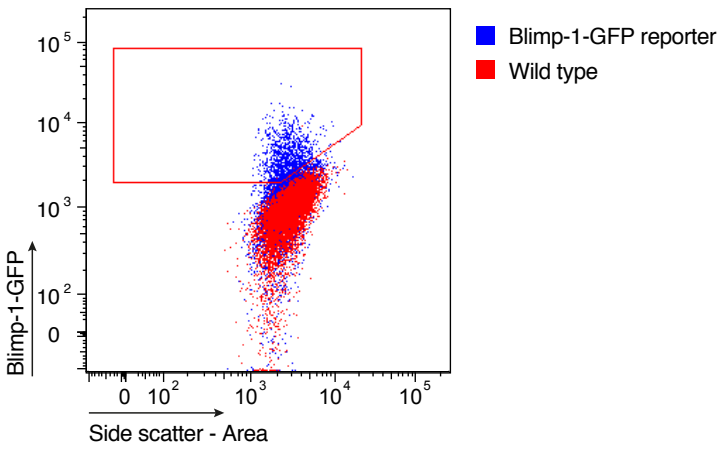

Figure 2.2: GFP+ gating for cell-cycle inhibited cells

Cells experiencing prolonged exposure (~24+ h) to cell cycle inhibitors increased in autofluorescence, particularly at around the 500 nm range, and hence interfered with standard GFP gating. Hence, a different strategy was used where GFP was gated against SSC; using inhibitor-treated wild type cells to set the GFP- gate.

2.9 Cell sorting

For sorting to isolate or exclude specific populations of cells, 5mL cultures of cells were harvested, pooled, and washed in PBS/0.1%BSA, before suspension in 1mL PBS/0.1%BSA. Where specified, cells were also labelled with IgG_1-APC as described above. Cells were then washed and resuspended at 10^7 cells/mL. The cell suspensions were pipetted carefully to disperse any clumps, and filtered through a 35μM mesh into pre-wet tubes to ensure a single cell suspension. PI was added (0.5 μM final) for dead cell exclusion. Cell sorting was conducted on a BD FACS Aria with the assistance of WEHI technical staff. Sorted samples were collected into sterile 5mL tubes containing 1mL of 50% FCS and 50% AdvBCM. Cells were then washed twice in AdvBCM (or AdvBCM-F - phenol-red-free base media if used for filming), counted, and re-cultured with stimuli as before.

2.10 Chamber slide preparation

For time-lapse imaging, cells were placed into chamber slides lined with a microgrid array of cell 'paddocks' to prevent aggregation.

Due to the extended duration of cell culture during live cell imaging, only the centre four chambers of 8-well slides (Ibidi μ-Slide 8 well, cat#80826) were used to ensure equal evaporation from all conditions. For experiments requiring more than four conditions (Chapter 4), an adapter was constructed in-house to allow the microscopy stage to hold more than one chamber slide. Unused wells were filled with standard AdvBCM as a buffer for humidity, and as a visual readout of pH, indicating CO_2 availability.

Microscopy chambers were each lined with an inert polydimethylsiloxane (PDMS) grid, imprinted with a 64 x 64 array of 50 μm square 'paddocks' (Microsurfaces MGA-050-02). Chambers were sterilized with filtered pure ethanol and 20 minutes of exposure to UV light in a sterile environment (class II biosafety cabinet), then left to dry completely. The drying step was essential to prevent the grids from lifting off the bottom during the next steps; 30 minutes in a 37°C incubator would help with this process (excess ethanol removed, lid on).

The PDMS microgrids were hydrophobic, and with 50 μm indents, excelled at catching rogue air bubbles if media is not introduced properly. Hence, dried chambers were carefully wet with a second round of ethanol (approximately 100 μL), excess run-off removed, and the chamber slowly filled with 250 μL of AdvBCM-F. Chambers and grids were slowly washed ten times with AdvBCM-F, ensuring the grids do not dry between washes. Chambers were then filled with 250 μL media (AdvBCM-F for filming or AdvBCM for unused chambers) and placed in a 37°C incubator overnight for any remaining bubbles to dissolve.

Prior to imaging, chambers and PDMS grids were exposed to 470 nm light emitting diodes (LEDs) (custom made) for at least 30 minutes, to photobleach the polymer and reduce autofluorescence in the GFP channel. Cells were subsequently added by removing existing media, and replacing with 250 µL AdvBCM-F containing $5x10^4$ cells/mL and the relevant stimuli. This density maximises the availability of paddocks seeded with only a single cell.

2.11 Microscopy

Images used in Chapter 3 were acquired on a Zeiss Axiovert 200M inverted widefield fluorescence microscope, fitted with a Zeiss Plan-Apochromat 20x objective (numerical aperture 0.8). Images in the bright field and GFP channels were acquired with a Zeiss AxioCam MRm (1.4 megapixels) camera, mounted in the light path coupled to a 0.63x C-mount. Image acquisition was automated using Zeiss AxioVision software, covering 141 positions across three conditions at 15-minute intervals. 360 time points were covered over 89.75 hours.

Microscopy images used in Chapter 4 were acquired on a Zeiss Axio Observer.Z1 after a system upgrade. This setup was equipped with a PCO.edge scientific complementary metal-oxide-semiconductor (CMOS) camera with greater resolution than previously available. A 10x objective lens was used to tile the nine conditions with 108 positions at 6-minute intervals. 619 frames were imaged over 61.8 hours. Image acquisition was automated using Zen 2 (Blue Edition) software to control the motorised stage.

Images were acquired in the GFP channel using a filter block with 500/20nm bandpass (BP) for excitation, 515 nm farb teiler (FT) beam splitter, and 535/20 BP filter for emission. Fluorophores were excited using 470 nm excitation from a Colibri Light-Emitting Diode (LED) system. Transmission images were also acquired for every position and time point.

Either microscopy system was equipped with an environmental control chamber, regulating temperature (37°C), CO_2 (5%), and humidity.

2.12 Image processing

Raw microscopy images were processed prior to scoring cell fates, using established methods [128]. Images acquired in the GFP channel were corrected for uneven illumination of the microscopy stage, thresholded for fluorescence over background, binarized, and noise corrected. Individual wells were cropped from images of the entire position, and time-lapse images compiled for side-by-side review in the bright field, raw GFP, processed GFP, and overlaid channels.

Images for Chapter 3 were processed by John Markham, and for Chapter 4 by Andrey Kan using established methods [128]. The processing methods run automatically off custom code, and threshold values computed using a formula relative to the pixel intensities across the entire image. ie. threshold level should be insensitive to fluctuations in background fluorescence values.

2.13 Image analysis

Time-lapse images were loaded into VirtualDub (GNU General Public License) or Quicktime (Apple) for review and frame-by-frame inspection. Cell paddocks containing single, undifferentiated cells were identified, and those that divided once were followed to record the fates of their offspring. Frame numbers were recorded for the following events: first observed mitosis, differentiation, death, or second observed mitosis. Fates of undivided, generation 0 cells were also followed in Chapter 4.

Bright field images were used to manually track and follow individual cells based on their location, size, granularity, morphology and trajectory; and using these properties, identify cell division and death. Cell division was recorded as the first frame in which the cell membrane is observed to contract during cytokinesis, resulting in cleavage of the two new cells in subsequent frames. Cell death was regarded as the first frame in which membrane blebbing occurred, causing cell edges to lose definition accompanied by a sharp increase in cell granularity or disturbance of transmitted light. Differentiation to ASC was recorded as the first frame in which the binarized image for GFP produced positive pixels, and positive pixels remained present in at least two subsequent frames. Raw GFP images were used to validate stray pixels due to noise, or the slow accumulation of GFP signal within the cell. Once producing GFP, this additional signal could also be used to aid in distinguishing sister cells.

Frame numbers were converted to times for further analyses.

2.14 Model fitting

Times to cell fates were transferred into Prism (GraphPad), where Kaplan-Meier (KM) survival estimates were plotted as a means of untangling competition between cell fates. Division was regarded as being censored by death, death by division, and differentiation to ASC was censored by both. Lost cells and cells that survived until the end of the experiments were also included as censoring events. Resulting curves depict events of interest as a fraction of the remaining population, while censoring events in cells where the event of interest becomes no longer observable are represented as check marks, indicating subjects that leave the cohort.

For model fitting in Chapter 4, log-normal cumulative distribution functions (CDFs) were fitted to KM survival estimates using the least sum of squared differences. Excel's 'solver' tool was used to find mean (μ), standard deviation (σ), and propensity (p) values which would

produce a lognormal CDF that most closely resembles the KM data, and hence generate the lowest possible value for sum of squared differences. Free fits were conducted with three parameters (μ, σ, p) per condition, while constrained fits were conducted by implementing equivalent parameters across conditions and minimizing the sum of squared differences over multiple conditions. The propensity for death is constrained as 1, given that all cells will eventually die. Censoring events after the last event of interest was excluded from the fitting, as any remaining plateau skews the fit with disproportionate weighting.

Pearson's rho was used to calculate the correlation in times to intercellular concordant and intracellular fate outcomes. For empirical data, 95% CI were calculated using Fisher's z' transformation and obtaining the standard error of z'. For calculating the expected levels of intracellular fate correlations that would arise from the fitted parametric model (Chapter 3), a bootstrapping method was used to sample events and calculate the mean and 95% CI. For this method, uncensored distributions from the parametric fitting were used to randomly sample independent differentiation and division or death times for hypothetical populations of cells. To do this, Matlab's random(lognormal,μ,σ) function was used to generate a list for each fate outcome, and the values randomly paired between fates. The sample size was the sum of division and death events observed in the condition being tested. For bootstrapped 'cells', each given a differentiation and division or death time, events were discarded where differentiation times were longer than the assigned division or death time; as these cells would not have been observed to differentiate. Pearson's correlations were calculated between differentiation and either division or death from 1000 iterations of these samples, the mean was plotted as the modelled expectation, and the values at the 2.5% and 97.5% percentiles used to assign the 95% CI.

2.15 Cell cycle inhibition

Cell cycle inhibitors were used to prevent division, thus removing it as a censoring factor to directly observe differentiation to ASC. Various inhibitors were acquired as powders and dissolved as suggested in the product specification sheets (see Appendix IV).

Cell cycle inhibition was generally commenced three days after stimulation, once divided cells are distributed across a number of generations and have the opportunity to undergo division-linked differentiation. These cells were harvested from 5 mL cultures, pooled, and re-cultured in 200 μL wells with fresh stimuli and the appropriate concentrations of cell cycle inhibitors.

2.16 AlamarBlue assay

For large scale screening of cell cycle inhibitor efficacy, alamarBlue (AbD Serotec) was used to measure metabolism as an indication of proliferation. Inhibitor-treated cells were cultured with stimuli for 33 hours at 10^4 cells per 100 µL well, before 10 µL of alamarBlue was added and the mix incubated for a further 10 hours until a colour gradient was visible across the 96 well plates (blue → pink in wells with highest metabolic activity). Fluorescence values were measured on a Hidex Chameleon plate reader (560nm excitation / 590nm emission), where a large number of cells (and hence increased metabolites) produce a high fluorescence readout. Relative fluorescence values were calculated with:

$$\frac{\text{Sample fluorescence} - \text{average fluorescence with no cells}}{\text{Average fluorescence with no drug} - \text{average fluorescence with no cells}}$$

Control wells containing no cells, untreated cells, or cells treated with Etoposide were measured from the same plate.

2.17 ELISpot assay

Enzyme-linked immunospot assays were conducted to test Blimp-1-GFP+ cells for antibody secretion. Plates were first coated overnight with primary capture antibodies for mouse Ig (goat anti-mouse Ig-unlabelled, 1/500; Southern Biotech) in coating solution (pH 9.1 carbonate buffer: 500 mL distilled H_2O, 0.36g Na_2CO_3, 0.95g $NaHCO_3$). RPMI 10% FCS was used to block non-specific binding for 1 hour at 37°C. Cells were counted and a dilution of known cell numbers were prepared in a separate 96 well plate. ELISpot plate was washed three times with RPMI, and 100 µL of cell suspension transferred into wells at diluting densities. Plates were left undisturbed in an incubator for 4-5 hours at 37°C, 5% CO_2 for the capture of secreted antibodies. Cells were washed out using three rinses each of RPMI, PBS-0.05% Tween-20, PBS, then water. Secondary antibody anti-Kappa-biotin (goat anti-mouse kappa-biotin, 1/1000; Southern Biotech) was added in 100 µL of PBS/0.1% BSA and incubated overnight at 4°C. Plates were washed 3x with PBS-0.05% Tween-20. 100 µL of streptavidin-alkaline phosphatase was added to each well (1/1000), and incubated at room temperature for 1 hour. Plates were washed 4x with PBS-Tween, rinsed 2x with PBS, and 100 µL of BCIP/NBT (Mabtech, diluted ½) added for the substrate reaction. Spots would develop within 2-7 minutes, at which point plates were rinsed thoroughly with tap water to stop the reaction. Plates were dried overnight, then spots measured and counted on an AID ELISpot reader. The number of counted spots as a proportion of known cells added generates the proportion secreting.

CHAPTER 3

The Quantitative Impacts of CD40 on Multiple B cell Fates

3.1 Introduction

This chapter includes the publication 'Stochastically timed competition between division and differentiation fates regulates the transition from B lymphoblast to plasma cell', where the relationship between division, death, and differentiation times in response to different levels of CD40 stimulation were explored.

Higher levels of CD40 stimulation is associated with a larger B cell response, more antibody isotype switching and somatic hypermutation, and the eventual formation of a large number of antibody secreting plasma cells [138]. Despite this requirement of strong CD40 stimulation for producing large numbers of antibody-secreting cells (ASCs), weak CD40 stimulation has been observed to produce a larger *proportion* of antibody-secreting plasmablasts [70], after accounting for generation-linked differentiation.

The Cyton model of competing cell fates may shed some light on how this counterintuitive result can be achieved. The framework of independent, stochastic, and competing cell fates posits several hypotheses that could be studied in a systematic way (Figure 3.1). Low CD40 stimulation may:

1) Increase the proportion of cells with the capacity to become antibody secreting (increased propensity);

2) Shorten the time required for cells to become antibody secreting within each cell cycle, such that more cells differentiate before they divide or die (decrease mean times, with or without affecting the variance);

3) Delay times required to divide (increase mean times, with or without affecting variance), while differentiation times and probabilities remain consistent, such that more cells reach their differentiation outcome before the next mitotic event obstructs the differentiation time from being observed;

4) Or affect some combination of the above parameters.

Following the publication presented here, some further findings relevant to this chapter are included.

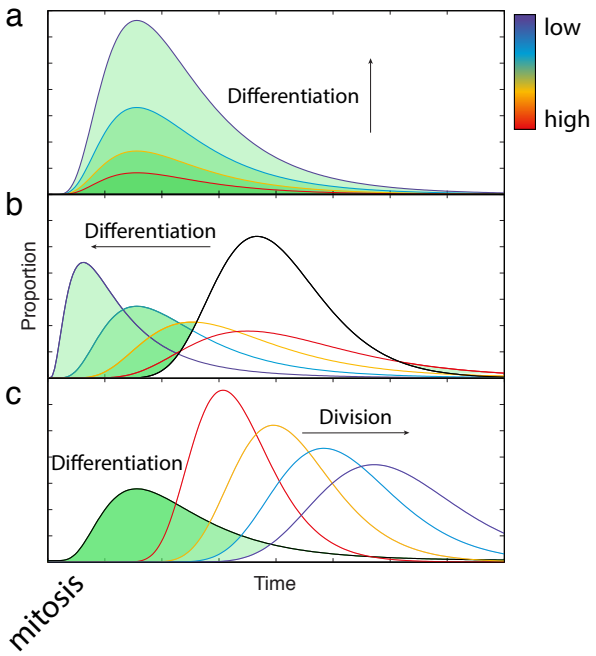

Figure 3.1: Hypothesis for differentiation controlled by CD40 stimulation.

Probability distribution functions illustrating the likelihood of undergoing differentiation to ASC (shaded green) or division (unshaded) over time, in the presence of competing cell fates. Low CD40 stimulation may **a)** increase the proportion of cells capable of undergoing differentiation (increase amplitude); **b)** shorten the time required for cells to differentiate (decrease mean, with or without changing the variance) such that more cells differentiate before they divide; or **c)** extend division times (increase mean with or without changing variance), giving more cells time to differentiate before they divide.

frontiers in Immunology

ORIGINAL RESEARCH
published: 10 September 2018
doi: 10.3389/fimmu.2018.02053

Stochastically Timed Competition Between Division and Differentiation Fates Regulates the Transition From B Lymphoblast to Plasma Cell

Jie H. S. Zhou[1,2], *John F. Markham*[1,3†], *Ken R. Duffy*[4‡] *and Philip D. Hodgkin*[1,2*‡]

[1] Immunology Division, The Walter and Eliza Hall Institute of Medical Research, Parkville, VIC, Australia, [2] Department of Medical Biology, The University of Melbourne, Parkville, VIC, Australia, [3] Victoria Research Laboratory, National ICT Australia, The University of Melbourne, Parkville, VIC, Australia, [4] Hamilton Institute, Maynooth University, Maynooth, Ireland

OPEN ACCESS

Edited by:
Benny Chain,
University College London,
United Kingdom

Reviewed by:
Kai-Michael Toellner,
University of Birmingham,
United Kingdom
Yi Hao,
Huazhong University of Science and Technology, China

***Correspondence:**
Philip D. Hodgkin
hodgkin@wehi.edu.au

†Present Address:
John F. Markham,
Peter MacCallum Cancer Centre,
Parkville, VIC, Australia

‡These authors have contributed equally to this work

Specialty section:
This article was submitted to B Cell Biology, a section of the journal Frontiers in Immunology

Received: 30 May 2018
Accepted: 20 August 2018
Published: 10 September 2018

Citation:
Zhou JHS, Markham JF, Duffy KR and Hodgkin PD (2018) Stochastically Timed Competition Between Division and Differentiation Fates Regulates the Transition From B Lymphoblast to Plasma Cell. Front. Immunol. 9:2053. doi: 10.3389/fimmu.2018.02053

In response to external stimuli, naïve B cells proliferate and take on a range of fates important for immunity. How their fate is determined is a topic of much recent research, with candidates including asymmetric cell division, lineage priming, stochastic assignment, and microenvironment instruction. Here we manipulate the generation of plasmablasts from B lymphocytes *in vitro* by varying CD40 stimulation strength to determine its influence on potential sources of fate control. Using long-term live cell imaging, we directly measure times to differentiate, divide, and die of hundreds of pairs of sibling cells. These data reveal that while the allocation of fates is significantly altered by signal strength, the proportion of siblings identified with asymmetric fates is unchanged. In contrast, we find that plasmablast generation is enhanced by slowing times to divide, which is consistent with a hypothesis of competing timed stochastic fate outcomes. We conclude that this mechanistically simple source of alternative fate regulation is important, and that useful quantitative models of signal integration can be developed based on its principles.

Keywords: B cells, anti-CD40 stimulation titration, fate regulation, lineage priming, competing stochastic timers

INTRODUCTION

Increased understanding of the regulation of cell differentiation, division and death is crucial in many fields of biology (1–5). While population-level consistency in the proportion of cells taking on distinct fates has long-since been observed, advancing technologies that enable direct observations of individual cells and their lineages reveal significant heterogeneity (6–14). In order to manipulate population-level fate allocation, determining the primary drivers of this cell-level heterogeneity is an essential precursor to designing interventions, and so the search for the sources of heterogeneity has been a topic of much recent research.

B lymphocytes are an essential component of the immune response and provide a useful model for assessing methods of fate control. During activation, they integrate signals from multiple sources that modify the resulting cell response by altering lifespan, the type of antibody made, the speed of cell proliferation, and the rate of development into antibody secreting plasma cells (15).

T cells provide one important source of signals that influence the B cell (16, 17). During an immune response, antigen captured by the B cell is presented to reactive T cells that are, in turn, induced to express CD40L on their surface. This ligand engages the constitutively expressed receptor CD40 found on the B cell surface. CD40 stimulation alone can activate and promote B cell proliferation, but its impact is amplified by T cell derived cytokines, such as IL-4 and IL-5, that further shape fate changes including isotype switching and the rate of development into Antibody Secreting Cells (ASCs) (18). Importantly for quantitative studies, a CD40 agonist and cytokines can replace the T cell, making it an excellent model system for studying the impact of variations in signals on fate outcomes *in vitro*.

Activated lymphocytes vary in the times they take to divide and, in culture, are usually found spread across multiple generations. Notwithstanding that, numerous studies report that the greater the number of divisions cells have experienced, the more likely they are to have undergone a change, regardless of time from stimulation. For example, isotype switching is linked to division, and is influenced by the concentration of switch-inducing cytokines (19–21). Similarly, the development into ASC also has been reported to be promoted by progressive passage through division cycles, and this likelihood, in turn, is modulated by the concentration of cytokine delivered signals (18, 22). These studies proposed that alternative division-linked cell changes, such as switching and development to ASC, could arise as the combination of a series of independent fate decisions underway in each cell (18, 20, 23–25).

This hypothesis of independent fate competition was evaluated and extended upon by Duffy et al. (26), by assessing data taken from experiments where individual B cells that had undergone given numbers of divisions, as determined by CTV staining, were sorted by flow cytometry and subsequently followed with long-term imaging. Once these cells were observed to divide, their sibling offspring were examined with times to divide, to die, to differentiate to ASC, and to antibody isotype-switch from last mitosis recorded. Probabilistic analysis established that the complex array of heterogeneous fate outcomes and times to fates were consistent with a simple hypothesis where, within each single cell, times to each fate (isotype switching, differentiation, death, and division) were selected independently from a probability distribution and behaved in competition with each other, such that short times to fate censor later fate outcomes (26). Sibling fates, however, had significantly greater commonality than unrelated cells of the same generation, indicating a substantial element of familial lineage priming.

As external regulators are known to influence the proportions of cells assuming fates at a population level, we reasoned that investigation of their impact at the single cell level would provide additional discriminating insight. Here we examine the cell-level impact of changing CD40 stimulation strength on ASC development. This analysis suggests that CD40 has no direct impact on differentiation rate or asymmetric fate changes, but exerts its influence by altering the time to divide distribution, thereby regulating the proportion of cells that differentiate as the result of alterations to the inherent cellular competition.

MATERIALS AND METHODS

Mice

Blimp-1-GFP reporter mice on a C57BL/6 background (22) were bred and maintained in specific pathogen free conditions at the Walter and Eliza Hall Institute (WEHI) animal facility according to institutional guidelines. All experiments were approved by the WEHI Animal Ethics Committee. Ten-week-old female reporter (Blimp-$1^{+/GFP}$) and wild type (Blimp-$1^{+/+}$) mice were used for the flow cytometry and filming experiments.

Cell Isolation and Labeling

Naïve, resting B cells were isolated from murine spleens using a discrete Percoll (GE Healthcare, cat#17089101) density gradient (50/65/80%, cells collected from 65/80% interface), followed by purification using magnetic beads (negative selection, mouse B cell isolation kit, Miltenyi Biotech cat#130-090-862). Enriched cells were verified to be >98% $B220^+$ and $CD19^+$ by flow cytometry. Cells were labeled with CellTrace Violet (Invitrogen, cat#C34557) at 7.5 μM final concentration, with 10^7 cells/mL in phosphate buffered saline containing 0.1% bovine serum albumin (PBS/0.1%BSA), and incubated in a 37°C water bath for 20 min. Cells were washed twice with cold culture medium prior to culture.

Cell Culture

For flow cytometry and for bulk cultures, cells were cultured in "B cell medium," made from Advanced RPMI 1640 (Gibco cat#12633-012) supplemented with 5% fetal calf serum (Gibco, cat#10099-141, Australian origin), 10 mM HEPES (Gibco, cat#15630-130), 2 mM GlutaMAX (Gibco, cat#35050-061), 10 U/mL penicillin, 100 μg/mL streptomycin (Penicillin/Streptomycin, Gibco, cat#15140-148), and 50 μM 2-mercaptoethanol (2-ME, Sigma-Aldrich, cat#M7522). For filming, cells were cultured in phenol red-free Advanced RPMI 1640 (Gibco custom order) with the same supplements. Imaged cells were stimulated with 1,000 U/mL IL-4 (WEHI), and 10, 2.5, or 0.625 μg/mL anti-CD40 antibody (1C10, WEHI Antibody Facility), and incubated at 37°C with 5% CO_2. Differentiation promoting effects of IL-4 were saturating at concentrations above 316 U/ml [(18) and data not shown].

Flow Cytometry

For flow cytometry experiments, 200 μL wells containing 10^4 cells were cultured in triplicates across 96 well flat-bottomed plates. Blimp-$1^{+/GFP}$ and wild type cells stimulated with IL-4 and 10, 2.5, or 0.625 μg/mL of anti-CD40 antibody, or IL-4 alone were harvested periodically for flow cytometry analyses (BD FACSCantoII). Propidium iodide (PI, 0.5 μg/mL final, Sigma cat#287075) for dead cell exclusion and 5,000 beads (Sphero Rainbow Calibration particles [6 peaks] 6.0–6.4 μm, BD Biosciences, cat#556288) for cell counting were added just prior to sample acquisition.

Cell Sorting and Long-Term Live Cell Imaging

For filming, 5 mL cultures (2×10^5 cells/mL) of cells stimulated with IL-4 and 10, 2.5, or 0.625 μg/mL of anti-CD40 antibody were harvested 85 h after stimulation. Cells were labeled for expression of IgG1 (clone X56, BD Pharmingen cat#550874), and sorted (BD FACSAriaIIu), for generation four cells that were undifferentiated (Blimp-1-GFP$^-$) and unswitched (IgG1-APC$^-$), to ensure that cells with a similar starting phenotype were tracked and compared in each CD40 stimulation condition.

Sorted cells were re-cultured in phenol red-free B cell medium with the same stimuli concentrations as prior to the sort, at 5×10^4 cells/mL. For each of the three anti-CD40 conditions, 250 μL of cell suspension was placed into a separate well of a pre-prepared chamber slide (Ibidi, cat#80826) where each well was lined with a polymer imprinted with a microgrid array of cell "paddocks" (Microsurfaces, cat#MGA-050-02) (27). Microgrids were prepared aseptically, rinsed with 100% ethanol for sterilization, then left to dry completely to ensure adherence; before wetting again with ethanol such that B cell medium could be introduced to the hydrophobic grids. Chambers were rinsed 10 times with B cell medium, prior to resting overnight in an incubator to aid the dissolution of any air bubbles. Chambers and polydimethylsiloxane (PDMS) microgrids were exposed to 470 nm LEDs (custom made) for at least 30 min prior to the addition of cells, to photobleach the grids and reduce autofluorescence during imaging. The seeding cell density was determined to yield not more than an average of one cell per paddock for filming.

Microscopy images were acquired using a Zeiss Axiovert 200M widefield inverted microscope, equipped with an incubation chamber (37°C, 5% CO_2, humidifier), plan-apochromat 20x objective (0.8 n.a.), 0.63x c-mount, and a Zeiss AxioCam MRm (1.4 MP) camera. Fluorescence (GFP) and bright field images were acquired for 141 positions, at 15-min intervals, encompassing 7,896 paddocks for the three culture conditions, across 360 time points over the following 89.75 h. The remainder of the sorted cells were placed into triplicate or duplicate cultures in 96-well plates for a concurrent flow-cytometry time course of events, and were run twice-daily for the duration of the filming experiment as a parallel control.

Single Cell Fates Were Manually Tracked With Visual Cues and Fluorescence Thresholding

For consistent tracking of imaged cells, fluorescence images were first processed using the pipeline reported by Duffy et al. (26). All images from the GFP channel were corrected for uneven illumination of the microscopy stage, thresholded for fluorescence, and binarized to produce an objective indicator of GFP positivity. The image processing method is automatic, and threshold values were computed relative to background illumination using intensity histograms for each image. Resultant images were cropped into individual paddocks, and the processed GFP, unthresholded GFP, and bright field images with GFP overlay for each paddock were concatenated for ease of viewing and stacked into time-lapse films.

Paddocks with individual, undifferentiated cells were identified, and those observed to divide were followed to record the fates of paired offspring. Bright field images were used to manually track cells using their location, size, shape, granularity and trajectory. These properties allowed for the reliable identification of division, as well as death. Shortly before division, cells appeared to lose adhesion and formed large spheres, before cleaving into two smaller cells that do not immediately produce pseudopodia. For death, cells sharply increased in granularity and the circumference of the membrane appeared ruffled, likely due to blebbing, several frames before cell fragmentation was observed, or the membrane perforated and the cell swelled from osmotic intake. This first change in texture was recorded as the cell death time.

For identifying differentiation to ASC, thresholded and binarized images in the GFP channel were followed as a reporter for Blimp-1 expression. Dim light settings are required for extended imaging to avoid phototoxicity, hence chosen voltage and exposure settings also allowed some noise to be detected above the low threshold, from the autofluorescence of the cells and grids. Consequently, differentiation times were only recorded when the cell's fluorescence remained above threshold for three or more consecutive frames (45 min), and then did not disappear for more than one frame at a time; GFP expression would later brighten and cover a larger area. Unthresholded images from the GFP channel were referenced for noise exclusion, and also used for cell identification and tracking based on differentiation status and level of fluorescence.

Sister cells fates were tracked until they either divided again or died. Some cells survived until the end of filming, or were lost due to falling out of focus, migration away from their paddock, or failure to maintain cell ID—these times were also recorded. Homotypic adhesion prevented the tracking of four or more cells using this experimental design.

Statistical Analysis

Data was processed in Matlab 2017b by custom software utilizing in-built functionality. Pearson's correlation coefficient was evaluated using `corr`, and the reported confidence intervals (CIs) were determined by Fisher's Transformation. We used Yule's Q, a traditional measure of association between pairs of variables, to quantify association between division and death or differentiation and no differentiation. Its asymmetric CIs were determined from a normal approximation to errors in the logarithm of the Odds Ratio. Non-parametric survival function (i.e., Kaplan-Meier) estimates were made using the censoring option of the in-built function `ecdf`.

Parametric Model Fitting Procedure

Custom software utilizing the Optimization Toolbox in Matlab 2017b was used for model fitting. The uncensored distributions were assumed to lie in the class of log-normal distributions. For all stimulation conditions, there was a single log-normal time to death T_{death} parameterized by a mean μ_{death} and covariance σ^2_{death}. For all stimulation conditions, there was a

probability, p_{diff}, that the differentiation process is active in the cell whereupon it occurs at a log-normally distributed time with parameters μ_{diff} and σ^2_{diff}. If the process was not on, then the differentiation time was set to be $+\infty$. For each of the three concentrations of 1C10 (0.625, 2.5 and 10 μg/mL), labeled j in (1, 2, 3), it was assumed there was a distinct probability, p^j_{div}, that the division process is active in the cell whereupon it occurs at a concentration-dependent log-normally distributed time with parameters μ^j_{div} and $\sigma^{2,j}_{div}$. If division was not active, the time was set to be $+\infty$.

For $\theta = (\mu_{death}, \sigma^2_{death}, p_{diff}, \mu_{diff}, \sigma^2_{diff}, p^1_{div}, \mu^1_{div}, \sigma^{2,1}_{div}, p^2_{div}, \mu^2_{div}, \sigma^{2,2}_{div}, p^3_{div}, \mu^3_{div}, \sigma^{2,3}_{div})$, a function was written that numerically calculates the likelihood of generating a data point $d \in D$ given that parameterization. For example, if a time-lapse frame is taken every h units of time, for a data point $d \in D$ in which a cell in stimulation condition j is observed to differentiate in the frame number f_{diff} and undergo death in the frame number f_{death}, the likelihood of generating that data point d given the model parameterization θ is

$$L(d|\theta) = P(f_{diff} \leq T_{diff}/h < f_{diff} + 1)P(f_{death} \leq T_{death}/h < f_{death} + 1)P(T^j_{div.}/h > f_{death.}),$$

where the cumulative distribution functions were evaluated using Matlab's `logncdf`. For a set D composed of the fates of stochastically independent cells, the likelihood of generating the set is the product of the likelihoods of generating each point in the data

$$L(D|\theta) := \Pi_{d \in D} L(d|\theta).$$

We used Matlab 2017b's Optimization Toolbox function `fmincon` to identify the maximum likelihood model parameters θ that would generate the data:

$$\theta_{MAP} := \text{argsup}_\theta L(D|\theta).$$

As sibling cells have correlated times to fate, they are not independent and so the function given above does not describe their likelihoods. Despite that, assuming symmetry in the joint underlying distribution of times to each fate of siblings, the maximum likelihood marginal parameters are obtained by optimizing over the same objective function given above computed on all data, including siblings.

Reshaped Distributions

Competition and censorship alters the underlying distributions of times to differentiation, division and death into those that are observed. For example, the observed marginal probability density function for division under stimulation condition j is related to the uncensored distributions for division and death through the following equation:

$$dP(T^{obs,j}_{div} \leq t)/dt = dP(T^j_{div} \leq t)/dt P(T_{death} > t)/\int dP(T^j_{div} \leq s)P(T_{death} > s),$$

which differs from the uncensored density of T^j_{div}. Similar expressions hold for $T^{obs,j}_{diff}$ and $T^{obs,j}_{death}$. Rather than perform numerical integrals to evaluate these, a Monte Carlo approach was taken where 10^6 samples were drawn from the uncensored distributions parameterized by θ_{MAP}, censoring rules were applied to the sampled values, and the resulting empirical distribution functions and densities of the observed variables were determined.

RESULTS

Population-Level Generation-Based Rate of Differentiation Is Increased by Weak CD40 Stimulation

To determine the effect of modulating CD40 signal strength, we utilized B cells from Blimp-1-GFP reporter mice to indicate expression of the ASC differentiation program within plasmablasts. In this system, cells expressing GFP secrete Ig at high efficiency (22). Purified resting naïve B cells from reporter mice were labeled with CellTrace Violet (CTV), and equal numbers of cells were placed in culture with varying concentrations of anti-CD40 agonist antibody (clone 1C10) (28) and saturating IL-4 (500 U/mL), and harvested over time (**Figures S1**, **1**). As expected, increasing concentrations of CD40 led to greater cell numbers and increased progression through consecutive generations (**Figures S1A,B**). Furthermore, division-linked effects on ASC development were apparent as a greater proportion of cells produced Blimp-1-GFP in the advanced generations (**Figures 1C,D**), consistent with published findings (18). These data also confirmed the observation of Hawkins et al. (29) that lower CD40 stimulation levels resulted in a greater proportion of ASC per generation when compared to equivalent generations in cultures with high CD40 stimulation (**Figures 1C,D**). An increased rate of differentiation was also measurable in the population as a whole (**Figure 1C**). Thus, modulating CD40 stimulation strength has two distinct effects on the B cell response: high concentrations promote increased proliferation, whilst low concentrations increase the rate of observed differentiation events per generation. To identify the mechanism that alters cell differentiation by changes in stimulation strength, we undertook direct observation by live imaging.

Long-Term Imaging Allocates Fate Assignments for Single Cells

B lymphoblasts stimulated by CpG can be tracked individually through multiple cell generations (30, 31). In contrast, observing differentiation by live imaging following CD40 stimulation is challenging due to homotypic adhesion. The development of cell aggregates restricts tracking of individual progenitor cells for more than one or two generations (30). A new method was introduced in Duffy et al. (32) to circumvent this problem. By harvesting and disaggregating CTV labeled, proliferating B cells after a few days in culture, then seeding sorted, individual cells into microgrids to maintain segregation,

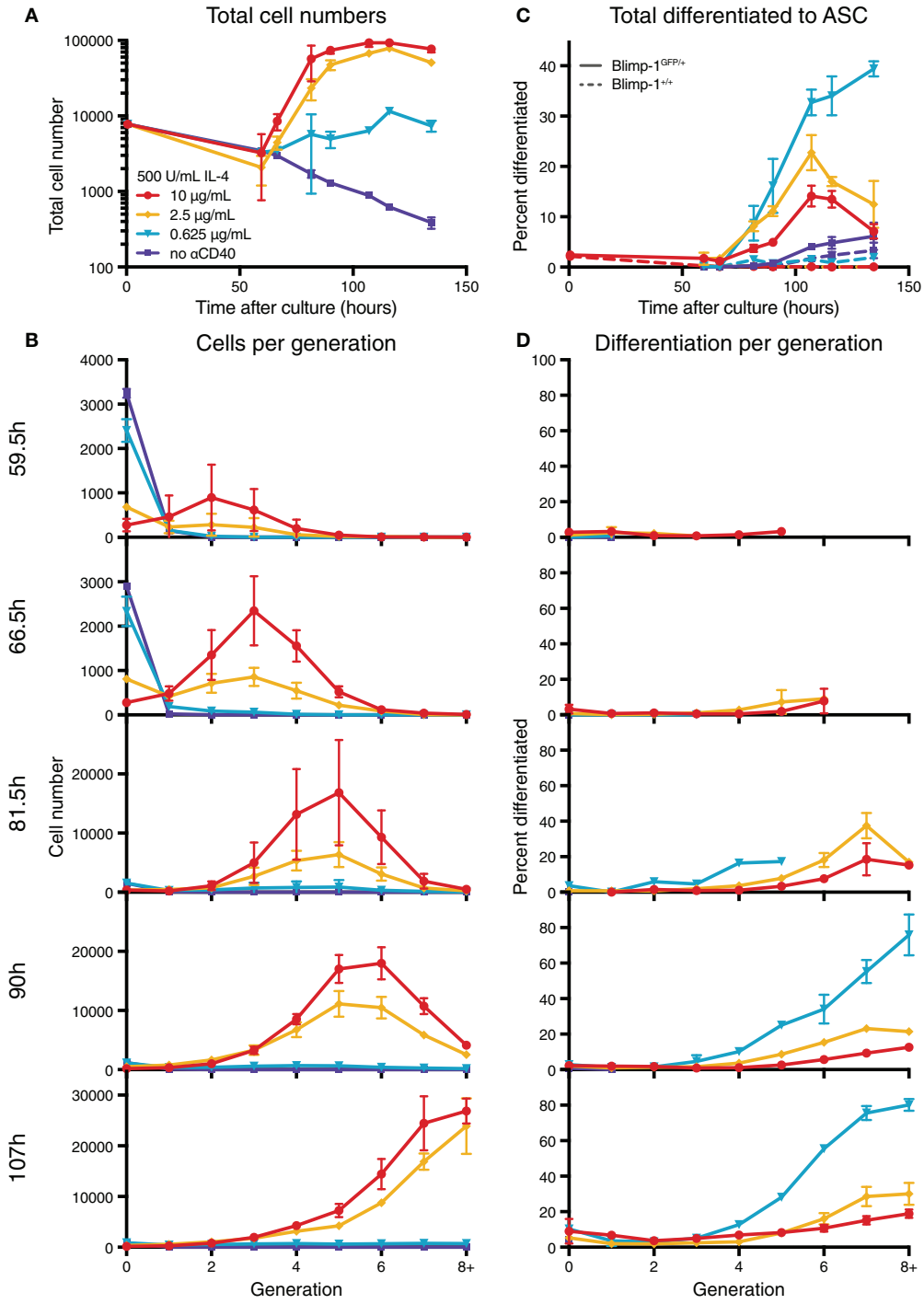

FIGURE 1 | Anti-CD40 concentration alters division and differentiation rates. CTV labeled resting Blimp-$1^{gfp/+}$ B cells were cultured in 500 U/mL IL-4 and 10, 2.5, 0.625, or 0 μg/mL anti-CD40 and harvested over time for flow cytometry analysis. **(A)** Total cell numbers over time. **(B)** Total cells found in each generation. **(C)** The proportion of total viable cells also GFP^+ (ASC). Dashed lines are from equivalent wild-type control cells used to set GFP gates. **(D)** The proportion of cells in each generation that were GFP^+. Data points are mean of triplicate cultures ± SEM, and representative of several repeated titration experiments.

(27) cells from different generations were observed to divide and their progeny followed until their next fate (32). Here we adapted this protocol, illustrated in **Figure 2**, to observe the effect of CD40 stimulation strength changes on differentiation and division times, as well as concordance in sibling fates.

In initial bulk cultures CTV labeled Blimp-1-GFP reporter B cells were incubated with IL-4 and varying concentrations of

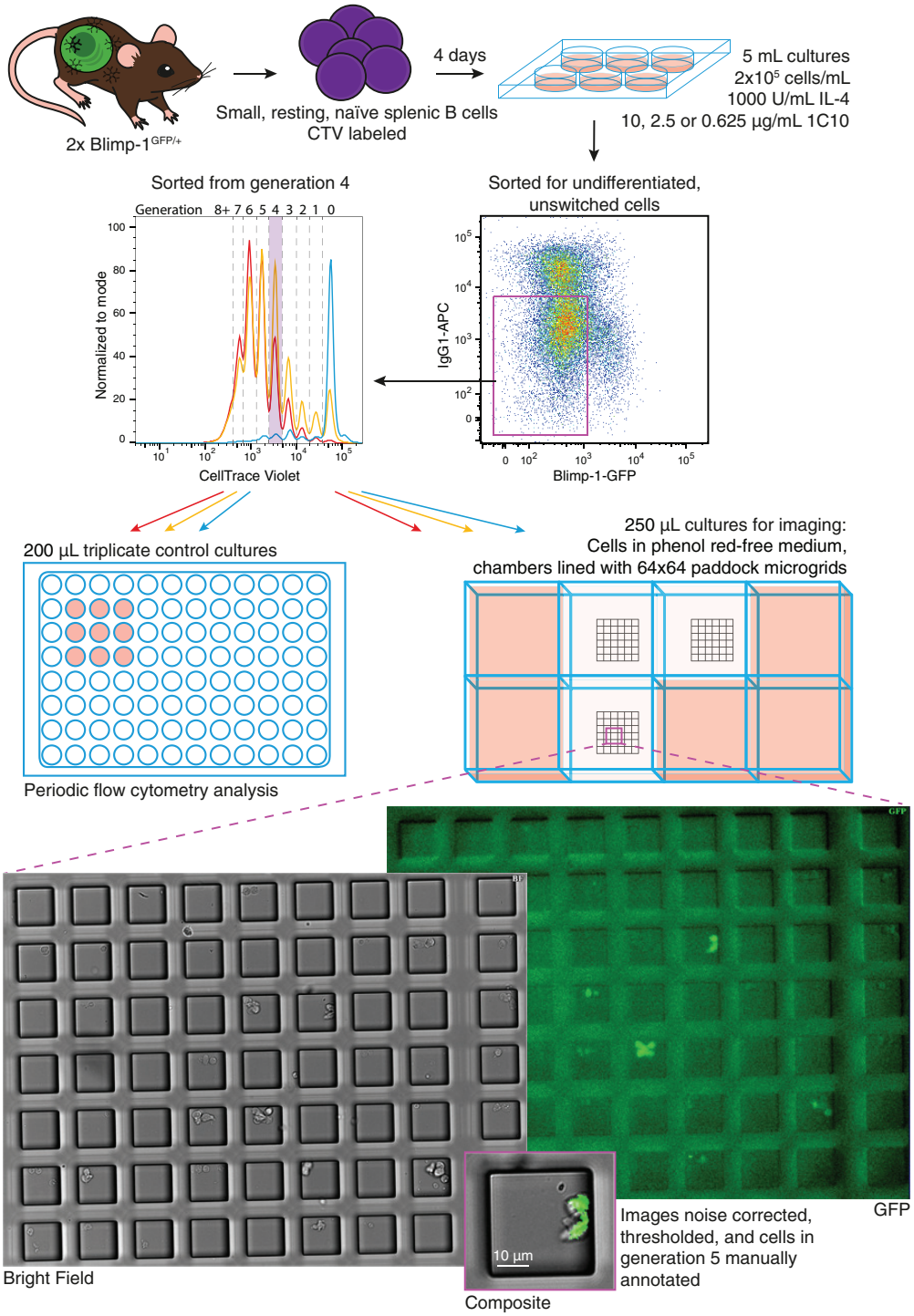

FIGURE 2 | Schematic of live cell imaging experiment. CTV labeled Blimp-$1^{gfp/+}$ B cells were incubated in two stages. Upper panels indicate the initial bulk culture at multiple anti-CD40 concentrations. After 85 h, cells were harvested, labeled with anti-IgG1, and unswitched, GFP^{-} cells identified and sorted from generation 4. Cells were returned to stimulation conditions identical to that prior to sorting, and a portion plated into control cultures for flow cytometry. For microscopy, phenol red-free media was used, and cells from each culture condition were placed into a separate chamber of an imaging slide, each lined with a microgrid of 50 µM cell paddocks. Once settled, the cell density was such that, on average one cell would randomly deposit within one paddock. Media containing pH indicator was placed in surrounding wells to buffer for evaporation and monitor CO^2 availability. Microgrids were tiled and imaged at 15 min intervals for 89.75 h. Acquired bright field and fluorescence images were processed and manually annotated to record cell fate.

anti-CD40 (10, 2.5, 0.625, and 0 μg/ml) for 4 days, resulting in the expected variation in division and differentiation rates (**Figure S1A**). To compare the subsequent fate of undifferentiated cells from the same generation, cells from each culture were sorted by flow cytometry for those in generation 4, and seeded into 250 μL chambers containing microgrids for a further 90 h of live cell imaging (see Materials and Methods). Control cell cultures were prepared in parallel at the same density in 96 well plates, and triplicate 200 μL cultures were analyzed periodically to ensure the overall population response of the sorted cells was consistent (**Figure S2**). Control analyses indicated that sorted cells were GFP^- and in generation 4 at the time they were re-cultured (**Figure S2B**). These cultures also confirmed that cells stimulated with higher concentrations of anti-CD40 divided faster, resulting in greater CTV dye dilution (**Figure S2B**), and higher total cell numbers (**Figure S2C**). Despite the variation in progression through generations, a greater proportion of cells in 2.5 μg/mL anti-CD40 were GFP^+ than in 10 μg/mL (**Figure S2D**). As these proliferation and differentiation features were consistent with earlier studies, manual tracking and analysis of the parallel single cell imaged cultures were undertaken.

Single Cell Data Recapitulated Fate Changes Seen at Population Level

Acquired images were processed and thresholded to facilitate GFP scoring, as described in Methods and illustrated in **Figure 3A**. After initial visual inspection, "paddocks" identified with single cells that undertook their first division as GFP^- cells were selected, and the resulting two siblings followed manually, to record their times to changes in fates (**Figure 3**). For the data presented here, the time of the cell's first division (therefore from generation 4 to 5) is set as time 0, the initiating event time, and the siblings being tracked are in generation 5. The complete annotated data set was converted to such times by calculating the times between the first observed division and subsequent fates (differentiation to ASC, division or death). Histograms of these times are plotted in **Figure 3B**, illustrating the heterogeneity in each outcome.

To visualize differences between culture conditions, observed proportions to undergo each fate are shown in **Figure 4A**, and mean times to reach each fate in **Figure 4B**. These data suggest that cells stimulated with high concentrations of anti-CD40 were more likely to divide and less likely to die (**Figure 4A**), and when they did divide they completed mitosis more quickly (**Figure 4B**) The proportion of cells observed to differentiate is also consistent with flow cytometry time courses, in that a higher proportion of cells differentiated to ASC with lower CD40 stimulation (**Figure 4A**). Thus, despite segregation into cell paddocks by the microgrids, the filmed cells recapitulated the fate outcomes measured by flow cytometry at the population level.

Stimulation Strength Does Not Affect Sibling Correlations or Concordance

Whether stimulation strength affected differentiation by influencing asymmetry in fate was first assessed. For each of the three concentrations (0.625, 2.5, and 10 μg/mL, respectively) 78, 68 and 75% (±8, 9, 8% as 95% CIs) of siblings take the same differentiation or no differentiation and death or division fates. **Figure 4C** plots Yule's Q, a measure of concordance for opposing fates (division vs. death, and differentiation vs. no differentiation) relative to their frequency of occurrence in the population. The consistent, high values of Q indicate the significant concordance found for both division-death and differentiation-no differentiation fates of siblings was not affected by CD40 stimulation strength. Thus, strong sibling concordances and correlations were found in this experiment, in line with earlier findings. Interestingly, these sibling similarities did not appear to be controlled by altered CD40 stimulation strengths, despite the marked changes in division times, and differentiation rates.

Uncensoring Cell Fate Time Distributions

Having eliminated modulation of asymmetric fates as a control feature regulated by anti-CD40 concentration, we turned to the theory of competing fates as a potential driver of heterogeneity. Under this hypothesis, autonomous processes leading to each fate are underway within the cell. The order in which they complete determines the fate that the cell is observed to take. As observed times to fate are heterogeneous, the mathematical framework of probability is necessary to describe them. It encapsulates the heterogeneity irrespective of whether its source is truly stochastic processes within each single cell, or arises as a result of unidentified heterogeneous lineage properties. The hypothesis suggests that the apparently complex correlation structures observed in cell fate data are a consequence of observed times to fate being the product of competition and censorship, and leads one to query the role of external regulation on each of the autonomous processes (26, 32).

Figures 4D,E shows the result of applying the standard non-parametric survival function estimator, the Kaplan-Meier estimator (33), to the raw cumulative frequency data for each fate (**Figure 4D**) to reveal the pre-competition, uncensored time-to-fate distributions (**Figure 4E**), assuming probabilistic independence of these underlying timed mechanisms. For these plots division is assumed to censor death, death censor division, and both division and death censor differentiation. In some instances, the remaining proportion is >0 (i.e., plot does not reach a height of 1), indicating the observation time was too short to capture all possible events in this category; or alternatively that the remaining proportion of cells were incapable of undergoing that fate.

Within this competing timers model, these results are consistent with the hypothesis that CD40 stimulation strength had a significant impact on cell division times with little direct effect on the underlying distributions of times to death or differentiation. Higher levels of anti-CD40 reduces division times, positively impacting the proportion of cells in the population that progress to the next generation, while reducing the proportion of cells that differentiate. Together, these results are consistent with the hypothesis that CD40 stimulation controls the time to divide, but not the times to differentiate or die.

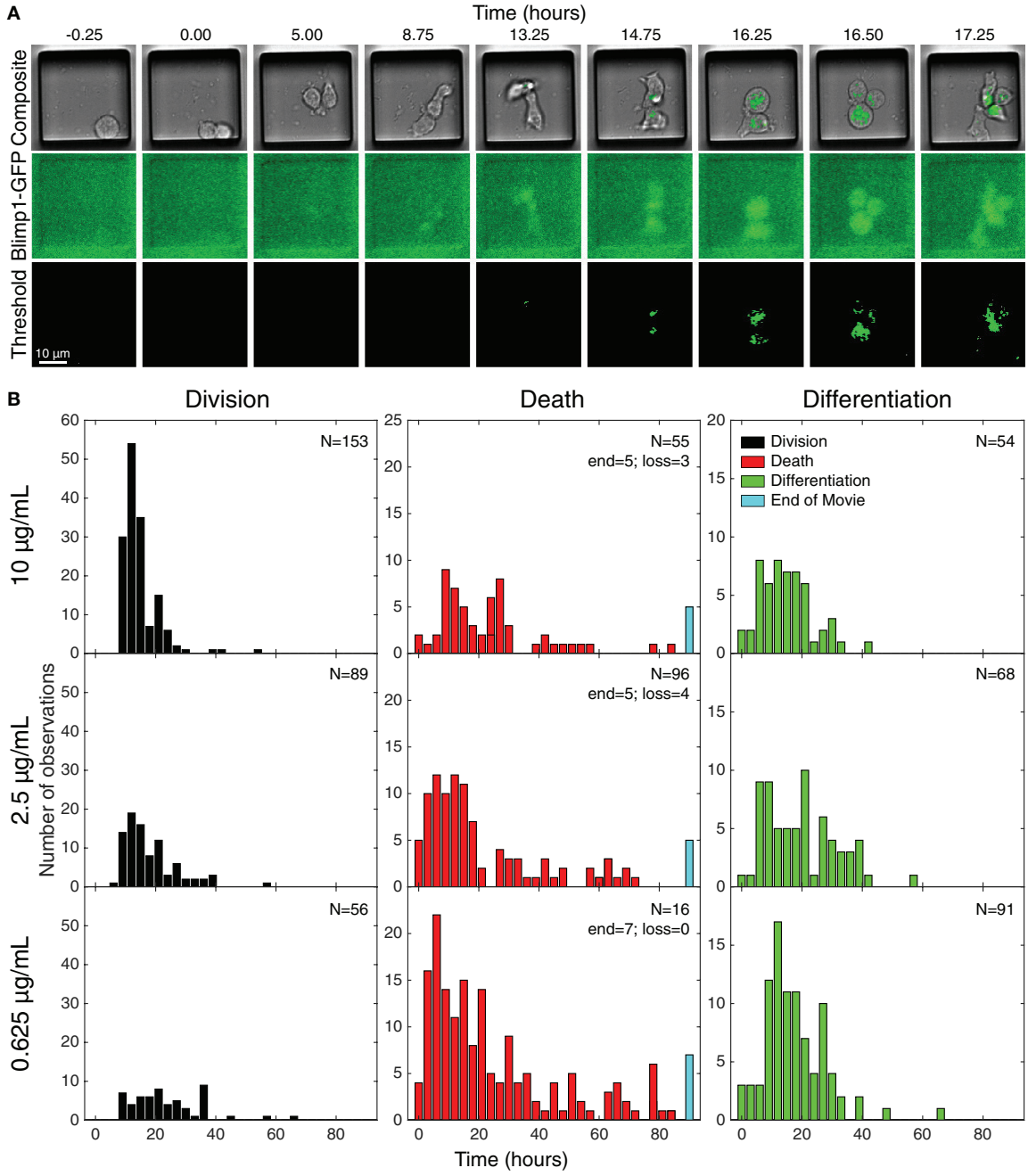

FIGURE 3 | Tracking individual cell fates over time. **(A)** Example microscopy images from one cell paddock, with selected frames from the bright field and GFP channels over time. Sorted cells (generation 4) observed to divide (generation 5) and, if still GFP^{-}, were tracked further to record subsequent division, death, and differentiation times. The initial mitotic event was assigned time = 0 in subsequent analyses. Division and death were visually discernible in the bright field channel (top row). Fluorescence images in the GFP channel (middle row) were corrected for uneven illumination, thresholded, and binarized for annotating differentiation to ASC (bottom row). **(B)** Histograms of the total data for each fate recorded, timed from first observed cell division and allocated to 3 h bins. Number of recorded cells indicated in panels (*N*). Cells that reached the end of the imaging period and had neither divided nor died were recorded as "end" and appear in the blue bar. Number of lost cells also indicated.

Parametric Model Based on Competition and Changes in Division Time Only

Under the stochastic competition hypothesis, not all processes need to be in operation in every cell. In particular, there is a possibility that neither differentiation nor division partake in the competition. To extract these propensities to differentiate and divide (i.e., likelihood that the underlying division or differentiation machinery is active within a cell), we created a

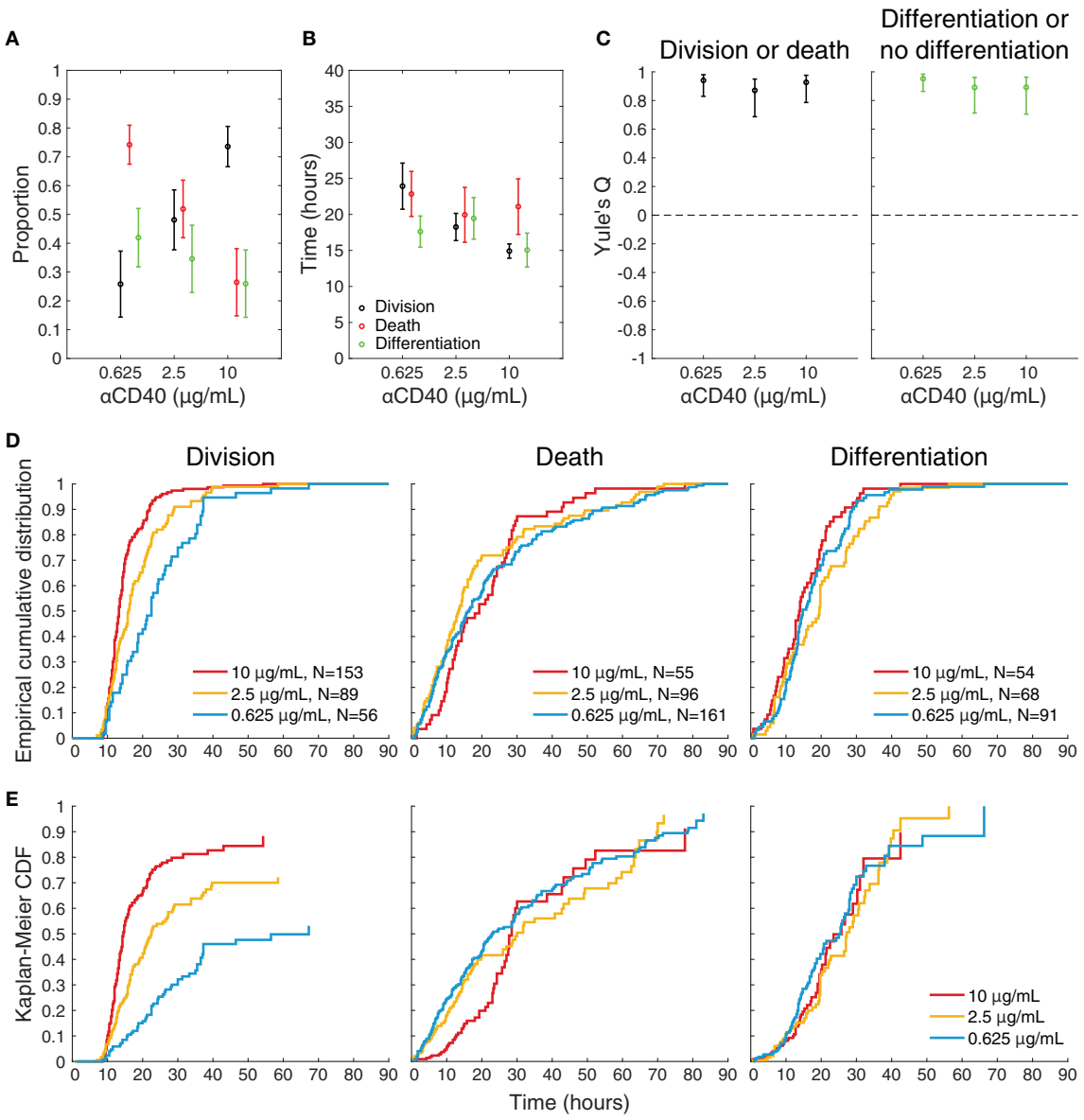

FIGURE 4 | Features of single cell imaged data. **(A)** The proportion of tracked single cells that underwent each fate. Fisher's exact test was performed to compare proportions of cells to undergo fates between 0.625 vs. 2.5, 0.625 vs. 10, 2.5 vs. 10 μg/mL anti-CD40. Division vs. death: $p = 4.18 \times 10^{-6}$, 1.77×10^{-23}, and 3.01×10^{-7}, respectively. Differentiation vs. no-differentiation: $p = 0.15$, 0.0007, and 0.078, respectively. **(B)** For cells reaching each fate the average time is shown with 95% CIs. Kruskal-Wallis test was performed to compare the times to fates between different anti-CD40 concentrations. Division: $p = 3.8741 \times 10^{-8}$, death: $p = 0.2386$ and differentiation: $p = 0.1354$. **(C)** Yule's Q, a measure of concordance in fate, shows that sibling fate selection (death or division, differentiation or no differentiation) is highly symmetric at all anti-CD40 stimulation levels with 95% CIs indicated by bars. **(D)** Cumulative frequency distributions of raw data for time to each fate. **(E)** Uncensored times to fate as determined by Kaplan-Meier survival function estimates overlaid for each anti-CD40 concentration. Division was uncensored from the influence of death, death was uncensored from division, and differentiation was uncensored from both division and death. Data from all tracked cells are included.

parametric statistical model by assuming that underlying time-to-fate distributions are log-normal given fate is in operation, but with a possibility that differentiation and division are inactive (discussed in Materials and Methods). Based on the observations from application of the Kaplan-Meier estimator, we assumed that the uncensored differentiation and death distributions were unchanging with stimulus and that only the division distribution and the propensity to divide were altered. This resulted in a single three-parameter description for differentiation (mean, variance, propensity to differentiate) and a two-parameter description for death (mean, variance) across all three stimulation conditions, along with a three-parameter description for division (mean, variance, propensity) per stimulation condition.

The uncensored lognormal curves with the highest likelihood of fitting to the data are shown in **Figure 5A** for comparison with the per-condition non-parametric uncensoring. The parametric

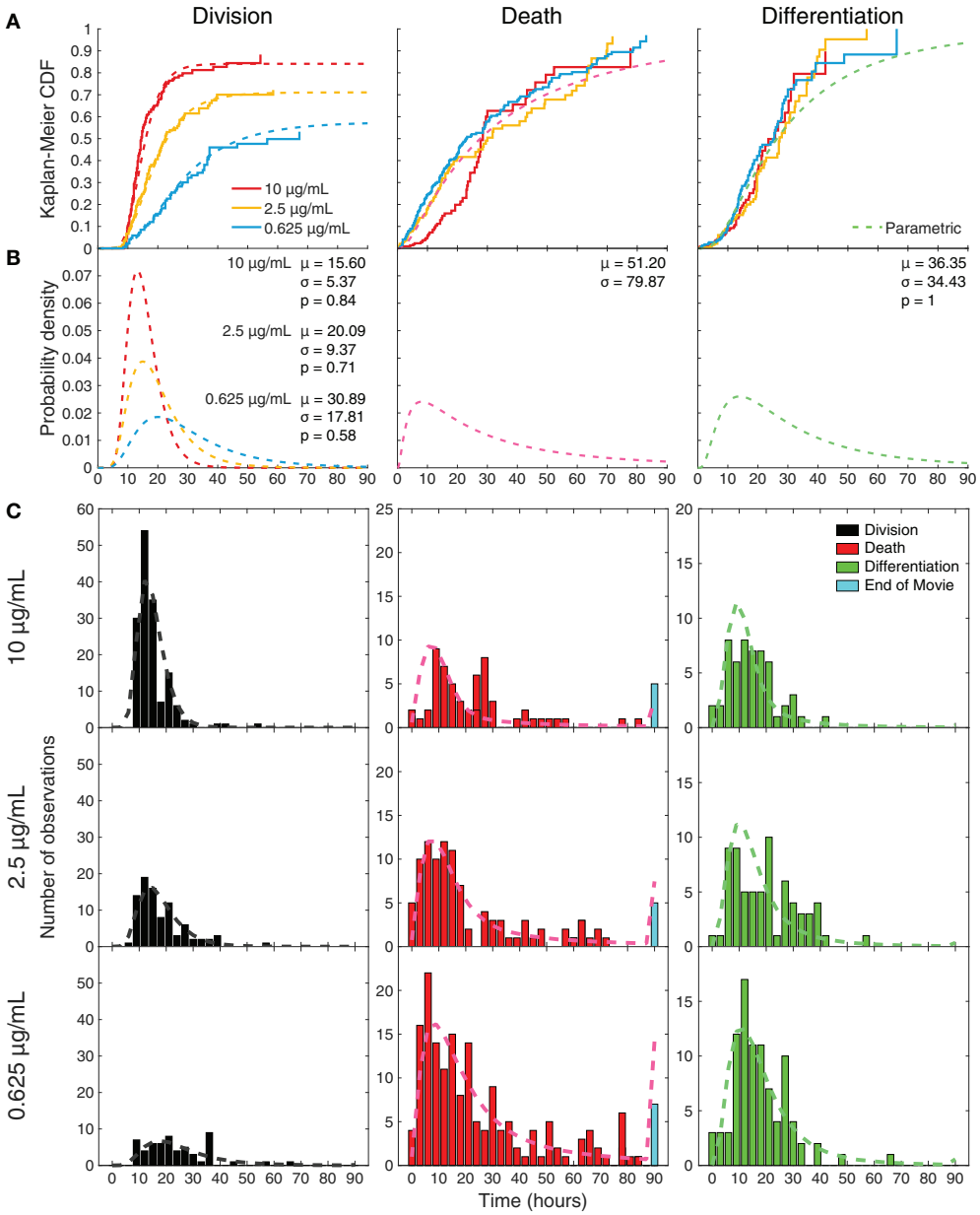

FIGURE 5 | Parametric model fitting with constrained parameters to censored data. **(A)** Maximum likelihood parametric model-fits to the data, under the constraints that death and differentiation time distributions were the same for all conditions, while the division time distribution and propensity for division could change with CD40 stimulation; overlaid with Kaplan-Meier analyses. **(B)** Uncensored parametric plots drawn as probability density functions; mean division times (μ) get longer with less CD40 stimulation, as variance (σ) increases and propensity (p) to divide decreases. **(C)** Predicted outcomes calculated from these constrained parametric distributions overlaid onto the observed data.

and non-parametric estimates are in good agreement, further supporting the hypotheses of the parametric model. Having ascribed lognormal curves to the probability distributions of times to fate, fitted parameters from different conditions could be compared for deviations in means, variations, and probabilities (**Figure 5B**). For decreasing anti-CD40 concentrations (10, 2.5, 0.625 μg/mL), the model fit division time distributions to the data with increasing mean (15.60, 20.09, 30.89 h) and variance (5.37, 9.37, 17.81 h), while the propensity for division being "on" in the cell decreased (0.84, 0.71, and 0.58, respectively). Death times (mean 51.20 h, variance 79.87 h) and differentiation times (mean 36.35 h, variance 34.43 h, propensity 1) were fitted with one distribution each for all of the CD40 stimulation concentrations, with the assumption that the probability of death is always ultimately 1. The best-fit propensity for differentiation was 1, suggesting that differentiation is always "on" in a

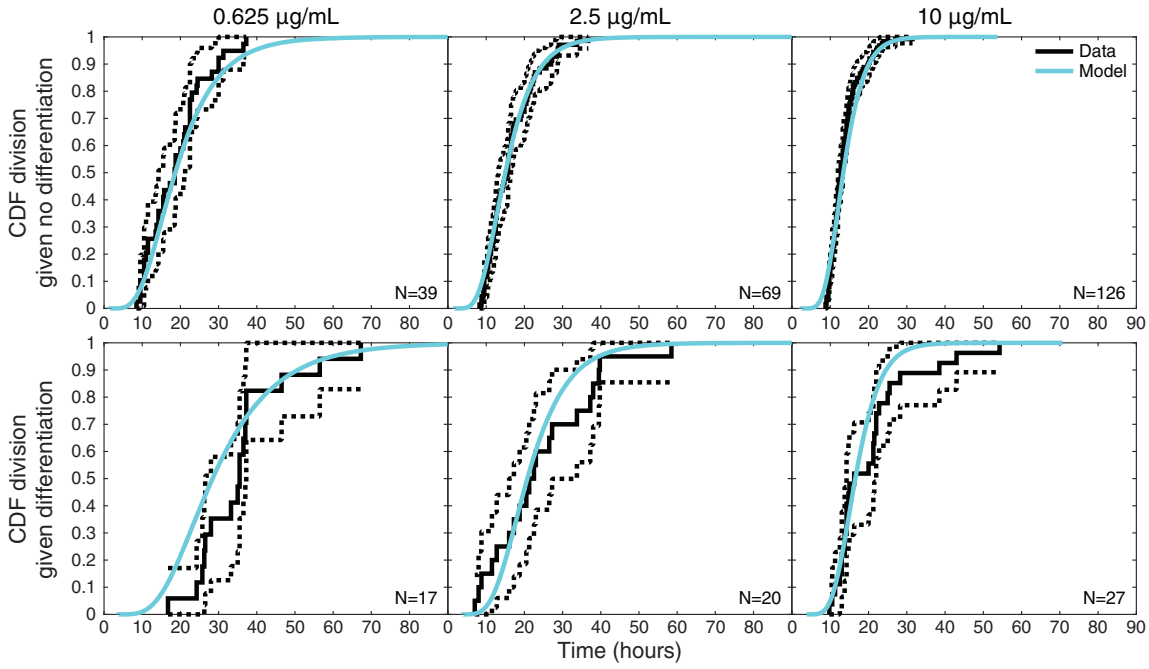

FIGURE 6 | Times to divide given differentiation or not. For each stimulation condition, upper panels display the empirical distribution of times to divide for cells that did not differentiate (solid black lines) with 95% confidence intervals (dotted black lines) computed with Greenwood's Formula. The lower panels display the same information for cells that were observed to differentiate before dividing. Also shown on both are the model-predicted distributions (cyan) of times to divide conditional on a cell differentiating or not, which differ as a consequence of the reshaping by competition.

stimulated cell and so is the default action that occurs when either division or death does not censor it. Overlaying the raw data, **Figure 5C** provides the extrapolation from these best-fit uncensored probability distribution functions to what they predict would be observed as a consequence of competition and censorship. The model predicts that a small proportion of cells will take their fate, typically death, after cessation of filming. A small number of cells are, indeed, observed to have neither died nor divided by the end of the microscopy session, and these are plotted at the end of the death-time histograms, according well with the out-of-sample model prediction.

Further Features of the Data Consistent With Competition

Figure 6 plots an additional interesting feature of the data that might appear to require an involved explanation. The upper panels display the empirical cumulative distribution of the times to divide of cells that did not differentiate for each stimulation condition, while the corresponding lower panels display the times to divide for cells that were observed to differentiate. For each condition, these two distributions are distinct, with division times being—on average—longer for cells that differentiated. The equivalent plots for times to death can be found in **Figure S3**, where the same phenomenon is exhibited.

Outside of the competition model, this seems to suggest distinct distributions for times to division or death fates dependent on whether a cell differentiates or not. Within the competition hypothesis, however, it is instead an intrinsic consequence of the model structure. Also displayed in the upper panel of **Figure 6** is the conditional distribution of the time to divide given that the cell did not differentiate as determined by the model, while the lower panel displays the model's conditional distribution of the time to divide given a cell did differentiate. Within the competition model, these two observed distributions are expected to be distinct as a consequence of censoring: knowing that a cell differentiates ensures a lower bound on the time to divide, conditioning it to be larger. Thus, the competition model inherently anticipates and accounts for these apparently involved features of the data within one mechanistically simple hypothesis that would otherwise require a model with significantly more parameters to explain.

DISCUSSION

The B lymphocyte is an ideal model system for studying cell fate control, being highly tractable to *in vitro* manipulation and sensitive to many alternative receptor driven signals that alter its behavior. Here we adopted this system and sought an answer to how varying the strength of one significant signal, transmitted through CD40 on the B cell surface, could affect the rate of development to ASC. This question is of particular interest as earlier studies noted the effect to be "paradoxical": weaker stimulation leads to a greater rate of differentiation with each generation (29). Building on previous filming experiments (26, 30), chamber slides were used to sustain and image cells in varying levels of anti-CD40 stimulation. Miniature paddocks

segregated the individual cells and reduced interference from homotypic adhesion (27). These data consisted of the recorded times to fates of hundreds of sibling pairs, making it suitable for quantitatively challenging hypotheses.

Analyzing these data allowed the elimination of the hypothesis that the paradoxical differentiation effect was due to changes in asymmetric cell division, as siblings had a high concordance in fate that was unaffected by stimulation strength. Our attention turned to ask whether the theory of competing fates (26, 32) could explain the phenomena. We hypothesized that increased differentiation could arise by cells transitioning faster within each generation, or by division times slowing, and thus allowing cells more time to differentiate before they divided again. Consistent with the latter hypothesis, the data, when uncensored, revealed that CD40 stimulation level regulated division times and division proportions, but had no effect on either differentiation or death times. Parametric fitting to differentiation times only required one set of parameters (mean, variance, propensity), whereas constraining division times to a single set of parameters would have produced poorly fitted outcomes. Hence, assuming independently timed control of fates, we were able to reject the hypothesis that CD40 stimulation was controlling either the proportions of cells capable of differentiating to ASC, or the time required for cells to differentiate. Instead, changes in division times were sufficient to re-create the differentiation patterns seen with flow cytometry.

This analysis supported the hypothesis that low CD40 stimulation slows division times, and consequently allows more time for cells to differentiate. Thus, regulation of division time by stimulation strength is identified as a controlling feature of fate decisions by the stimulated B cell. An influence of cell cycle length on differentiation has been noted in other cell systems suggesting this may be a biologically widespread regulatory mechanism (34, 35). We also assume the likelihood of differentiation is dependent on, and in turn altered by, the concentration of cytokines in culture. Further experiments will be required to assess this possibility.

These studies raise the question of how signals and internal molecular processes alter the time to different fates. One mechanism reported to date posits accumulation of transcriptional regulators. Kueh et al. (36) imaged hematopoietic progenitor cells and noted the choice between becoming a macrophage-lineage cell or a B cell was dependent upon the timed accumulation of transcriptional regulator PU.1. The longer cells took to divide, the more likely they were to accumulate the higher levels of PU.1 needed for macrophage commitment. A variant of this mechanism requiring both timed production and loss was noted by Heinzel et al. (37) for expression of Myc as a controller of division progression. Myc accumulated in proportion to signal strength and decayed at a constant rate, independently of division, eventually leading to a timed cessation of mitosis. As transcriptional regulators are important drivers for many fate changes, equivalent timed changes in expression level based on accumulation are likely

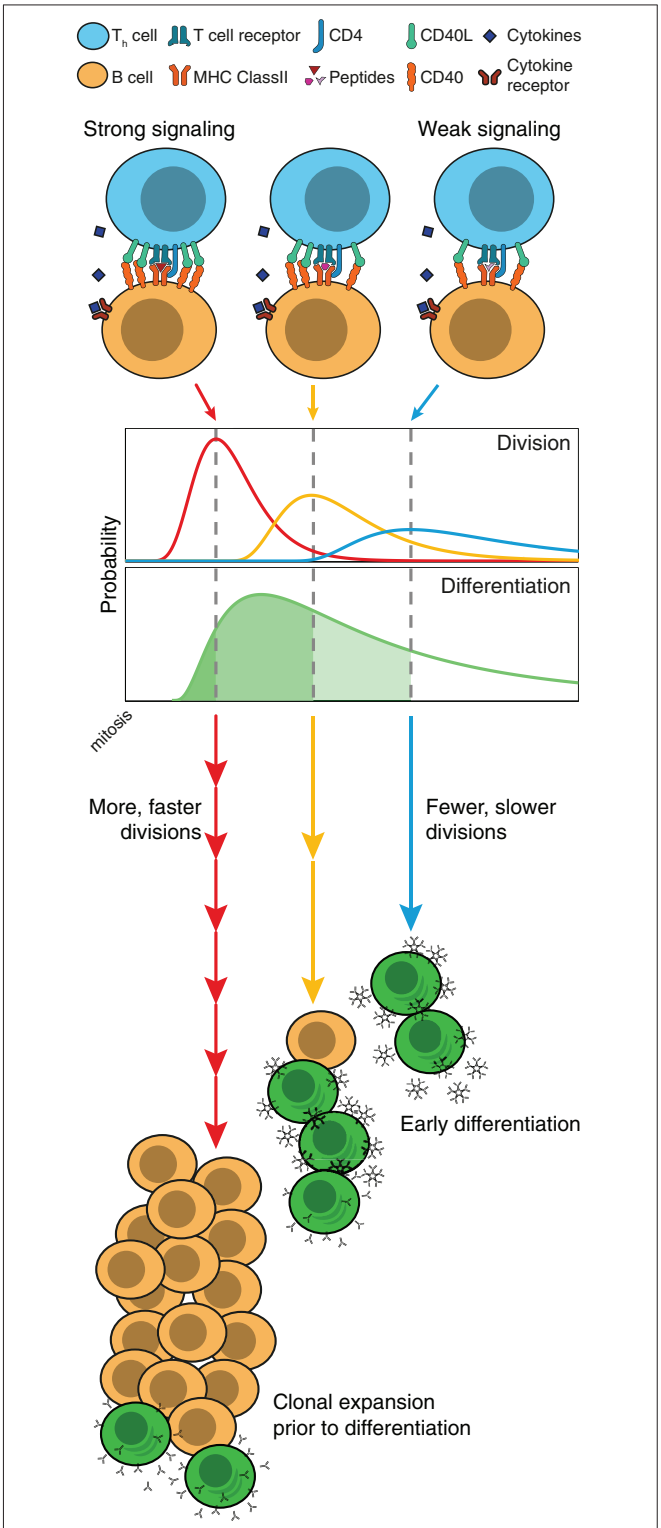

FIGURE 7 | Model of division-based control of B cell fate. Quantitative differences in CD40 signaling leads to proportional differences in division times, as well as the number of divisions completed. Even without modifications to underlying differentiation times, cell populations can differentiate as a result of competing cell fates. With slow divisions, the multitude of weakly stimulated

(Continued)

FIGURE 7 | cells automatically differentiate, and rapidly form large numbers of unswitched, low affinity antibody secreting cells. Meanwhile, those cells that receive strong stimulation divide rapidly, and hold back their differentiation mechanism until the clone has undergone expansion and isotype modifications, thus leading to an increased net number of higher affinity plasmablasts.

to be in operation in mature B cells. Further experiments measuring levels of transcriptional regulators and correlating levels with fate outcomes in individual cells will be informative to identify this and other putative molecular mechanisms (15).

These findings also offer insights into the controlling systems for antibody generation during a T-dependent immune response. T and B cell cooperation is an active process that occurs in two distinct sites during an immune response. Initial engagement occurs in the extrafollicular zones of lymphoid tissue and leads to the heterogeneous production of antibody secreting plasmablasts, that are typically short-lived and of weak to moderate affinity (38). Effective T and B cell collaboration requires an unbroken sequence of graded quantitative events that begins with antigen capture by the B cell receptor (BCR) and upregulation of T cell costimulatory surface molecules such as CD28, class II MHC and CD40 (39, 40). For effective stimulation by T cells, antigen must also be internalized by the B cell and presented on the cell surface, providing further opportunities for quantitative titration of the outcome (41). These variables in turn determine the level of stimulation received by an engaged T cell and subsequently the level of CD40L expression, and the rate of cytokine production provided to the B cell during the collaborative event (42). While the combinatorial possibilities are large, given the results here, we can identify a key principle in operation: even if holding all other variables constant, quantitative differences in CD40L, as the result of the chain of early events, will lead to proportional variations in average division times as well as the number of divisions completed (43). By slowing division, the weaker cells automatically assume a greater likelihood of differentiating and of dying. The more strongly stimulated cells will divide rapidly, automatically holding back their differentiation to ASC and leading to greater selection and expansion. Based on these findings we suggest that, as stimulated cells lose access to T cells, B cells slow division and automatically transition to secreting plasmablasts, provided cytokines are also present. Thus, the more avid and competent B cells are naturally selected for expansion while their differentiation is suppressed, leading, ultimately, to an increased net number of higher affinity plasmablasts overall (illustrated in **Figure 7**). This model is consistent with the studies of Paus et al. showing greater proliferation and overall generation of plasmablasts by higher affinity B cells (44). As antibody isotype switching is also strongly linked to progressive division and unaffected by the strength of CD40 stimulation (18, 19), this selection mechanism will, without additional cellular machinery, result in higher affinity clones that transition, automatically, to produce specialized antibody subtypes. It seems likely that the quantitative relation between all of these processes has evolved to provide an optimal balance for generating protective antibody over time.

An important second site of T-B cell collaboration is the germinal center. A subset of activated T and B cells migrate to primary follicles to initiate and sustain this reaction (45–47). At this site B cells undertake successive rounds of somatic hypermutation and selection that generates fully differentiated plasma cells and long-lived high affinity, memory B cells. Selection of B cell clones in the germinal center is critically dependent upon T cells and CD40-CD40L interactions (17, 48, 49). B lineage cells in the germinal center are distinct from those generated *in vitro*, and seen in extrafollicular sites (50). However, labeling studies *in vivo* have determined that the division rate is affected by the strength of stimulation provided by T cell help (51, 52). These observations taken together with the *in vitro* findings of the present paper, imply a general mechanism where the rate of proliferation is linked to, and tempers, the fate of competent, highly stimulated cells to achieve an optimal dynamic outcome with minimal direct control over differentiation.

AUTHOR CONTRIBUTIONS

JZ, PH, and KD designed all experiments and analyzed and interpreted experiments and wrote manuscript. JZ performed experiments and undertook all data annotation. JM developed the data pipeline, conducted the image processing, and oversaw microscopy setup.

ACKNOWLEDGMENTS

This work was supported by the National Health and Medical Research Council via Project Grants 1010654 and 1057831, and Program Grant 1054925, and fellowships to PH and Science Foundation Ireland grant No. 12IP1263 to KD. This work was made possible through Victorian State Government Operational Infrastructure Support and Australian Government NHMRC Independent Research Institutes Infrastructure Support Scheme Grant 361646. JZ was supported by an Australian Postgraduate Award. JM was supported by National ICT Australia (NICTA), which was funded by the Australian Research Council and the Australian Department of Broadband, Communications and the Digital Economy. We thank S. Nutt and A. Kallies for Blimp-1-GFP reporter mice.

SUPPLEMENTARY MATERIAL

The Supplementary Material for this article can be found online at: https://www.frontiersin.org/articles/10.3389/fimmu.2018.02053/full#supplementary-material

REFERENCES

1. Sun J, Ramos A, Chapman B, Johnnidis JB, Le L, Ho YJ, et al. Camargo: clonal dynamics of native haematopoiesis. *Nature* (2014) 514:322–7. doi: 10.1038/nature13824
2. Carulli AJ, Samuelson LCS. Schnell: unraveling intestinal stem cell behavior with models of crypt dynamics. *Integr Biol (Camb).* (2014) 6:243–57. doi: 10.1039/c3ib40163d
3. Livesey FJ, Cepko CL. Vertebrate neural cell-fate determination: lessons from the retina. *Nat Rev Neurosci.* (2001) 2:109–18. doi: 10.1038/35053522
4. Homem CC, Knoblich JA. Drosophila neuroblasts: a model for stem cell biology. *Development* (2012) 139:4297–310. doi: 10.1242/dev.080515
5. Tyson JJ, Novak B. Control of cell growth, division and death: information processing in living cells. *Interface Focus* (2014) 4:20130070. doi: 10.1098/rsfs.2013.0070
6. Naik SH, Perie L, Swart E, Gerlach C, van Rooij N, de Boer RJ, et al. Diverse and heritable lineage imprinting of early haematopoietic progenitors. *Nature* (2013) 496:229–32. doi: 10.1038/nature12013
7. Papalexi E, Satija R. Single-cell RNA sequencing to explore immune cell heterogeneity. *Nat Rev Immunol.* (2018) 18:35–45. doi: 10.1038/nri.2017.76
8. Altschuler SJ, Wu LF. Cellular heterogeneity: do differences make a difference? *Cell* (2010) 141:559–63. doi: 10.1016/j.cell.2010.04.033
9. Rodriguez-Fraticelli AE, Wolock SL, Weinreb CS, Panero R, Patel SH, Jankovic M, et al. Camargo: clonal analysis of lineage fate in native haematopoiesis. *Nature* (2018) 553:212–216. doi: 10.1038/nature25168
10. Pei W, Feyerabend TB, Rossler J, Wang X, Postrach D, Busch K, et al. Polylox barcoding reveals haematopoietic stem cell fates realized *in vivo*. *Nature* (2017) 548:456–460. doi: 10.1038/nature23653
11. Paul F, Arkin Y, Giladi A, Jaitin DA, Kenigsberg E, Keren-Shaul H, et al. Transcriptional heterogeneity and lineage commitment in myeloid progenitors. (2016) *Cell* 164:325. doi: 10.1016/j.cell.2015.12.046
12. Perie L, Duffy KR, Kok L, de Boer RJ, Schumacher TN. The branching point in erythro-myeloid differentiation. *Cell* (2015) 163:1655–62. doi: 10.1016/j.cell.2015.11.059
13. Gerlach C, Rohr JC, Perie L, van Rooij N, van Heijst JW, Velds A, et al. Heterogeneous differentiation patterns of individual $CD8^+$ T cells. *Science* (2013) 340:635–9. doi: 10.1126/science.1235487
14. Buchholz VR, Flossdorf M, Hensel I, Kretschmer L, Weissbrich B, Graf P, et al. Disparate individual fates compose robust $CD8^+$ T cell immunity. *Science* (2013) 340:630–5. doi: 10.1126/science.1235454
15. Nutt SL, Hodgkin PD, Tarlinton DM, Corcoran LM. The generation of antibody-secreting plasma cells. *Nat Rev Immunol.* (2015) 15:160–71. doi: 10.1038/nri3795
16. Crotty S. A brief history of T cell help to B cells. *Nat Rev Immunol.* (2015) 15:185–9. doi: 10.1038/nri3803
17. Vinuesa CG, Linterman MA, Yu D, MacLennan IC. Follicular helper T cells. *Annu Rev Immunol.* (2016) 34:335–68. doi: 10.1146/annurev-immunol-041015-055605
18. Hasbold J, Corcoran LM, Tarlinton DM, Tangye SG, Hodgkin PD. Evidence from the generation of immunoglobulin G-secreting cells that stochastic mechanisms regulate lymphocyte differentiation. *Nat Immunol.* (2004) 5:55–63. doi: 10.1038/ni1016
19. Hodgkin PD, Lee JH, Lyons AB. B cell differentiation and isotype switching is related to division cycle number. *J Exp Med.* (1996) 184:277–81.
20. Deenick EK, Hasbold J, Hodgkin PD. Switching to IgG3, IgG2b, and IgA is division linked and independent, revealing a stochastic framework for describing differentiation. *J Immunol.* (1999) 163:4707–14.
21. Hasbold J, Lyons AB, Kehry MR, Hodgkin PD. Cell division number regulates IgG1 and IgE switching of B cells following stimulation by CD40 ligand and IL-4. *Eur J Immunol.* (1998) 28:1040–51. doi: 10.1002/(SICI)1521-4141(199803)28:03<1040::AID-IMMU1040>3.0.CO;2-9
22. Kallies A, Hasbold J, Tarlinton DM, Dietrich W, Corcoran LM, Hodgkin PD, et al. Plasma cell ontogeny defined by quantitative changes in blimp-1 expression. *J Exp Med.* (2004) 200:967–77. doi: 10.1084/jem.20040973
23. Hawkins ED, Turner ML, Dowling MR, van Gend C, Hodgkin PD. A model of immune regulation as a consequence of randomized lymphocyte division and death times. *Proc Natl Acad Sci USA.* (2007) 104:5032–7. doi: 10.1073/pnas.0700026104
24. Duffy KR, Subramanian VG. On the impact of correlation between collaterally consanguineous cells on lymphocyte population dynamics. *J Math Biol.* (2009) 59:255–85. doi: 10.1007/s00285-008-0231-x
25. Subramanian VG, Duffy KR, Turner ML, Hodgkin PD. Determining the expected variability of immune responses using the cyton model. *J Math Biol.* (2008) 56:861–92. doi: 10.1007/s00285-007-0142-2
26. Duffy KR, Wellard CJ, Markham JF, Zhou JH, Holmberg R, Hawkins ED, et al. Activation-induced B cell fates are selected by intracellular stochastic competition. *Science* (2012) 335:338–41. doi: 10.1126/science.1213230
27. Day D, Pham K, Ludford-Menting MJ, Oliaro J, Izon D, Russell SM, et al. A method for prolonged imaging of motile lymphocytes. *Immunol Cell Biol.* (2009) 87:154–8. doi: 10.1038/icb.2008.79
28. Heath AW, Wu WW, Howard MC. Monoclonal antibodies to murine CD40 define two distinct functional epitopes. *Eur J Immunol.* (1994) 24:1828–34. doi: 10.1002/eji.1830240816
29. Hawkins ED, Turner ML, Wellard CJ, Zhou JH, Dowling MR, Hodgkin PD. Quantal and graded stimulation of B lymphocytes as alternative strategies for regulating adaptive immune responses. *Nat Commun.* (2013) 4:2406. doi: 10.1038/ncomms3406
30. Hawkins ED, Markham JF, McGuinness LP, Hodgkin PD. A single-cell pedigree analysis of alternative stochastic lymphocyte fates. *Proc Natl Acad Sci USA.* (2009) 106:13457–62. doi: 10.1073/pnas.0905629106
31. Mitchell S, Roy K, Zangle TA, Hoffmann A. Nongenetic origins of cell-to-cell variability in B lymphocyte proliferation. *Proc Natl Acad Sci USA.* (2018) 115:E2888–97. doi: 10.1073/pnas.1715639115
32. Duffy KR, Hodgkin PD. Intracellular competition for fates in the immune system. *Trends Cell Biol.* (2012) 22:457–64. doi: 10.1016/j.tcb.2012.05.004
33. Cox DR, Oakes, D. *Analysis of Survival Data.* London; New York, NY: Chapman and Hall (1984).
34. Calegari F, Huttner WB. An inhibition of cyclin-dependent kinases that lengthens, but does not arrest, neuroepithelial cell cycle induces premature neurogenesis. *J Cell Sci.* (2003) 116(Pt 24):4947–55. doi: 10.1242/jcs.00825
35. Coronado D, Godet M, Bourillot PY, Tapponnier Y, Bernat A, Petit M, et al. A short G1 phase is an intrinsic determinant of naive embryonic stem cell pluripotency. *Stem Cell Res.* (2013) 10:118–31. doi: 10.1016/j.scr.2012.10.004
36. Kueh HY, Champhekar A, Nutt SL, Elowitz MB, Rothenberg EV. Positive feedback between PU.1 and the cell cycle controls myeloid differentiation. *Science* (2013) 341:670–3. doi: 10.1126/science.1240831
37. Heinzel S, Binh Giang T, Kan A, Marchingo JM, Lye BK, Corcoran LM, et al. Myc-dependent division timer complements a cell-death timer to regulate T cell and B cell responses. *Nat Immunol.* (2017) 18:96–103. doi: 10.1038/ni.3598
38. MacLennan IC, Toellner KM, Cunningham AF, Serre K, Sze DM, Zuniga E, et al. Extrafollicular antibody responses. *Immunol Rev.* (2003) 194:8–18. doi: 10.1034/j.1600-065X.2003.00058.x
39. Harwood NE, Batista FD. Early events in B cell activation. *Annu Rev Immunol.* (2010) 28:185–210. doi: 10.1146/annurev-immunol-030409-101216
40. Linterman MA, Vinuesa CG. Signals that influence T follicular helper cell differentiation and function. *Semin Immunopathol.* (2010) 32:183–96. doi: 10.1007/s00281-009-0194-z
41. Batista FD, Neuberger MS. Affinity dependence of the B cell response to antigen: a threshold, a ceiling, and the importance of off-rate. *Immunity* (1998) 8:751–9.
42. Crotty S. Follicular helper CD4 T cells (TFH). *Annu Rev Immunol.* (2011) 29:621–63. doi: 10.1146/annurev-immunol-031210-101400
43. Rush JS, Hodgkin PD. B cells activated via CD40 and IL-4 undergo a division burst but require continued stimulation to maintain division, survival and differentiation. *Eur J Immunol.* (2001) 31:1150–9. doi: 10.1002/1521-4141(200104)31:4<1150::AID-IMMU1150>3.0.CO;2-V
44. Paus D, Phan TG, Chan TD, Gardam S, Basten A, Brink, R. Antigen recognition strength regulates the choice between extrafollicular plasma cell and germinal center B cell differentiation. *J Exp Med.* (2006) 203:1081–91. doi: 10.1084/jem.20060087
45. Phan TG, Paus D, Chan TD, Turner ML, Nutt SL, Basten A, et al. High affinity germinal center B cells are actively selected into the plasma cell compartment. *J Exp Med.* (2006) 203:2419–24. doi: 10.1084/jem.20061254
46. Shlomchik MJ, Weisel, F. Germinal centers. *Immunol Rev.* (2012) 247:5–10. doi: 10.1111/j.1600-065X.2012.01125.x

47. Victora GD, Nussenzweig MC. Germinal centers. *Annu Rev Immunol*. (2012) 30:429–57. doi: 10.1146/annurev-immunol-020711-075032
48. Liu YJ, Joshua DE, Williams GT, Smith CA, Gordon J, MacLennan IC. Mechanism of antigen-driven selection in germinal centres. *Nature* (1989) 342:929–31. doi: 10.1038/342929a0
49. Foy TM, Laman JD, Ledbetter JA, Aruffo A, Claassen E, Noelle RJ. gp39-CD40 interactions are essential for germinal center formation and the development of B cell memory. *J Exp Med*. (1994) 180:157–63.
50. Victora GD, Dominguez-Sola D, Holmes AB, Deroubaix S, Dalla-Favera R, Nussenzweig MC. Identification of human germinal center light and dark zone cells and their relationship to human B-cell lymphomas. *Blood* (2012) 120:2240–8. doi: 10.1182/blood-2012-03-415380
51. Victora GD, Schwickert TA, Fooksman DR, Kamphorst AO, Meyer-Hermann M, Dustin ML, et al. Germinal center dynamics revealed by multiphoton microscopy with a photoactivatable fluorescent reporter. *Cell* (2010) 143:592–605. doi: 10.1016/j.cell.2010.10.032
52. Gitlin AD, Mayer CT, Oliveira TY, Shulman Z, Jones MJ, Koren A, et al. Humoral Immunity. T cell help controls the speed of the cell cycle in germinal center B cells. *Science* (2015) 349:643–6. doi: 10.1126/science.aac4919

Conflict of Interest Statement: The authors declare that the research was conducted in the absence of any commercial or financial relationships that could be construed as a potential conflict of interest.

Supplementary figures

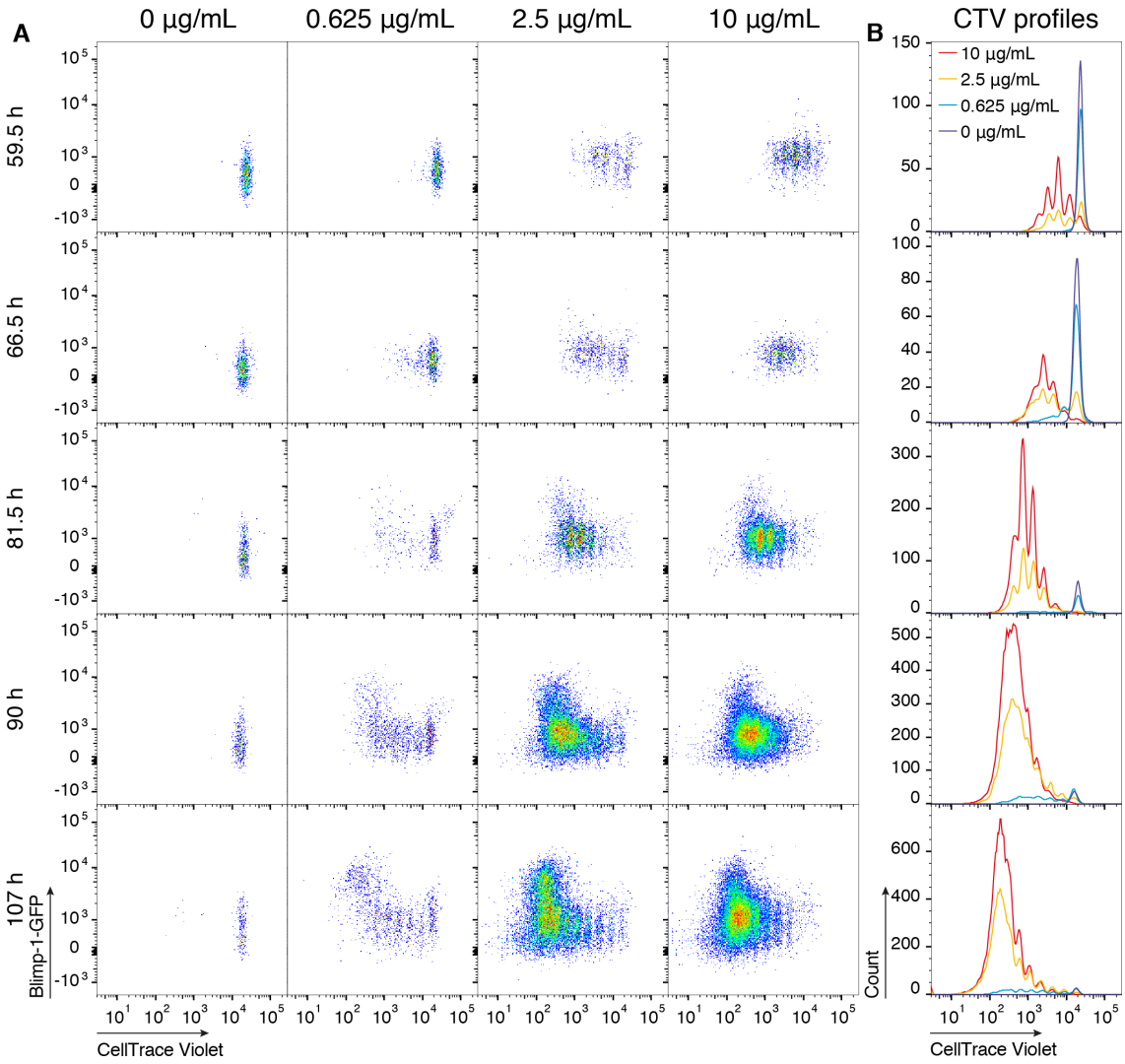

FIGURE S1 | B cell proliferation and differentiation is affected by anti-CD40 concentration. CTV labelled resting Blimp-1$^{gfp/+}$ B cells were cultured in the indicated concentrations of anti-CD40 with constant IL-4 and harvested over time. **(A)** Plots of CTV vs Blimp-1-GFP showing increases in GFP^{+} cell frequency with advancing divisions. **(B)** CTV histograms of total live cells overlaid to compare division progression in response to different anti-CD40 levels. Data representative of multiple CD40 titration experiments.

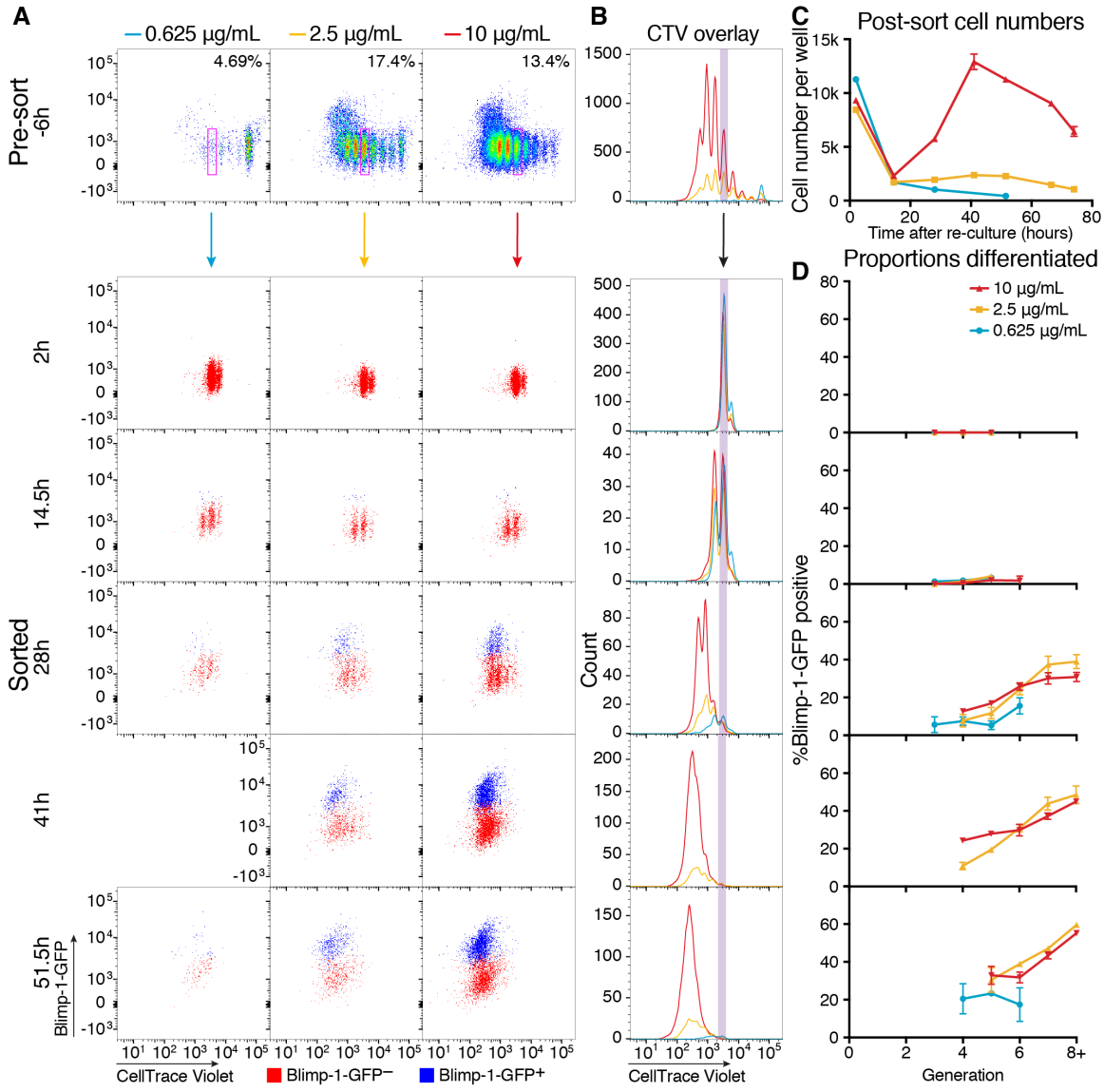

FIGURE S2 | Control cultures for long-term imaging campaign. CTV labelled resting Blimp-1$^{gfp/+}$ B cells were cultured in the indicated concentrations of anti-CD40 with IL-4 and harvested after 4 days. **(A)** Cells analyzed by flow cytometry showing CTV versus Blimp-1-GFP. Pre-sort row (- 6 h) indicates varying proliferation and differentiation in each culture. Sorted cell rows (2 – 51.5 h) show successive harvests of control cells after cytometric sorting of undifferentiated cells from generation 4 (gating box shown in pre-sort dot plot). Blimp-1-GFP^{+} cells indicated in blue. **(B)** CTV histograms overlaid indicating differences in division progression of presorted cultured cells and subsequent control cultures of sorted generation 4 cells. Shaded bar provides reference for generation 4. **(C)** Shows cell numbers recovered over time from re-culture of sorted cells, where '0' is 91 h after initial stimulation. **(D)** The proportion of GFP^{+} cells upon re-culture of sorted cells shows progressive changes with division.

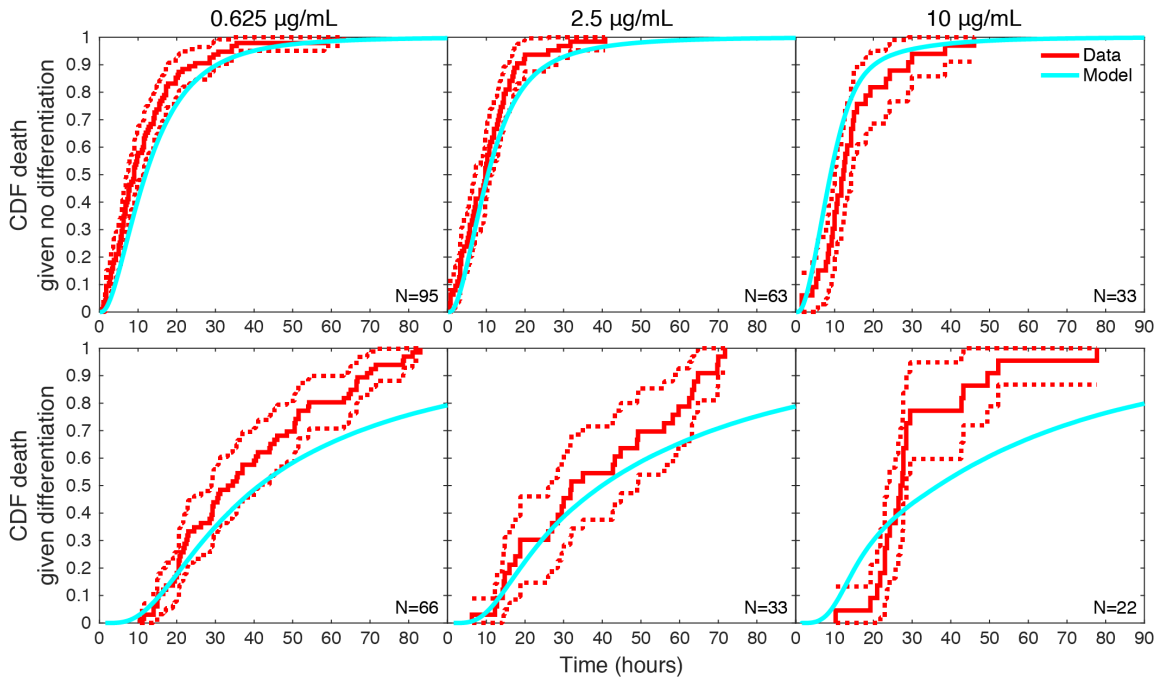

FIGURE S3 | Times to death given differentiation or not. For each stimulation condition, upper panels display the empirical distribution of times to death for cells that did not differentiate (solid red lines) with 95% confidence intervals (dotted red lines) computed with Greenwood's Formula. The lower panels display the same information for cells that were observed to differentiate before dying. Also shown on both are the model-predicted distributions (cyan) of times to death conditional on a cell differentiating or not.

3.2 Further Results

3.2.1 The independence between alternate cell fates was not affected by CD40 stimulation strength

The Cyton model's assumptions of independence between cell fates was further interrogated by investigating the correlations between alternate fates outcomes. To illustrate this analysis, two hypothetical situations for times to fates are compared in **Figure 3.1a** as an example.

In the top panels, each simulated point is randomly assigned a time to event X and another time to event Y. Either fate is log-normally distributed with the same mean and standard deviation, however each are designated independently of the other, and so the correlation (ρ) is 0 (top left panel). When events where $Y \leq X$ cannot be observed, such as where division censors long differentiation times, the data set is reduced to only $Y > X$ pairs (top right panel). As a consequence of censorship, a correlation is observed between two independent events; and this value can change depending on the level of competition between the two fates. In the bottom panels, simulated times to fates are drawn from two markedly different, but independent distributions, W and Z. After censorship, the correlation expected between fates Z and W is much lower than if there were more overlap between the probabilities for the two times to fates [125].

Using this technique, Pearson's ρ was calculated for each of the three CD40 conditions under scrutiny, for both differentiation vs division, and differentiation vs death (**Figure 3.2b**). These observed values were compared with that predicted using times to fate distributions calculated from parametric fits of the data (**Figure 3.2c**). To do this, the fitted, uncensored distributions from the parametric model were used to sample simulated populations of the same size as each data set. After censoring those events where differentiation is longer than either division or death, the mean Pearson's Correlations from 1000 simulations are plotted in (Figure 3.2c 'modelled'), with 95% confidence intervals (CIs) for the true mean. There are large degrees of overlap between the 95% CIs for the observed data compared with the modelled data; in particular, the observed Pearson's correlations for 0.625ug/mL 1C10 fell within the 95% CIs for both differentiation-division and differentiation-death correlations. Thus, these data further support the hypothesis that differentiation to ASC is independent of both division and death times, and that long division times in low CD40 stimulation conditions allow more cells to fulfil the time required for them to differentiate.

a Cyton: censorship produces signature correlations when times to fates are independent and in competition.

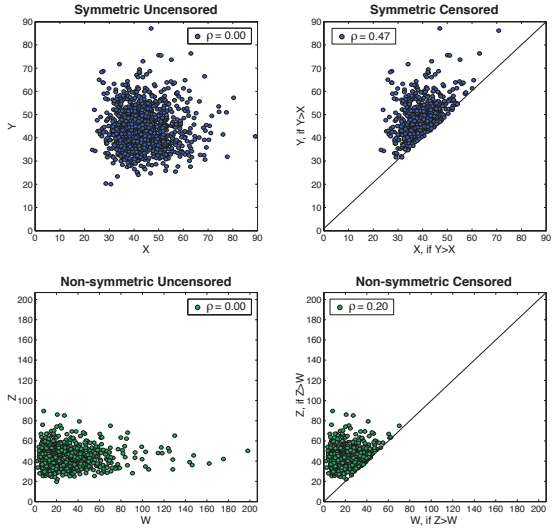

b Correlations between alternative intracellular fates from observed data:

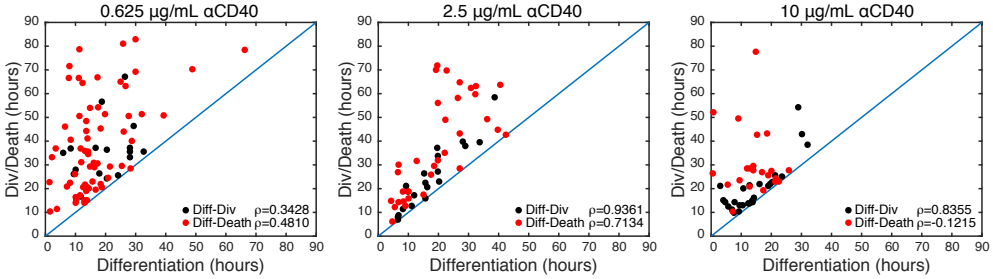

c

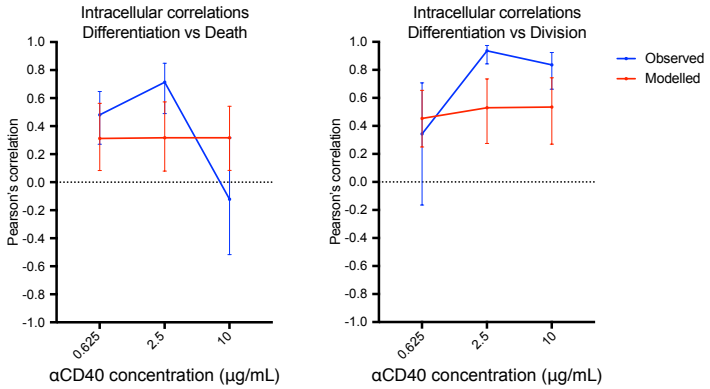

Figure 3.2: Intracellular fate correlations

a) Simulated data for times to independent fates taken from the same log-normal distribution (X and Y) or different log-normal distributions (W and Z). As these distributions are independent, Pearson's correlation is expected to be close to 0 (left panels). With censorship, values where X≥Y or W≥Z are unobservable (right panels), and the resulting distribution produces a signature correlation value. Adapted from Ken Duffy [125]. **b)** Observed intracellular fate correlations between differentiation times and either division or death times. **c)** Observed Pearson's correlations (blue) compared with modelled predictions (red) for intracellular correlations between cell fates (95% CI).

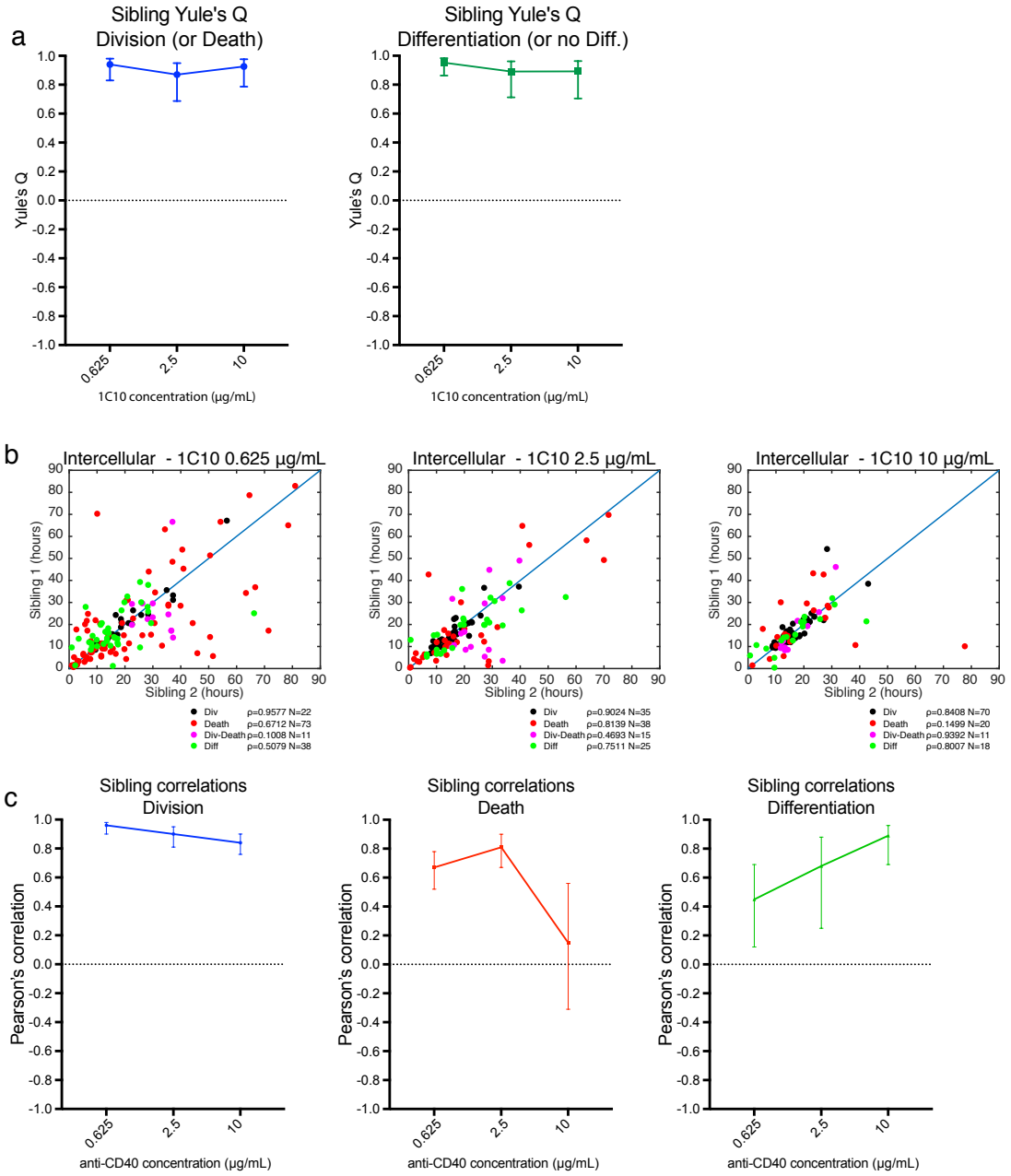

Figure 3.3: Intercellular correlations between sibling cells

a) Yule's Q for concordance between sibling cells that divide or not, or differentiate or not. 95% CI. **b)** Scatter plots of times to cell fates where both sibling cells attained the same event. **c)** Dose-response changes in correlations between times to fates (95% CI).

3.2.2 CD40 stimulation strength does not affect sibling correlations or concordance

After examining single cell fates and the effects of independent but competing fate outcomes, it remained of interest whether CD40 stimulation strength would affect sibling cell fate relations. Very high correlations in fate outcomes and concordance in times required to achieve cell fates have been seen previously [128], and was also observed in this experiment (Figure 3.3).

For generation 5 cells that divided, their sibling was also highly likely to divide, and the converse was also true for death. Similarly, whether one cell differentiated or not, their sibling was also likely to follow the same fate. Yule's Q for quantifying these sibling concordances are plotted in Figure 3.3a, and appears not to be affected by CD40 stimulation strength.

Sibling cells that undergo the same fate (differentiation, division, or death) have their times to fate plotted in Figure 3.3b for each stimulation condition. The levels of correlation between siblings' times to concordant fates were found to be high for each fate outcome, and CD40 stimulation had little impact on this correlation (Figure 3.3c).

3.3 Further Discussion

In using a technique for observing and recording the times to fates of individual cells, these data could then be analysed using mathematical methods to uncensor underlying times to cell fates. The uncensored data revealed that CD40 signalling controlled division times and division proportions, but had no effect on either differentiation or death times. Parametric fitting to differentiation times was successful with only one set of parameters (mean, variance, P), whereas constraining division times to a single set of parameters would have produced poorly fitted outcomes. Hence, we were able to reject the hypotheses that CD40 stimulation was controlling either the proportions of cells capable of differentiating to ASC, or the time required for cells to differentiate, at the levels of CD40 stimulation tested. Instead, the changes in division times were found to be sufficient for producing the differentiation patterns seen with flow cytometry; these data and the subsequent tests for independence and competition supported the last hypothesis, where low CD40 stimulation slows division times, and consequently allows more cells time to differentiate. These characteristics would not have been uncovered without collecting the heterogeneous array of times to fates for individual cells, and uncensoring analyses.

CHAPTER 4

Generation-linked Differentiation

4.1 Introduction

Differentiation typically occurs several days after commencement of the B cell response, by which time most activated cells have undergone multiple rounds of cell division. For both T-dependent and -independent stimulation, plasmablasts begin to appear 3-4 days after *in vivo* antigen challenge, around the same time that antibody isotype switching is also detected [49, 139, 140].

The observation that plasmablasts appear several days after B cell activation is also mirrored in *in vitro* experiments. These differentiation changes are measurable by staining for differentiation marker CD138 (Syndecan-1) and antibody secretion [67], or using the Blimp-1-GFP reporter mouse [70, 114]

An important clue for how the characteristic timing of plasmablast appearance was controlled and delayed arose with the application of division tracking dyes such as CFSE [98]. The utility of these dyes made it possible to observe cell differentiation behaviours in individual generations, as the cell population divides over the course of the lymphocyte response. When examined in this way, both antibody isotype switching and differentiation to ASC were found to exhibit strong division-linked behaviour. Regardless of time from stimulation, or cell numbers per generation, CFSE-labelled cells produced consistent proportions of cells that were antibody isotype switched, depending on the number of times divided and the stimulation conditions [92, 103]. Similar results were found for differentiation to ASC [67], where cells that had divided more times produced antibody secreting cells at greater frequency. This was observed in both bulk flow cytometry analyses and experiments where cells were sorted from single, consecutive generations and re-cultured for subsequent analysis [67, 102].

How division progression imposes such a striking influence on cell differentiation is not well understood at either the cellular or molecular levels. In this chapter, the production of antibody secreting cells in different cell generations was examined in relation to the theory of competition between cell fates. The higher frequency of ASCs among cells that undergo more divisions has a number of possible explanations if consistent with the competing fate hypothesis explored and supported in the previous chapter. It may be due to:

1) Changes in the times to differentiate altered by division progression;
2) Poor survival of lymphoblasts in late generations;
3) Faster division times censoring and impeding differentiation in earlier generations;
4) A mixed permutation of altered times and cell fates as in 1 - 3.

To distinguish between these possibilities, the filming method used in the previous chapter [128, 141] was adapted with a number of further modifications. In order to facilitate and improve the ability to monitor differentiation, an attempt was made to reduce the influence of a major competing fate, cell death, by using a mouse strain overexpressing the pro-survival oncogene Bcl-2. Bcl-2 belongs to a family of anti-apoptotic proteins responsible for inhibiting or sequestering pro-apoptotic molecules [142-144]. Bcl-2 and its family of apoptotic regulators are key components of the programmed cell death pathway, and so are constitutively expressed in all mammalian cell types. The dysregulation of Bcl-2 contributes towards malignancies such as chronic lymphocytic leukaemia (CLL) or other lymphomas, as Bcl-2 overexpression enhances cell survival, one of the hallmarks of cancer [145]. Here, we use these properties of enhanced survival in Vav-bcl-2-69 transgenic mice [146] to inhibit death as a competing cell fate, as a means of directly 'uncensoring' differentiation.

The previous chapter demonstrated how changing division times alone can modulate the rate of antibody secreting cell production. In this chapter, the use of single cell imaging was applied to examine how the passage through multiple division rounds controls differentiation to ASC.

4.2 Results

4.2.1 Generation-linked differentiation is enhanced by IL-5

To promote division-linked differentiation and therefore increase the sensitivity of the proposed experiments, the cytokine interleukin-5 (IL-5) was evaluated. This T cell derived cytokine has been reported to promote division linked differentiation without effects on other fates, including isotype switching, proliferation or survival [67, 86].

To assess the effects of IL-5 in our culture system, purified, naïve splenic B cells were CTV labelled and incubated with 10 µg/mL anti-CD40, 500 U/mL IL-4, and varying concentrations of IL-5 in the established culture system (Methods 2.3 – 2.8). Triplicate 200 µL cultures were harvested and analysed by flow cytometry on days 0, 3, 4, 5 and 6, and assessed for total cell numbers, as well as cells per generation. Total cell numbers, and the distribution of cells per generation, were largely unaffected by IL-5 concentrations (**Figure 4.1a,b**). Differentiation to ASC, however, was increased in the presence of IL-5. Proportions of total ASCs produced in the population were higher with greater IL-5 stimulation (**Figure 4.1c**). When examined by generation, the enhancement in differentiation

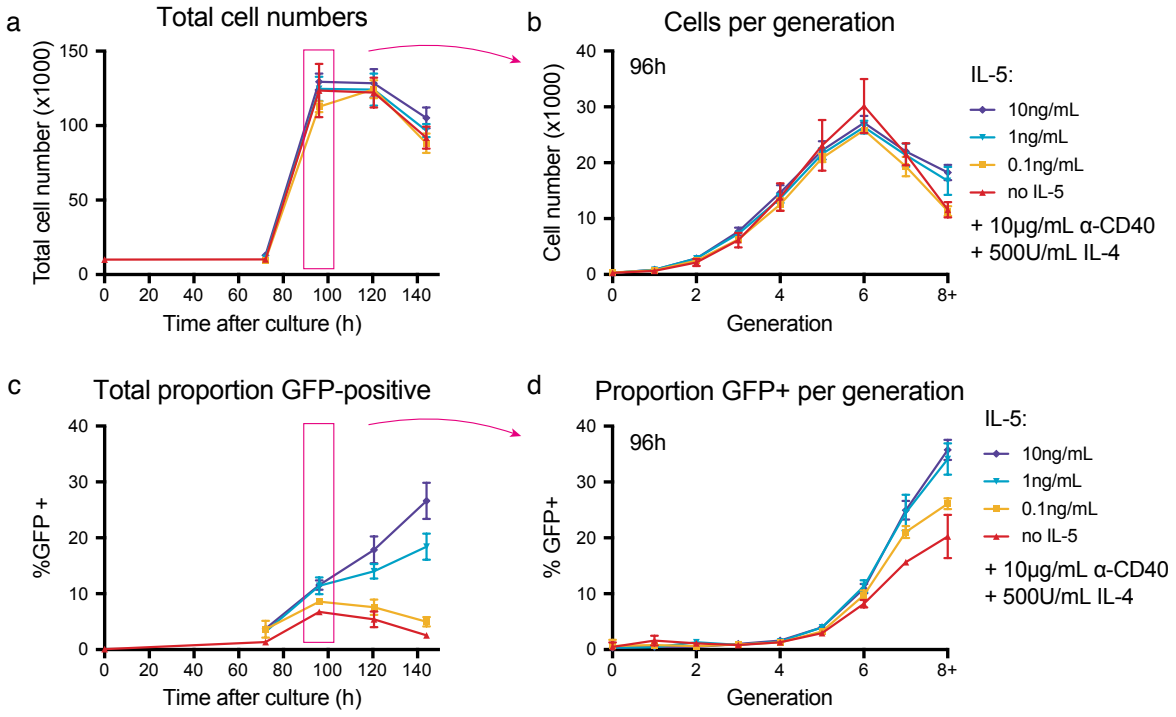

Figure 4.1: Differentiation is generation-linked, and enhanced with the addition of IL-5.

a) Total cell numbers over time for cells cultured with 10 µg/mL anti-CD40, 500 U/mL IL-4, and varying concentrations of IL-5. **b)** Cell numbers per generation as determined by CTV gating, at 96 h post-stimulation. **c)** Total proportions of differentiated cells (Blimp-1-GFP-positive) as they appeared over time in each culture condition. **d)** Proportions of Blimp-1-GFP-positive cells from each generation 96 h after stimulation, indicative of differentiation to ASC. Mean +/- SEM. Data representative of 3 independent experiments.

was revealed as a consistent increase with successive divisions (**Figure 4.1d**), despite very little differences in cell numbers at the varying IL-5 concentrations. Thus, IL-5 was included in subsequent experiments to amplify differentiation outcomes without affecting division or death as competing cell fates.

4.2.2 Long-term imaging identified the effect of generation progression on differentiation outcomes

In order to better understand cell fate allocation behaviours that produce division-linked differentiation, times to single cell fates from last mitosis were measured using long-term imaging. Healthy Bcl-2-overexpressing mice (VavP-Bcl2-69, Methods 2.1 – 2.2) were included as a means of either removing or delaying cell death as a competing fate, and filmed alongside mice that were wild-type for this gene. All experiments here used cells from Blimp-1-GFP reporter mice, with the exception of the C57BL/6 (wild type) controls used to set the GFP positive/negative thresholds for both flow cytometry and microscopy image-processing.

4.2.2.1 Experimental design

As illustrated in **Figure 4.2**, naïve B cells were harvested and purified from the spleens of two Bcl-2 transgenic, Blimp-1-GFP reporter mice (Bcl-$2^{Tg/+}$ Blimp-$1^{GFP/+}$, henceforth referred to as 'Bcl-2-Tg'); two Bcl-2 wild type, Blimp-1-GFP reporter mice ($Bcl2^{+/+}$ Blimp-$1^{GFP/+}$, 'Bcl-2-WT'), and one C57BL/6 wild type mouse ($Bcl2^{+/+}$ Blimp-$1^{+/+}$, 'WT' control) in preparation for filming. Cells from each genotype were cultured at 10^5 cells/mL in 6 mL media, with low anti-CD40 (2.5 µg/mL), high IL-4 (500 U/mL), and IL-5 (5 ng/mL) to maximise observable differentiation events, while maintaining a steady rate of proliferation. Concurrent control samples with identical stimulation conditions were cultured at 5 x 10^4 cells/mL in 200 µL triplicate wells, for monitoring by flow cytometry over the next four days of culture (**Figure 4.3**).

On day 4, after cells had begun proliferating and were distributed across approximately nine generations including an undivided cohort, the Bcl-2-WT and Bcl-2-Tg populations were harvested and sorted for undifferentiated (Blimp-1-GFP negative) cells in generations 0, 2, 4, and 6. These eight populations were seeded into individual wells of two chamber slides, at 5 x 10^4 cells/mL in 250 µL filming media (Advanced BCM-F, phenol red free) with fresh stimuli, where each well was lined with a 50 µm microgrid to isolate individual cells into paddocks for tracking (Methods 2.10). Remaining cells were distributed across six plates in duplicate or triplicate cultures at 5 x 10^4 cells/mL in 200 µL with stimuli for a concurrent flow cytometry time course, and analysed at twice-daily time points for the duration of the imaging experiment (**Figure 4.4, 4.5**).

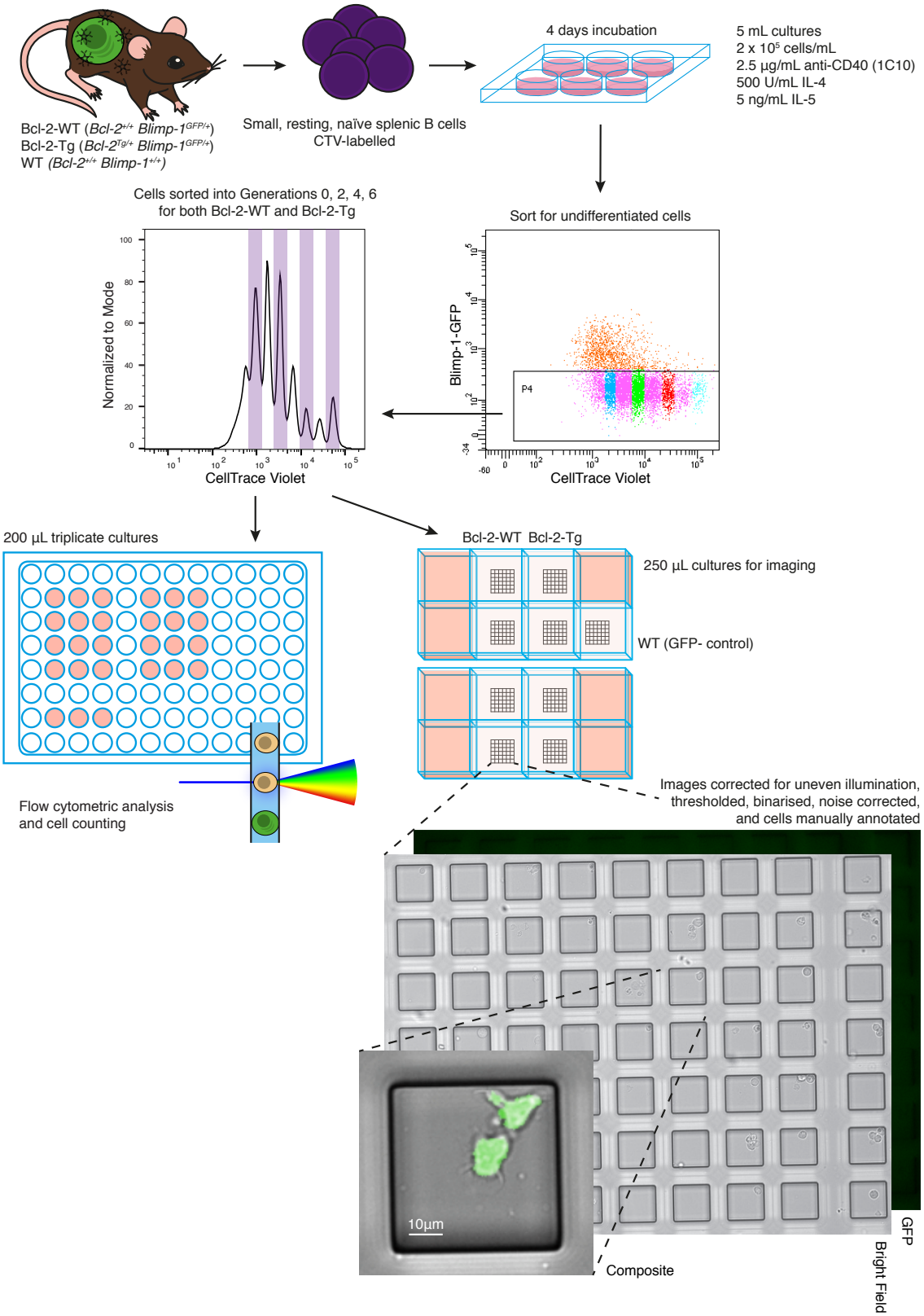

Figure 4.2: Protocol for imaging Bcl-2-Tg and Bcl-2-WT cells sorted into individual cell generations.

Cells from Bcl-2-Tg mice or Bcl-2-WT mice (and C56BL/6 controls) were cultured in 5 mL 2.5 µg/mL anti-CD40, 500 U/mL IL-4, and 5 ng/mL IL-5 for four days prior to imaging. (Concurrent 200 µL cultures were set up for flow cytometry analyses.) Cultures for filming were harvested 84h after initial stimulation, and sorted for Blimp-1-GFP-negative cells occupying generations 0, 2, 4, or 6. Sorted cells were cultured with stimuli in phenol-red-free media (Advanced BCM-F) for imaging, and remaining cells plated for concurrent culture and analyses by flow cytometry.

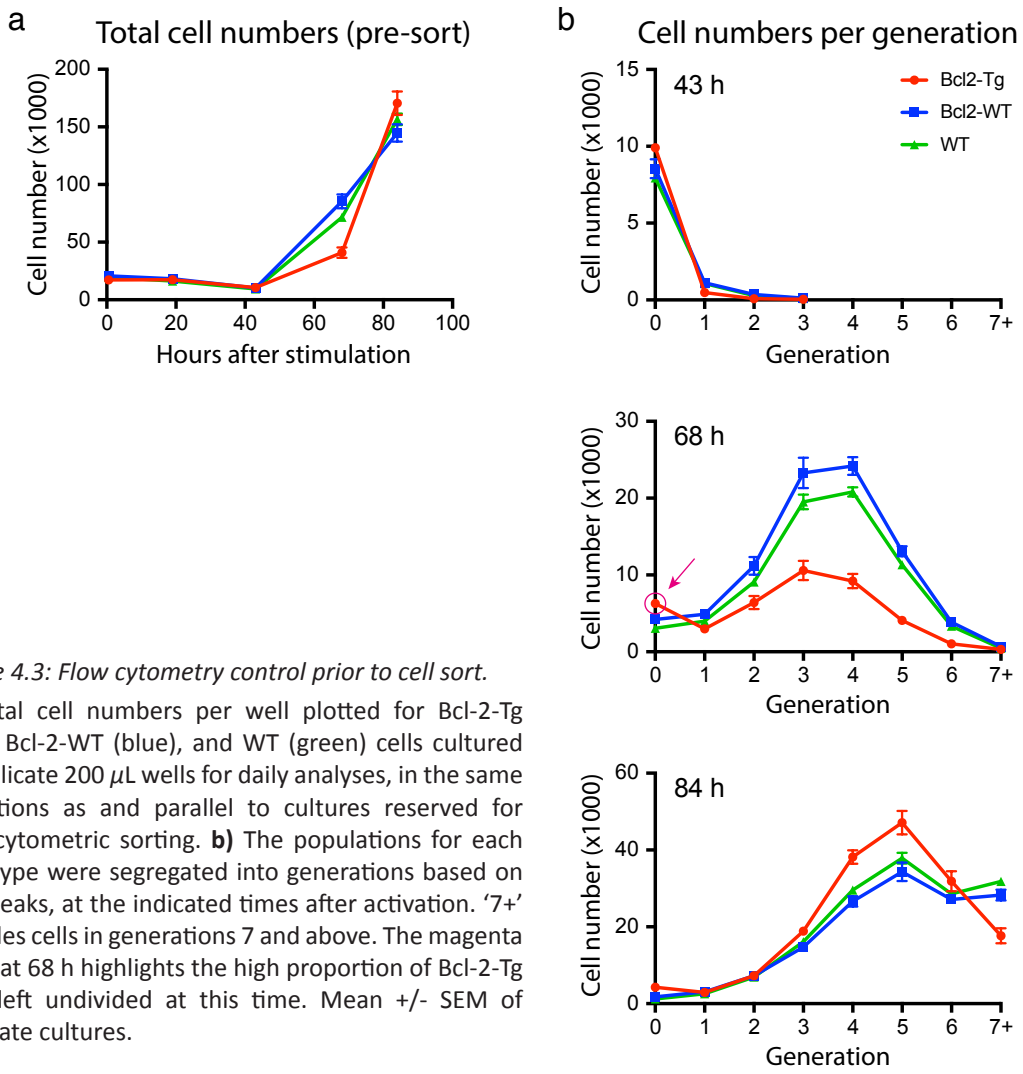

Figure 4.3: Flow cytometry control prior to cell sort.

a) Total cell numbers per well plotted for Bcl-2-Tg (red), Bcl-2-WT (blue), and WT (green) cells cultured in triplicate 200 μL wells for daily analyses, in the same conditions as and parallel to cultures reserved for flow cytometric sorting. **b)** The populations for each genotype were segregated into generations based on CTV peaks, at the indicated times after activation. '7+' includes cells in generations 7 and above. The magenta circle at 68 h highlights the high proportion of Bcl-2-Tg cells left undivided at this time. Mean +/- SEM of triplicate cultures.

Time-lapse images were acquired on a Zeiss Axio Observer.Z1 inverted microscope equipped with a PCO.edge scientific CMOS camera, in the GFP and transmission channels (refer to Methods 2.11). Each microgrid was tiled in a 3 x 4 fashion, totalling 108 positions (including C57BL/6 controls), imaged every 6 minutes over the following 61.8 hours.

4.2.2.2 Population controls confirm division-linked differentiation and Bcl-2 mediated survival advantage

Upon completion of the experiment, flow cytometry data of the bulk control populations were analysed first. To assess the effects of Bcl-2 overexpression on cell fates at the population level, total cell numbers were monitored over the initial four days after stimulation. Bcl-2-Tg cells differed slightly from the Bcl-2-WT and WT controls, as total cell numbers were lower at the 68 h time point soon after commencement of cell division (**Figure 4.3a**). This effect is likely due to a delayed entry into first division, as previously noted [147, 148], and confirmed

by the higher undivided fraction in the Bcl-2-Tg population (**Figure 4.3b**, 68 h). Notably, the Bcl-2-Tg populations had surpassed the controls in cell number by 84 h post-stimulation, suggesting no impediment in proliferation. Since the CTV distribution and hence division profiles between Bcl-2-Tg and Bcl-2-WT remained very similar (**Figure 4.3b**, 84 h), Bcl-2 overexpression did not appear to affect division rate.

Control populations of cells sorted from different generations were also followed by flow cytometry (**Figure 4.4**). Both the Bcl-2-WT and Bcl-2-Tg cultures continued proliferating after re-culture, although for both groups, cells sorted from the undivided portion (generation 0) were significantly slower to increase in number (**Figure 4.4a, b**) compared to the other generations. Cells sorted from generations 2, 4, and 6 expanded rapidly, and based on CTV profiles, appeared to successfully progress through multiple further generations (**Figure 4.4b**). For generation 0, however, a large proportion of the sorted cells remained undivided. A comparison between Bcl-2-WT and Bcl-2-Tg indicated that cells overexpressing Bcl-2 typically accumulated more divisions, and also reached higher cell numbers compared to their WT counterparts across the time series, presumably as a consequence of enhanced survival allowing more cells to divide.

For the above control cultures, proportions of cells that differentiated to ASC from each sorted population were also compared by relation to generation number (**Figure 4.5**). Cells sorted from generation 6 differentiated more quickly per division than those from generation 4, which in turn accumulated ASCs faster than cells from generation 2, consistent with generation-linked changes in rates for differentiation reported previously [67]. Generation 0 cells appeared to differentiate at a similar low rate to those sorted from generation 2 (**Figure 4.5a, b**). Despite differences in cell numbers, the rate of differentiation observed over time was found to be similar for both Bcl-2-WT and Bcl-2-Tg when compared in this manner.

Thus, segregation into generations using CTV peaks demonstrated that the proportion of cells differentiated to ASC were comparable between the Bcl-2-WT and Bcl-2-Tg cultures at both the population (**Figure 4.5a, b**) and generation levels (**Figure 4.5c**).

Overall, the features of differentiation and proliferation for population data were as expected: Despite the small early difference in cell numbers between Bcl-2-Tg and Bcl-2-WT cells, differentiation behaviour was similar, and demonstrated generation-linked behaviour across time, regardless of generation. Having confirmed the population controls indicated the culture conditions were successful, microscopy images were then analysed for single cell fate outcomes.

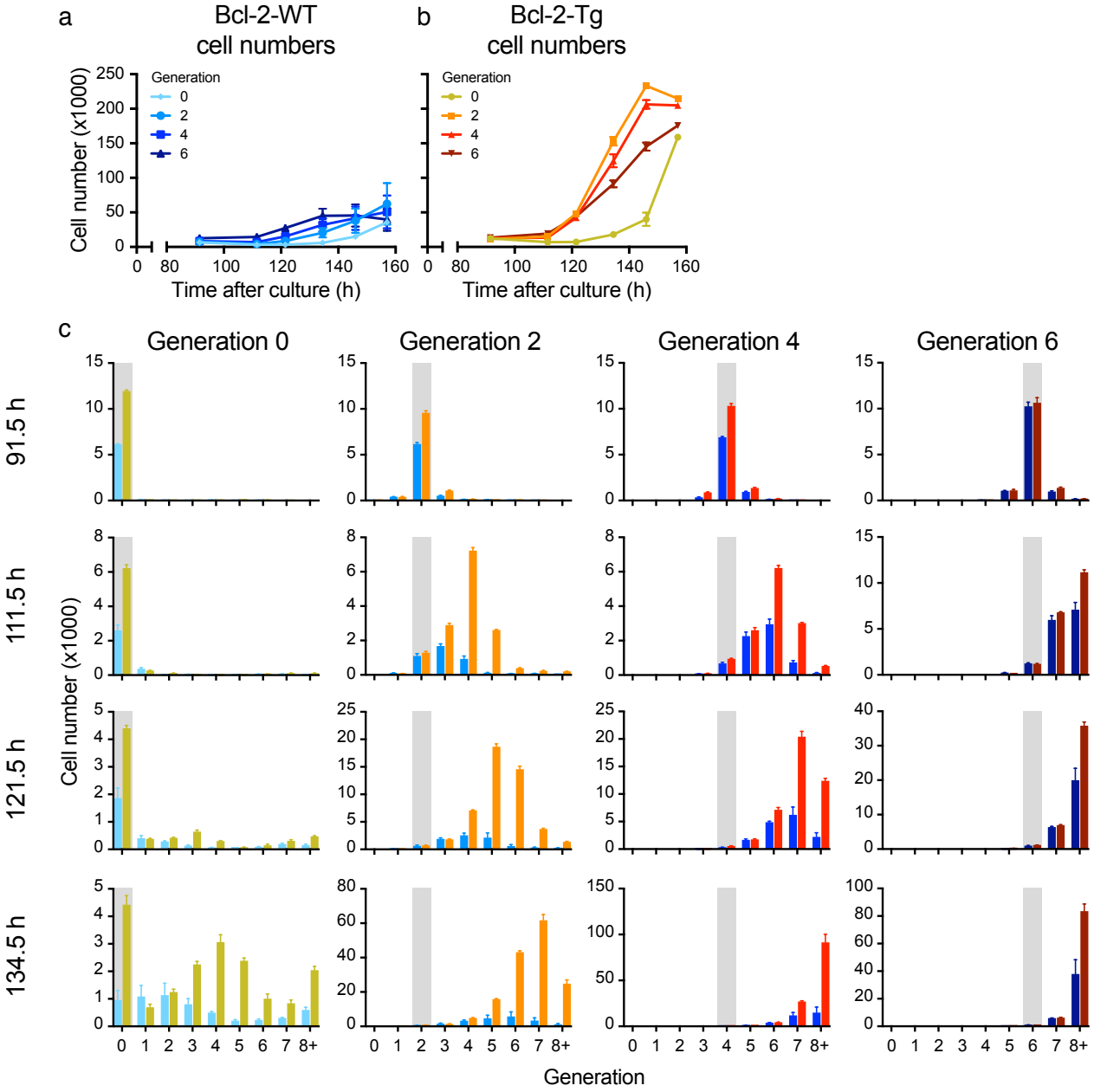

Figure 4.4: Flow cytometry analyses of cells sorted into generations: proliferation.

Total cell numbers over time of cell populations sorted 84 h after culture, into generations 0, 2, 4, or 6 from **a)** Bcl-2-Tg or **b)** Bcl-2-WT populations. Sorted cells were restimulated 89 h after initial culture, and plated into triplicate wells in replicate plates for flow cytometric analyses. **c)** Cells from the first four time points, where CTV resolution was optimal, were segregated into generations for either Bcl-2-Tg (red) or Bcl-2-WT (blue) and plotted for comparison. Mean +/- SEM

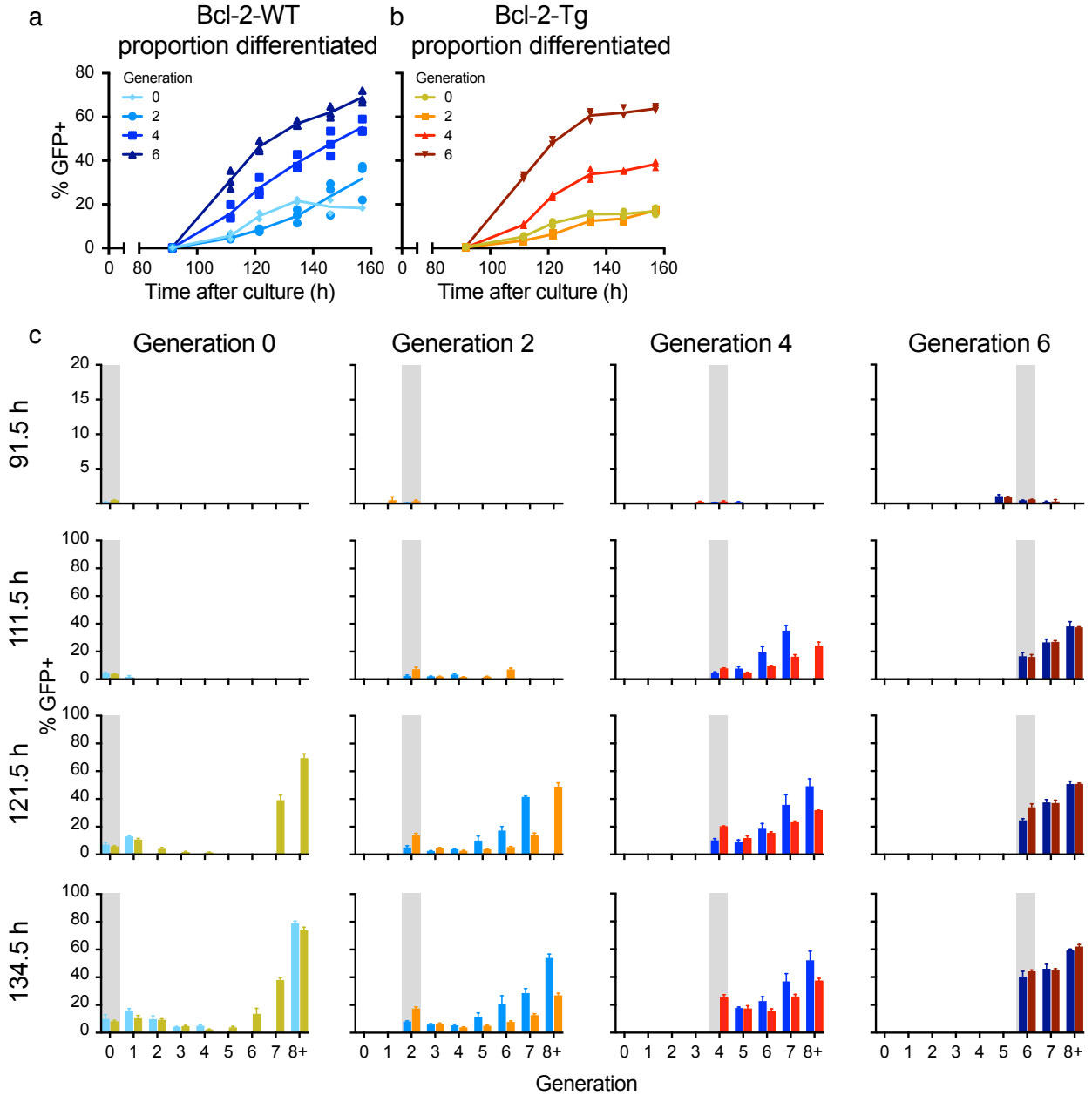

Figure 4.5: Flow cytometry analyses of cells sorted into generations: differentiation.

Proportion of cells differentiated over time for cell populations sorted 84 h after culture, into generations 0, 2, 4, or 6 from **a)** Bcl-2-Tg or **b)** Bcl-2-WT populations. Sorted cells were restimulated 89 h after initial culture, and plated into triplicate wells in replicate plates for flow cytometry analyses. **c)** Proportion of differentiated cells per generation for either Bcl-2-Tg (red) or Bcl-2-WT (blue) cells, when 100 or more cells were analysed from each gate in the indicated generation. Mean +/- SEM

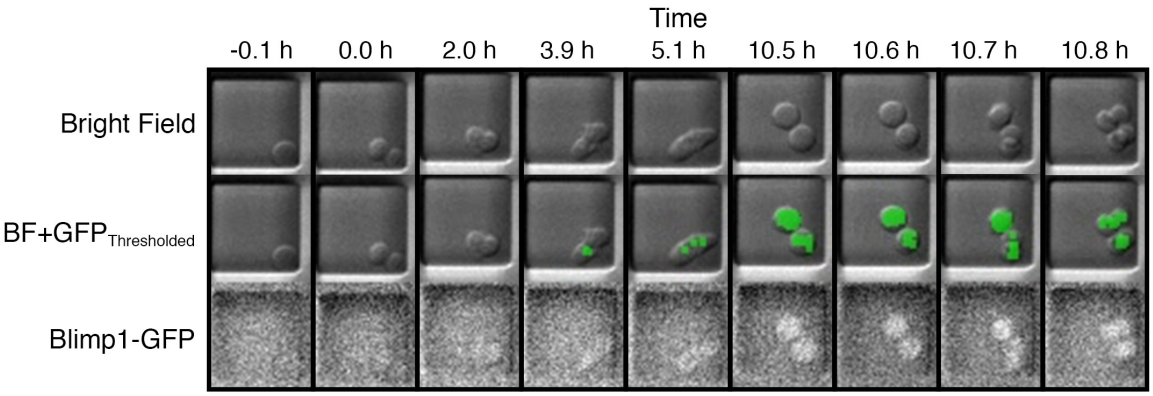

Figure 4.6: Manual tracking of cell fates using live cell imaging.

B cells from Blimp-1-GFP reporter mice that either over-expressed Bcl-2 (Bcl-2-Tg) or were wild type at the Bcl-2 locus (Bcl-2-WT) were stimulated with anti-CD40 antibody, IL-4, and IL-5. On day 4, undifferentiated cells were sorted into generations 0, 2, 4, or 6, and placed into separate wells of a chamber slide for filming. Chambers contained microgrid inserts to separate individual cells into 'paddocks'. Images were acquired in the transmission and GFP channels using a Zeiss Axio Observer.Z1 equipped with environment chamber to maintain 37°C, 5% CO_2, and humidity. Automated rounds of 108 positions were acquired at 6 minute intervals. Raw images in the GFP channel were corrected for uneven illumination, noise, thresholded, and binarised for visual scoring. Cells that occupied individual wells were followed and their first division event recorded. Subsequent daughter cells were tracked for their differentiation, division, and death times. Sample images from one paddock are shown, with the first division assigned as 'time 0'. One daughter differentiates into an ASC at 3.9 h and divides at 10.8 h, the other differentiates at 5.1 h and divides at 10.7 h.

4.2.3 Bcl-2 delayed death times and increased the proportions dividing cells

Time-lapse microscopy images were processed using a pipeline developed by Andrey Kan (WEHI) as a series of MatLab scripts, to objectively identify differentiation times as the Blimp-1-GFP reporter cells began to produce GFP (Methods 2.12). These steps were similar to those used previously (Chapter 3, [126, 128, 141]). Resulting images were cropped into individual paddocks and compiled into time-lapse movies for manual analysis, with the same paddock displayed in the bright field and raw GFP channels, and an additional panel for bright field overlayed with thresholded and binarised GFP fluorescence (**Figure 4.6**).

Paddocks which contained a single cell that would go on to divide were identified and tracked, and the fates of at least 50 starting cells and their 100 or more daughters were recorded for each of the populations sorted from generations 2, 4, or 6, for both the Bcl-2-Tg and Bcl-2-WT populations. Meanwhile, for cells sorted from undivided populations (generation 0), 164 progenitor cells were followed from Bcl-2-Tg and 165 cells from Bcl-2-WT regardless of fate. Frame numbers were recorded for when cells divided, died, or started expressing Blimp-1-GFP, and cells were tracked until they either died, divided again, or could no longer be tracked (classified as 'lost') due to movement away from the field and/or plane of view, or imaging ceased as the experiment ended (see Methods 2.13). These values were then translated into times to fates from mitosis for generations 1, 3, 5, and 7, or for generation 0, time from the commencement of filming, 90.75 h after initial stimulation.

A large number of cell 'losses' were recorded for generations 0 and 1 (**Figure 4.7a**), predominantly due to the fraction of cells that survived the extent of the imaging without either dividing or dying (see section 4.2.6). In contrast, the proportions of fates followed for generations 3, 5, and 7 were high, with 87% or more of cells traced until division or death. Due to this apparent discrepancy in generation 1 selecting for a small proportion of cells with delayed entry to first division by their progenitors, we focussed our initial analyses upon cells sorted from generations which were actively proliferating at the time of cell sorting (ie. generations 2, 4 and 6).

Inspection of the raw filming data revealed non-uniform distributions for division, death, and differentiation when timed from mitosis, for both Bcl-2-WT (**Figure 4.7b**) and Bcl-2-Tg (**Figure 4.7c**). Division times in particular appeared to conform approximately to right skewed distributions, predominantly occupying narrow time ranges in the first 20 h, as previously observed [128]. Death times were more broadly distributed than division times, and as expected, tended to occur later for Bcl-2-Tg populations than for Bcl-2-WT. The majority of differentiation events occurred within 40 h of mitosis. By contrast, cell loss events appeared not to relate to mitosis time and showed no consistent pattern, as would be expected for a randomly occurring event.

Proportions of cells that underwent division, death, or differentiation were enumerated (**Figure 4.8a**), in conjunction with mean times to each fate (**Figure 4.8b**). Comparisons between genotypes revealed that smaller proportions of cells died with Bcl-2-Tg, compared to Bcl-2-WT. Conversely, Bcl-2 overexpression also increased the proportions of cells observed to divide. Meanwhile, for the proportions of cells that differentiated to ASC, Bcl-2 overexpression had little, if any, effect. Across the generations, the proportions of cells observed to undergo each fate remained largely the same (**Figure 4.8a**), while times to GFP expression appeared to decrease with increasing generation number (**Figure 4.8b**). As complex simultaneous changes in multiple fates are expected if competition is operating, Kaplan-Meier (KM) analyses were employed to untangle censored fate times (**Figure 4.9**).

For this analysis, division times were considered censored by deaths and losses, death times by divisions and losses, and differentiation times by division, death, and loss outcomes. Uncensored KM estimates of times to each fate are illustrated in **Figure 4.9**. As noted in the previous chapter, this analysis indicates that under these culture conditions not all cells are destined to divide, even if they do not die (**Figure 4.9a**). Surprisingly the projected proportion of non-dividing cells per generation, indicated by the plateau, is different between Bcl-2-WT and Bcl-2-Tg cells (50% compared to approx. 80%). Despite the larger frequency of dividing cells, Bcl-2 overexpression did not appear to affect the time taken for those cells to divide (**Figure 4.9a**). In each condition, the majority of cells that divided achieved their fate by approximately 22 h, regardless of genotype or generation number. From there, the

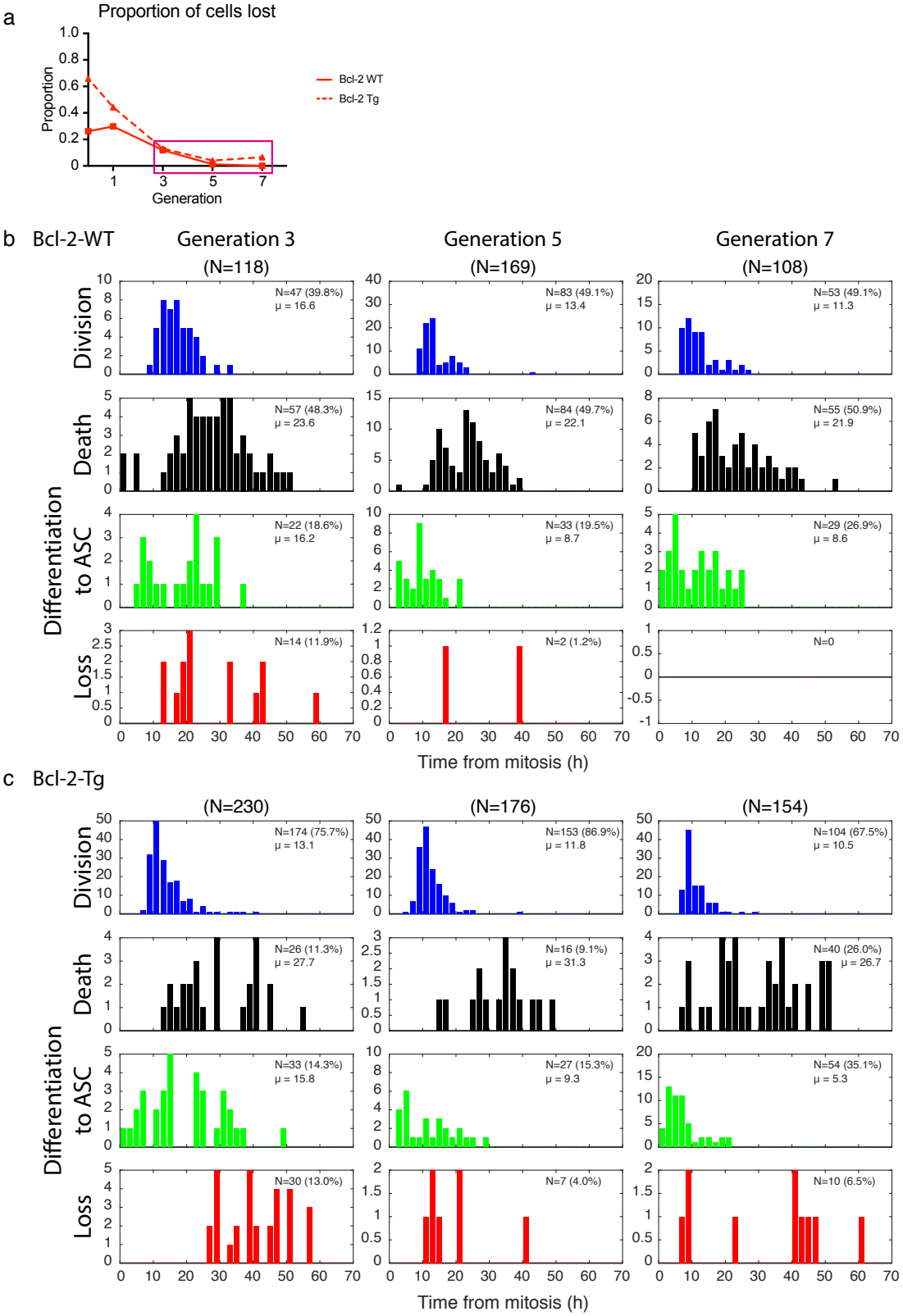

FIgure 4.7: Quantifying filming data.

a) Proportions of cells which could not be tracked until division or death, and were deemed 'lost'; largely due to the cessation of imaging. For generations 3, 5, and 7, where the vast majority of cells divided or died within the microscopy experiment, histograms are plotted of times to divide (blue), die (black), differentiate to ASC (green), or when cells were lost (red) for both **b)** Bcl-2 WT and **c)** Bcl-2 Tg populations. Times to fates were calculated from last mitosis. μ = geometric mean event time (h).

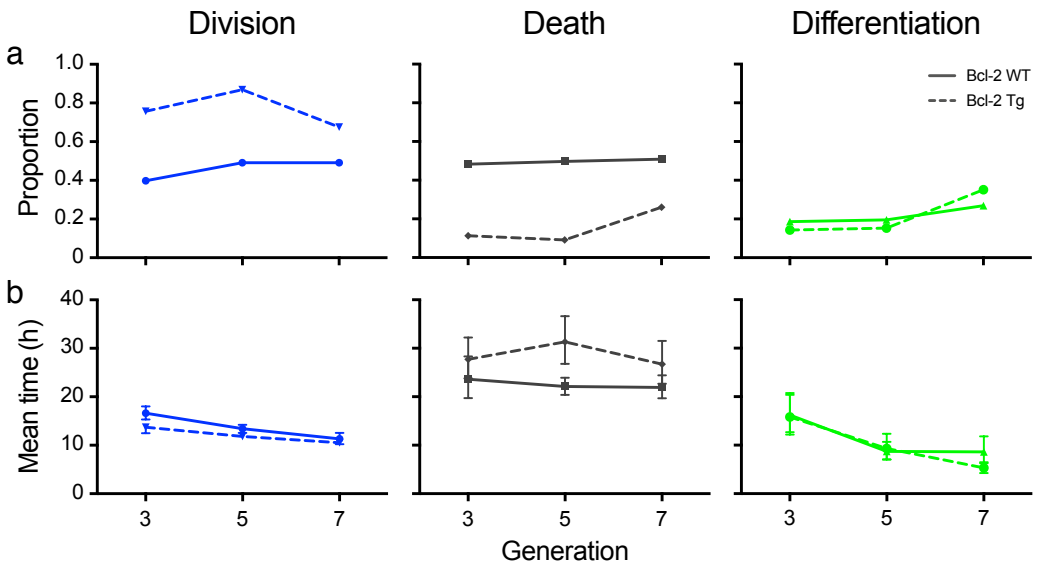

Figure 4.8: Summary of filming data.

a) Proportions of Bcl-2-WT (solid) or Bcl-2-Tg (dashed) cells observed to undergo division, death, or differentiation, tracked from generations 3, 5, and 7. **b)** Geometric mean times between initial mitosis and observed cell fates (95% CI).

KM plots began to plateau, indicative of a difference in the total proportion of cells capable of dividing between Bcl-2-Tg and Bcl-2-WT (dashed line, **Figure 4.9a**).

The Bcl-2-Tg genotype was included in this experiment in an attempt to delay death, and therefore uncensor and observe more differentiation events. Both these requirements appeared to have been satisfied. Death was delayed by approximately 11.5 h in the Bcl-2-Tg populations (**Figure 4.9b**), and there was no statistical difference between differentiation times for Bcl-2-Tg compared to Bcl-2-WT for each generation (**Figure 4.9c**, Log-rank test in GraphPad Prism, using one randomly selected sibling of each pair).

4.2.4 Increasing generation number decreased the time required for cells to differentiate, without affecting proportions

This single cell data was explored in more detail to evaluate how generation number was influencing differentiation. KM survival estimates were plotted together to compare generations 3, 5, and 7, for both Bcl-2-WT (**Figure 4.10a**) and Bcl-2-Tg (**Figure 4.10b**), using one randomly selected cell from each sibling pair to fulfil the assumption of independence between events (see section 4.2.5 for linked sibling fates). Whereas the changes in distributions of times to fates between generations were ambiguous with the Bcl-2-WT populations, the inclusion of Bcl-2 overexpression, and hence delayed death and censorship, allowed the differences in uncensored distributions to be visualised more clearly (**Figure 4.10b**). Model fitting was thus attempted on the Bcl-2-Tg data (**Figure 4.11**).

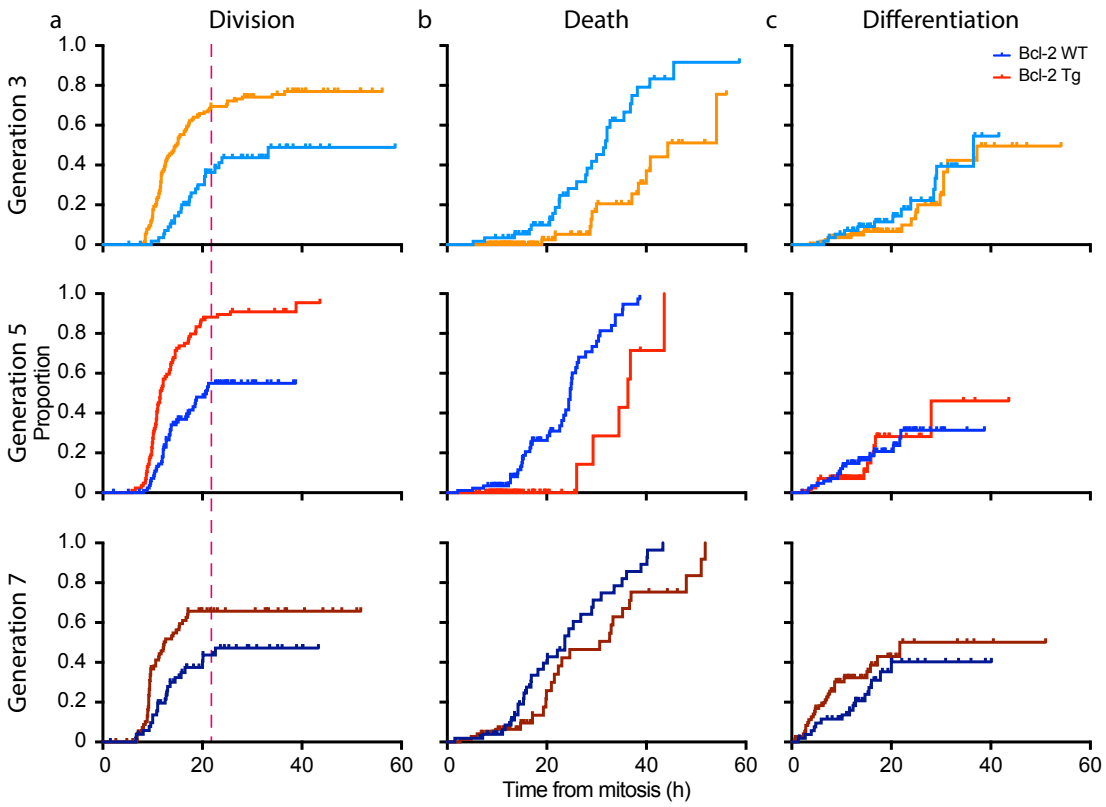

Figure 4.9: Uncensored division, death, and differentiation times.

Kaplan-Meier survival estimates of uncensored times to fates, calculated from last mitosis (0 h), depicting one randomly selected cell from each sibling pair in generations 3, 5, and 7. **a)** Proportions of cells divided over time, uncensored from deaths and losses. **b)** Proportions of cells that died over time, uncensored from divisions and losses. **c)** Proportions of cells differentiated over time, uncensored from divisions, deaths, and losses. 'Steps' mark each event of interest, while check marks indicate censoring events.

Log-normal cumulative distribution functions (CDFs) were fitted directly to the KM survival estimates, to quantify the probabilities of undergoing each fate over time (Methods 2.14). The survival estimates for each fate across generations 3, 5, and 7 were first fitted freely (with the exception of p=1 for death), using the least sum of squared differences between a log-normal CDF and the observed data. Resultant curves are overlaid in **Figure 4.11a**. These same CDFs were plotted as probability density functions (PDFs) in **Figure 4.11b**, listing model parameters of mean (μ) and standard deviation (σ) for the log-transformed data, and the propensity (p) for the fate to occur in the absence of censorship.

Inspection of modelled PDFs reinforced the observation that the distribution of division times changed little with increasing generation numbers. Meanwhile, for both differentiation and death, the mean times to fates reduced markedly with increasing generation numbers. Fitted curves were mapped only until the last event of interest, due to the lack of power in data towards the end of KM distributions, and to minimise any skew to the fitting due to the remaining censoring events. Nevertheless, the data suggested that only a limited proportion of cells are able to differentiate in each generation, and that the proportion remains the same regardless of division number. Consequently, constrained fits were

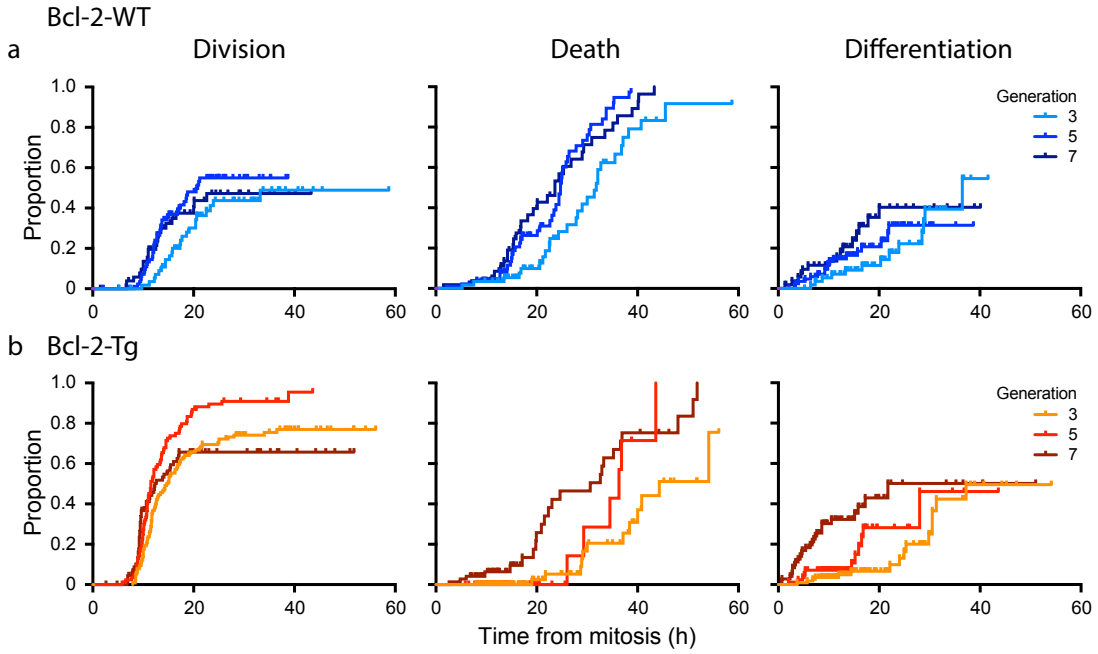

Figure 4.10: The effect of generation number on times to fates.

Kaplan-Meier survival estimates for uncensored division, death, and differentiation times were compared for generations 3, 5, and 7, in both **a)** *Bcl-2 WT, and* **b)** *Bcl-2 Tg populations. One randomly selected cell from each sibling pair is plotted.*

tested where a single optimal division time probability was mapped to all three generations (9 → 3 parameters; same μ, σ, p) (**Figure 4.11c**), and times to differentiate (μ, σ) varied between generations, but retained the same propensity (9 → 7 parameters, equal p) (**Figure 4.11d**). Resulting modelled fits deviated little from the data compared to the free fits, despite the fewer parameters (**Figure 4.11d**). This result suggests that approximately 50% of cells in each generation (p = 0.54) are committed to differentiate. Furthermore, that the median time to differentiate (calculated by exp^{μ}, μ = log-transformed mean) is reduced by 10 hours from generations 3 to 5, and by a further 12 hours from generations 5 to 7.

Together, analyses of the Bcl-2-WT, Bcl-2-Tg, and model-fitting data indicated that the number of divisions after B cell activation did not substantially affect division times from last mitosis, but shortened both death and differentiation times. Faster differentiation times with increasing generation number was consistent with the hypothesis that differentiation times would more frequently outcompete division or death in cells that undergo many divisions, leading to division-linked increases in differentiation frequency. Proportions of cells with the capacity to undergo each fate, however, appeared unaffected.

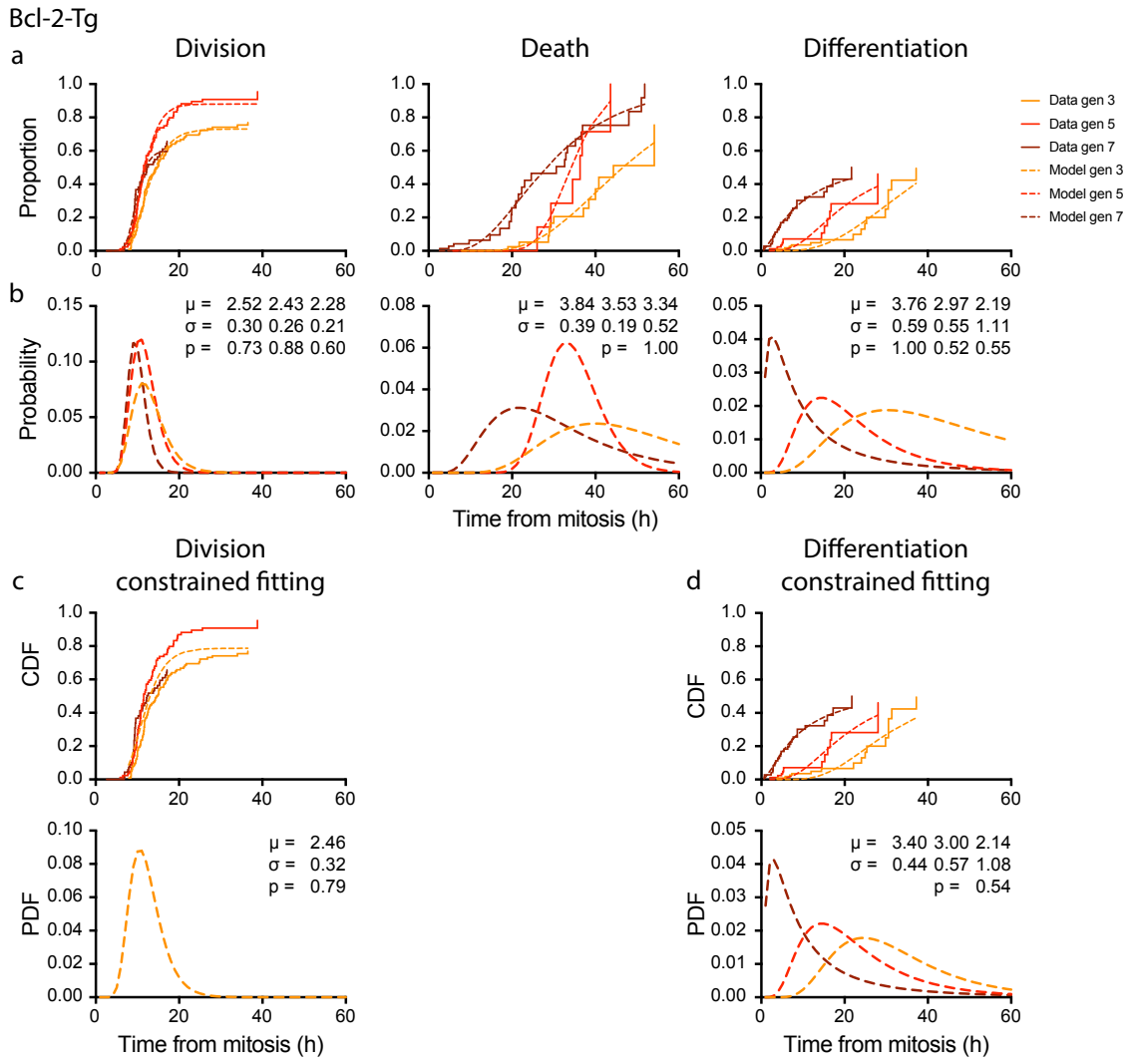

Figure 4.11: Model-fitting to Bcl-2 Tg data

a) Log-normal cumulative distribution functions (CDF) were fitted to the Kaplan-Meier estimates for generations 3, 5, and 7 for each fate, using the least sum of squared differences. Probability of death was constrained to 1, all other parameters were fitted freely. **b)** Fitted CDFs are plotted as probability distribution functions (PDFs). Log-transformed mean (μ) and standard deviation (σ), and probability (p) parameters are listed for generations 3, 5, and 7, respectively. **c)** Division times were re-fitted with the same distribution for each generation (9 → 3 parameters), and **d)** differentiation times were re-fitted with the constraint that probabilities were to remain the same between generations (9 → 7 parameters), resulting in $\exp^{\mu}$ = 29.96, 20.09, 8.50 h medians for generations 3, 5, and 7, respectively.

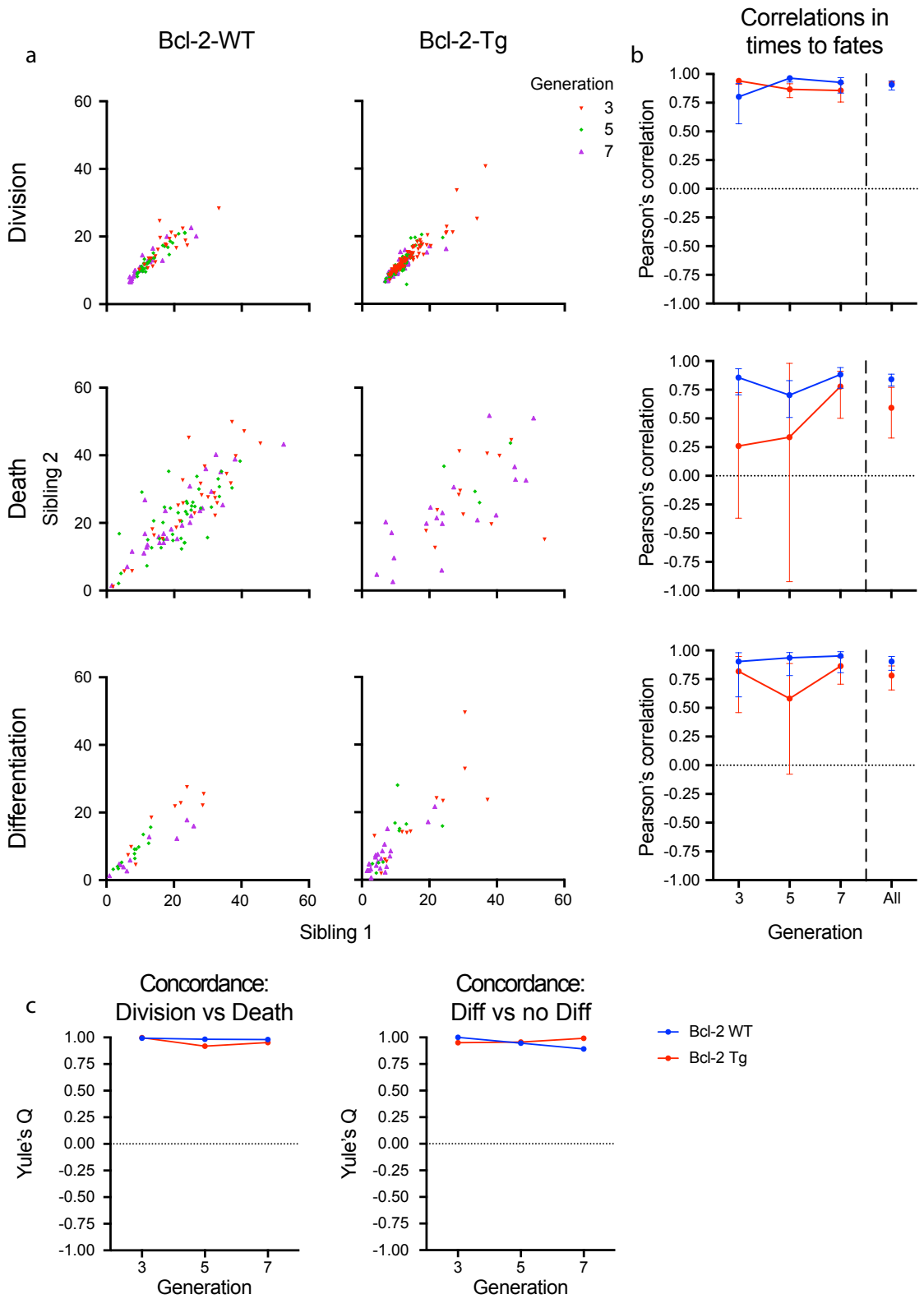

Figure 4.12: Sibling correlations in times to fate and concordances between fate outcomes.

a) Where sibling fate outcomes were concordant, the time for one cell to reach the indicated fate is plotted against the time for its sibling cell; sibling '1' or '2' is randomly assigned. **b)** Pearson's ρ measuring the correlation between sibling times to fates for generations 3, 5, and 7, as well as the pooled data from these generations. (95% CI) **c)** Yule's Q for sibling fate concordance, for division vs death (left), and differentiation vs no differentiation (right).

4.2.5 Sibling fate concordances and correlations remained high regardless of generation number

Statistical tests between times to fates excluded sibling data by randomly choosing one cell of a pair, as these tests assume independence between events, and sibling fates are known to be highly concordant (Chapter 3, [128]). Sibling fate outcomes and times were investigated for these data, to test whether generation number would influence the strong correlations and concordances previously observed.

Yule's Q, used previously for quantifying concordances between sibling fate outcomes [128], was used here as it conveniently reports a value of 0 for no concordance and 1 for perfect concordance [149]. The Yule coefficient of association (Q) is calculated by: (ad-bc)/(ad+bc), where a is the number of pairs in positive agreement, d is for negative agreement, b is where one event has a negative outcome and c is where the other has a negative result. The data demonstrated a very strong association between the fates of sibling cells for both division/death and differentiation (**Figure 4.12a**). Generation number appeared not to affect the high concordances observed, for either Bcl-2-WT or Bcl-2-Tg.

For siblings with concordant fate outcomes, the correlation in their times to divide, die, or differentiate were also determined. These are plotted in **Figure 4.12b**, with sibling '1' and '2' randomly assigned. Pearson's correlation coefficient (ρ) was measured for each fate (GraphPad Prism), for generations 3, 5, and 7 from both Bcl-2-WT and Bcl-2-Tg populations (**Figure 4.12c**). Generation number was found to have little influence on the correlations between times to sibling fate outcomes; consequently, the correlations for each genotype were also measured together for increased statistical power, regardless of generation number (**Figure 4.12c**, right column). Sibling cell fates for division, death, and differentiation were all found to be strongly correlated regardless of Bcl-2 expression.

Thus, these data demonstrate little or no effect of the number of divisions since B cell activation on either the linked fates of sibling cells, or the times required to achieve these fates.

4.2.6 Undivided cells can differentiate and upregulate Blimp-1-GFP many days after the addition of stimuli

In the above analyses, generation number executed a clear effect on differentiation times. From this conclusion emerged the question of whether differentiation required mitosis to occur, or whether division events enhanced the activity of an otherwise slow differentiation timer. To test between these possibilities, we returned to the recorded undivided cells and examined them for their capacity to differentiate to ASC prior to entry to first division.

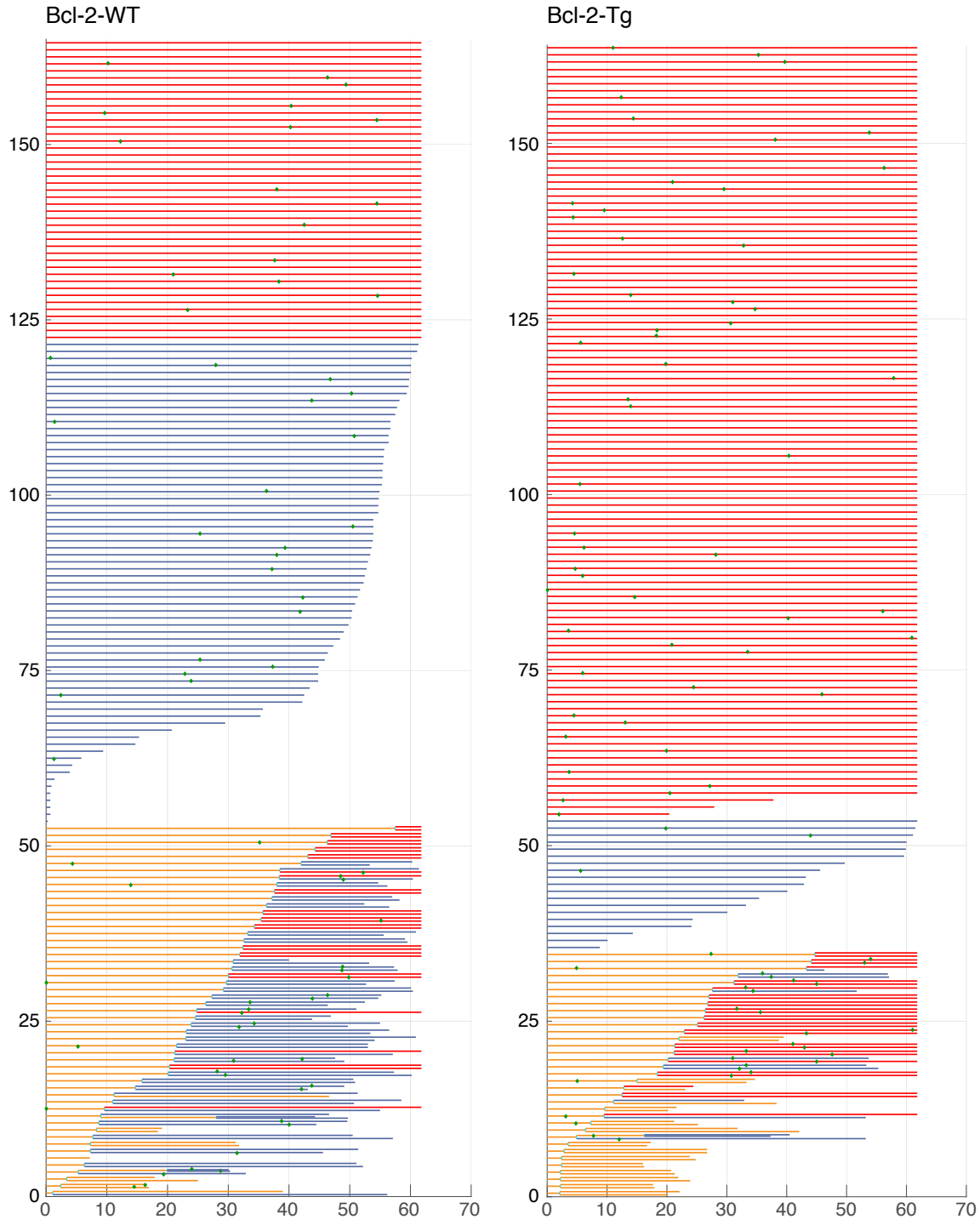

Figure 4.13: Tracked cell fates over time for cells sorted from generation 0.

Each line from the Y axis represents an individual cell that was tracked. Cell fates are colour-coded: red for cells that survived until the end of the imaging experiment, or were lost and unable to be tracked; blue for cells that died; orange indicates cells that divided; green marks are differentiation events. Time is along the X-axis, representative of the 61.8 hours of images. 165 progenitors were tracked from the Bcl-2-WT population, and 164 cells were followed from Bcl-1-Tg.

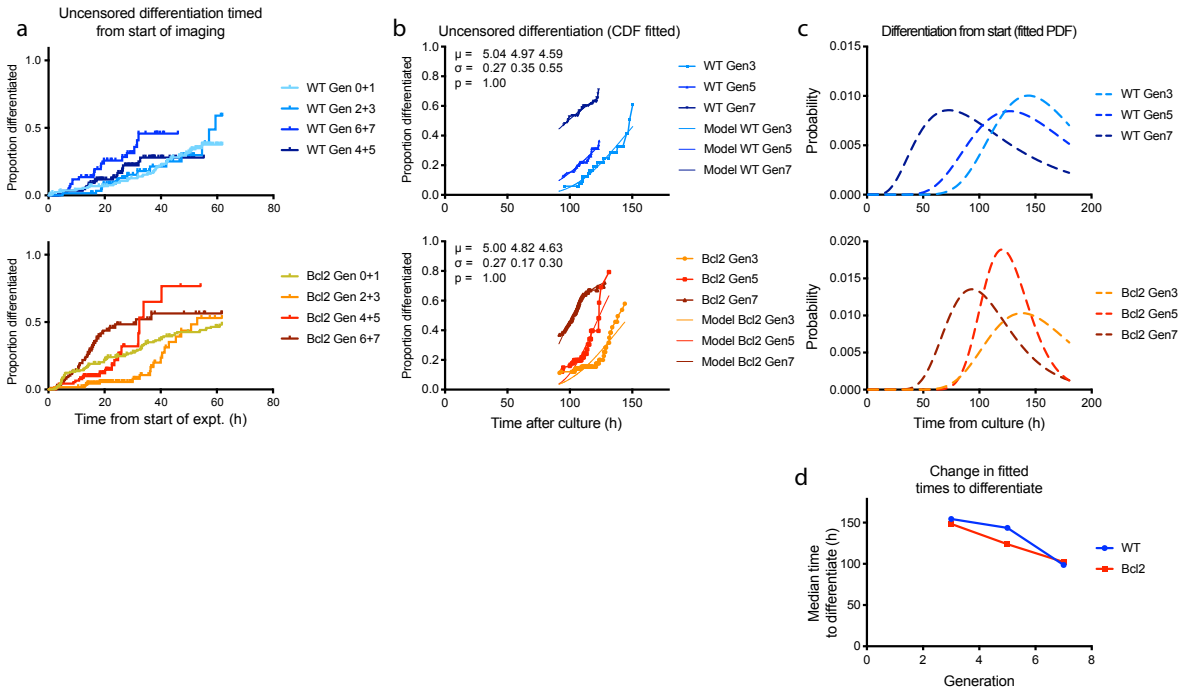

Figure 4.14: Exploring global differentiation timers.

a) Kaplan-Meier estimates of uncensored differentiation times calculated from the commencement of imaging. Included events are: all generation 0 cells, generation 2, 4, 6 cells that also divided, and one randomly selected sibling from each cell pair in generations 1, 3, 5, 7. Censoring events are a second division event, death, or losses of undifferentiated cells. **b)** Estimates of differentiation times adjusted for the existing proportion of differentiated cells at the time of sorting. Fitted log-normal CDFs are overlaid, under the constraint that p remains equal. Log-transformed mean (μ) and standard deviation (σ), and probability (p) parameters are listed for generations 3, 5, and 7, respectively. **c)** PDFs of fitted curves. **d)** Change in median ($\exp^{\mu}$) of modelled times to differentiate for each generation.

Cells sorted as 'generation 0' which were seeded into their own paddocks for filming were tracked from the commencement of filming (91 h after stimulation), regardless of eventual fate. Many did not divide over the next 62 h of imaging (67.9% from Bcl-2-WT, 78.4% from Blimp-1/Bcl-1), and instead died or simply survived until the cessation of the experiment (**Figure 4.13**). Of the fully tracked cells, 24.8% of Bcl-2-WT and 37.7% of Bcl-2-Tg populations were observed to become GFP-positive, indicative of differentiation to ASC, prior to entering any division.

Thus, taken together, these results suggested a hypothesis whereby differentiation did not require cell division, but were somehow accelerated in cells undergoing multiple divisions.

4.2.7 An alternative hypothesis where differentiation is timed from B cell activation

An alternative hypothesis, where differentiation is set in place and timed from initial stimulation, and increased by division, was explored further by plotting observed differentiation times from the commencement of filming (ie. 91 hours after cells were placed in stimulation conditions), rather than time from last mitosis.

For KM estimates from the start of imaging, differentiation times were assumed to be censored not by mitosis, but rather by when cells were no longer followed (ie. if underwent a second division, died, lost, or survived until filming ended). Uncensored times to fates are plotted in **Figure 4.14a**. Despite the cells from each generation having been exposed to stimuli for the same amount of time, different KM estimates emerged for each generation, thus rejecting the possibility that time from stimulation was the sole contributor to differentiation times.

To further visualise how division events could be modulating the likelihood of differentiation when timed from stimulation, the KM estimates for differentiation as timed from the beginning of the imaging experiment were adjusted to represent the observed section of the putative cumulative distribution function (CDF) for total differentiation times (**Figure 4.14b**). First, curves for each generation were shifted to the right by 91 h to account for the time from stimulation. Second, the proportion of unobserved cells that had differentiated between time of activation and cell sorting was estimated using the control flow cytometry data, recording the proportion of GFP-positive cells from the generation being sorted for (2, 4, or 6 to observe generations 3, 5, or 7, respectively). The beginning of each KM distribution was shifted up by the corresponding value for that generation. This step was necessary as exclusion of differentiated cells during cell sorting enriched for cells that remained undifferentiated by this time. As a result, the KM estimates were thus normalised to the remaining proportion of undifferentiated cells at 91 h post-stimulation.

Log-normal CDFs were fitted to each of these curves between the first and last differentiation events for each generation. Initial fits produced very similar total propensities (ie. scale factor p) for differentiation, and so these were constrained to remain constant between generations 3, 5, and 7. Fitted, constrained CDFs mapped to the data reasonably well, and are overlayed on **Figure 4.14b**, with PDFs illustrated in **Figure 4.14c**. These data remain consistent with the hypothesis that division events modify a differentiation likelihood, even if timed from stimulation, by reducing the mean time to differentiate for cells in successive generations.

Quantifying the change in mean times to differentiate between the sorted populations revealed a difference of approximately 25 h (**Figure 4.14d**) – incidentally approximating to the average time taken for two rounds of cell division: the difference between the sorted generations. This result opens up the possibility that differentiation events are not timed from exposure to stimuli, but from the subsequent activation that occurs as cells reprogram gene expression during the transition from quiescent to activated cells, prior to first division. The distinction here is that while all cells are exposed to stimuli at the same time, perhaps not all cells are activated and reprogrammed at the same time. Rather, they initiate gene expression changes across a distribution of times. It follows that cells which activated earlier will begin dividing earlier, and reach higher generation numbers at the time of sorting; while those that took longer to activate divide fewer times. Consequently, the difference between the

populations that were sorted may not have only been the number of divisions undergone, but also the time since cellular fate reprogramming. Under this alternative model, all cells follow a determined series of timed fate changes after an initiating event, but since cells that activate earlier also begin dividing earlier, those in higher generations would produce a greater proportion of differentiated cells compared to those lower generations for the bulk of the response.

Whether the differences observed here between the differentiation times for cells in generations 3, 5, and 7 were *caused* by the number of divisions undergone, or were a *consequence* of the cohort's earlier activation times remains ambiguous with this analysis. These new data shine a light on the question of when differentiation times might be set or changed, and merit further investigation for how they might conform to prior observations of competition with division timed from mitosis, as in the previous chapter.

4.3 Discussion

Single-cell imaging and the de-convolution of competing cell fates was used in the last chapter to record an influence of division times on fate allocations among activated B cell populations. Here, these same tools were utilised to investigate the fate-allocation behaviours behind division-linked differentiation, where cells have been observed to produce more antibody-secreting cells after multiple rounds of division [67].

Culture conditions were selected to maximise the proportions of ASCs produced while still maintaining a range of cell divisions. Consequently, low levels of anti-CD40 stimulation were used based on results from chapter 3, in combination with saturating IL-4. IL-5, a known enhancer of differentiation [67], was included to increase the frequency of differentiation independently of that caused by anti-CD40 levels.

Individual cells sorted from different generations were manually tracked to calculate the times taken from mitosis until cells differentiated, divided, died, or could no longer be tracked. These times to fates were examined both by inspection and using KM survival estimates under the assumptions of independent, competing cell fates.

B cells isolated from Bcl-2 overexpressing mice were included in the study as a means of directly reducing the impact of death as a competing cell fate. KM analyses uncensoring death times from competing division and loss outcomes found that Bcl-2 overexpression delayed the time for cells to die, as expected, by approximately 11.5h. Surprisingly, Bcl-2 also affected division, seemingly by modulating the proportions of cells capable of dividing in each generation, but not the distribution of division times for those cells that do undergo mitosis. Since Bcl-2 has been identified principally as a survival molecule [142], this finding is suggestive of a number of possibilities. For instance, it is possible that high levels of Bcl-2 affect not only survival, but also a cell's decision to divide and prevent the normal cessation of proliferation seen in lymphocytes, known as 'division destiny' [73]. Another possibility exists where by classic cell cycle 'checkpoint molecules', known regulators of apoptosis that trigger cell death when cells are under excessive duress [150], may have alternate or secondary roles in permitting cell division when the cells are producing survival factors in excess. Alternatively, there remains the possibility that a subset of naïve cells which would have terminated with negative selection, instead survived with Bcl-2 overexpression, and after stimulation contributed disproportionately to the higher percentage of dividing cells.

These results appear to contradict early findings that Bcl-2 overexpression reduces the proportion of cells proliferating in both B and T lymphocytes [151, 152]. However a possible explanation for the incongruity becomes more apparent when studying the population as a whole, as with the generation 0 population where all single cells were tracked. Bcl-2 expression

prolonged the survival of these activated but undivided cells, leading to an accumulation of cells that would otherwise have died in the absence of cell divisions. Consequently, when measuring population turnover and proliferation rates, these surviving cells essentially dilute the proliferating population, producing a smaller total proportion of proliferating cells in the presence of more Bcl-2.

For survival times, the use of Bcl-2-Tg revealed a clear decrease in times to die as cells progressed through divisions. Between undivided and actively dividing cells, a large difference in survival times was also observed, and is indicative of reprogramming after B cell activation. Although Bcl-2 enhances survival of both populations, the ~40 h survival times of divided cells is still incomparable to the ~120h or longer survival times of undivided B cells. Earlier studies document the independent effects of Bcl-2 on cell cycle entry and cell survival [153, 154], and these data support the need for assigning separate parameters for 'entry to first division' and subsequent division and death times [94].

Use of the Bcl-2-Tg cells produced no significant impact on uncensored differentiation times compared to Bcl-2-WT. Bcl-2 overexpression did, however, enhance our ability to measure the differences in differentiation rates when comparing across multiple generations. In contrast to CD40 stimulation data, where division times changed and affected differentiation outcomes as a result of competition, control of differentiation to ASC by generation number demonstrated the inverse. Here, with the aid of Bcl-2-Tg to directly remove death as a competing fate, it was shown that increasing division numbers decreased the time required to differentiate, with little change to division times. In the generations analysed here, median differentiation times decreased by over 20 hours between generations 3 and 7, allowing differentiation to not only outcompete death times, but also division times in later generations.

By modelling to the data with a constrained set of parameters, it was found that the underlying propensity for differentiation likely remains consistent regardless of generation number. This result is visually similar to findings presented in [128], however the untangling of multiple competing fates left the previous data set difficult to model using constrained parameters. The use of Bcl-2-Tg here helped reveal underlying patterns of fate control, and the results remain consistent with the competition hypothesis.

Curiously, the propensity for differentiation modelled here was found to be short of 100%. This inconsistency with the previous chapter (where $p = 1$) may be due to the lower concentration of IL-4 used (500 U/mL as opposed to 1000 U/mL), a known driver of differentiation [67]. Although division parameters were deemed to be saturated at both these concentrations (IL-4 titration, data not shown), there may be a difference in saturation thresholds for the two independent cell fates. Further, the finding that not all activated cells have the propensity to differentiate is of interest, given that the lymphoblast gene regulatory network appears to be

a system which *suppresses* Blimp-1 and the plasmablast program [110, 155]. Ultimately the usefulness of a B cell lies in its ability to secrete antibody, and hence expanding cells without the capability of becoming effector cells at first appears wasteful. An explanation may lie in the generation of memory cells – low affinity cells that appear during the germinal centre response, exit the B cell reaction until repeat exposure to antigen, and importantly, do not differentiate to ASC [156]. Indeed, the overexpression of Bcl-2 has been demonstrated to enhance memory cell production [157].

Although all cells sorted from generation 0 were filmed and tracked, they were excluded from our initial analyses searching for trends across generations as the length of the films was not enough to encompass the division or death events in a large proportion of cells, particularly from the Bcl-2-Tg. Surprisingly, however, these undivided cells were still observed to differentiate, as indicated by Blimp-1-GFP expression; a finding not previously reported in B cells. This indicated that mitosis was not required for differentiation and led to the hypothesis that undivided, stimulated cells are already harbouring an active, 'differentiation timer'. Further, it raised the possibility that this timer might be heritable, and influence differentiation time in the progeny of each founder cell. Evidence for heritable timers governing B and T cell fate has recently been shown to regulate the time for division progression [135] as well as survival in other stimulation systems. These studies provided a precedent that led us to examine this possibility for differentiation after CD40 stimulation.

Model-fitting was attempted on differentiation in generation 0 under the assumption of a heritable time to become ASC. Fitted data was consistent with a hypothesis that cells differentiate at a particular rate after activation, modulated by mitotic rounds, but an alternate hypothesis where differences in differentiation arise from variation in times from a putative 'activation' time rather than number of divisions undergone could not be excluded.

By this model, cells are programmed to differentiate at some point between exposure to stimuli and entry to first division, and the designated times to differentiate follows the same distribution for all cells, calculated from time of activation. Therefore, cells that activate earlier are also expected to differentiate earlier, and cells that activate later take longer to become ASC, such that when sampled from a population where division times are consistent, those cells observed to have divided more times also activated earlier and have a shorter wait time until differentiation (**Figure 4.15**). This form of differentiation timer may also remain independent of division times, such that for cells activated at the same time, those that divide more slowly take the same length of time to differentiate as those that divide quickly, consistent with earlier results (Chapter 3). The possibility remains that differentiation times may be insensitive to division number (although limited by phases of the cell cycle that allow changes in gene expression), and investigating this is hindered by our inability to track self-adherent B cells over multiple divisions.

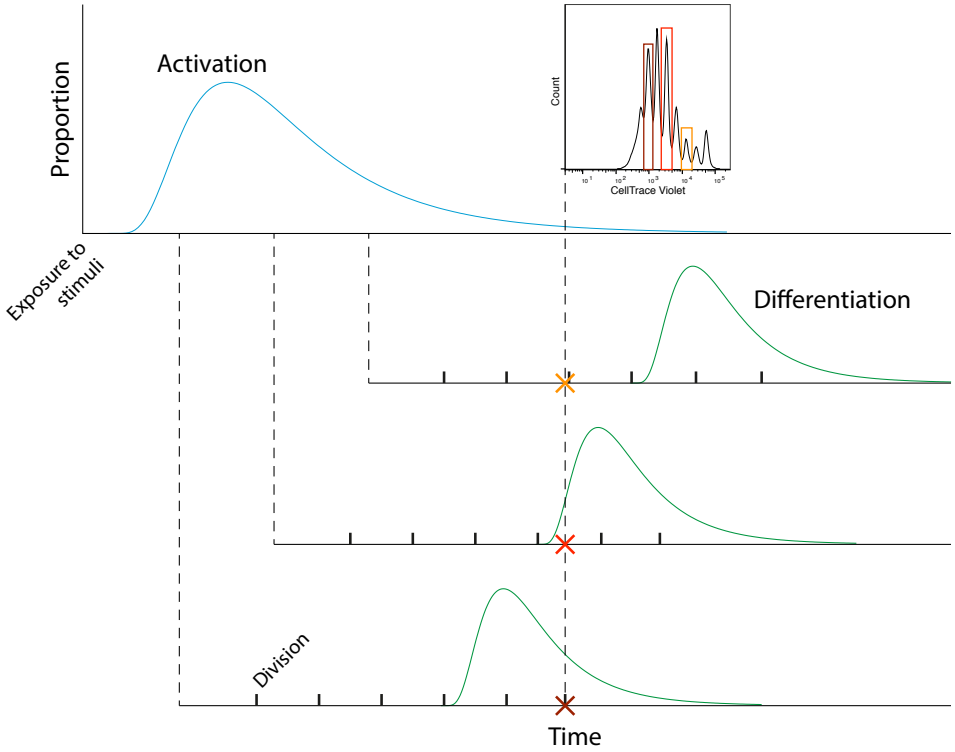

Figure 4.15: An alternate model for differentiation: a global timer regulates time to ASC.

For this model, cells are programmed to differentiate at a set time after 'activation', which occurs some time after exposure to stimuli, and also sets the time of the first division. Division and differentiation otherwise still operate independently, with differentiation time insensitive to the frequency or rate of cell divisions. In a system where divisions progress at a similar rate regardless of activation time or generation number, the observer will see cells distributed across multiple generations, reflective of their activation time and time to first division (CTV profile, inset). Those cells occupying higher generation numbers thus differentiate sooner, due to their earlier activation time.

Whether the observed differences in differentiation times arose from a mechanism that counts the number of divisions undergone, or a count down from activation time, remains indistinguishable without further experiments. Consequently, for the next chapter, the use of cell cycle inhibitors were pursued in an attempt to modulate division times, and directly uncensor differentiation fates.

CHAPTER 5

Manipulating Division times to Uncensor Death and Differentiation Outcomes

5.1 Introduction

The earlier chapters, and previous studies of CD40/IL-4 stimulated B cells provide evidence supporting the presence of independent, competing fates within individual cells. Collectively these data support a concept [125] where upon division, each daughter cell has created, effectively, a set of molecular programs that dictates a pre-determined time to die, a determined time to divide, and a determined time to differentiate, where each of these fate timers are shared with a sibling cell. Data from the previous chapter also supports an alternative extension to this hypothesis for differentiation. By this revision, the timed fate outcome is not initiated de novo by mitosis, but a time to differentiate is set and carried from earlier generations (likely before the first division) and transmitted through the subsequent descendants.

These experiments highlight how statistical analyses and modelling can give insight to the hidden mechanisms behind complex systems, their modes of operation and potential interactions in influencing the outcome of a cell population. Occasionally, multiple models may generate similar outputs, and thus further empirical data is required to distinguish between the possibilities. For the competition hypothesis, a method for removing one or more of the competing fates to directly observe otherwise censored outcomes would be experimentally valuable, and facilitate the study of cell fate allocation under a variety of different stimulation conditions.

In the last chapter, Bcl-2 overexpression was used to successfully delay cell death and enhance the comparison between the differentiation times of the populations under observation. Division times, however, particularly when short, still obscured the direct observation of potential differentiation events. A prediction of the model of competing cell fates is that if division times could be lengthened, even artificially, the likelihood of differentiation would be increased. A further prediction is that blocking cell division would uncensor and reveal the intrinsic cell death time, usually reset upon mitosis. In this chapter, the ability of cell cycle inhibitory compounds to 'uncensor' cell death and differentiation was assessed, and findings used to test the competition hypothesis and its predictions for hidden cell fates.

The use of cell cycle inhibitors to promote differentiation has a precedent in T cell studies. In murine helper T cells, Richter, Löhning and Radbruch [158] exposed naïve, stimulated cells to cell cycle inhibitors with different modes of activation. Days later, cells prevented from dividing were observed to differentiate into IL-4, IL-10, or IL-2 producing T cells, in some cases in greater proportions than in the absence of inhibitors, where cells progressed through multiple divisions. These data are consistent with the model of competing cell fates,

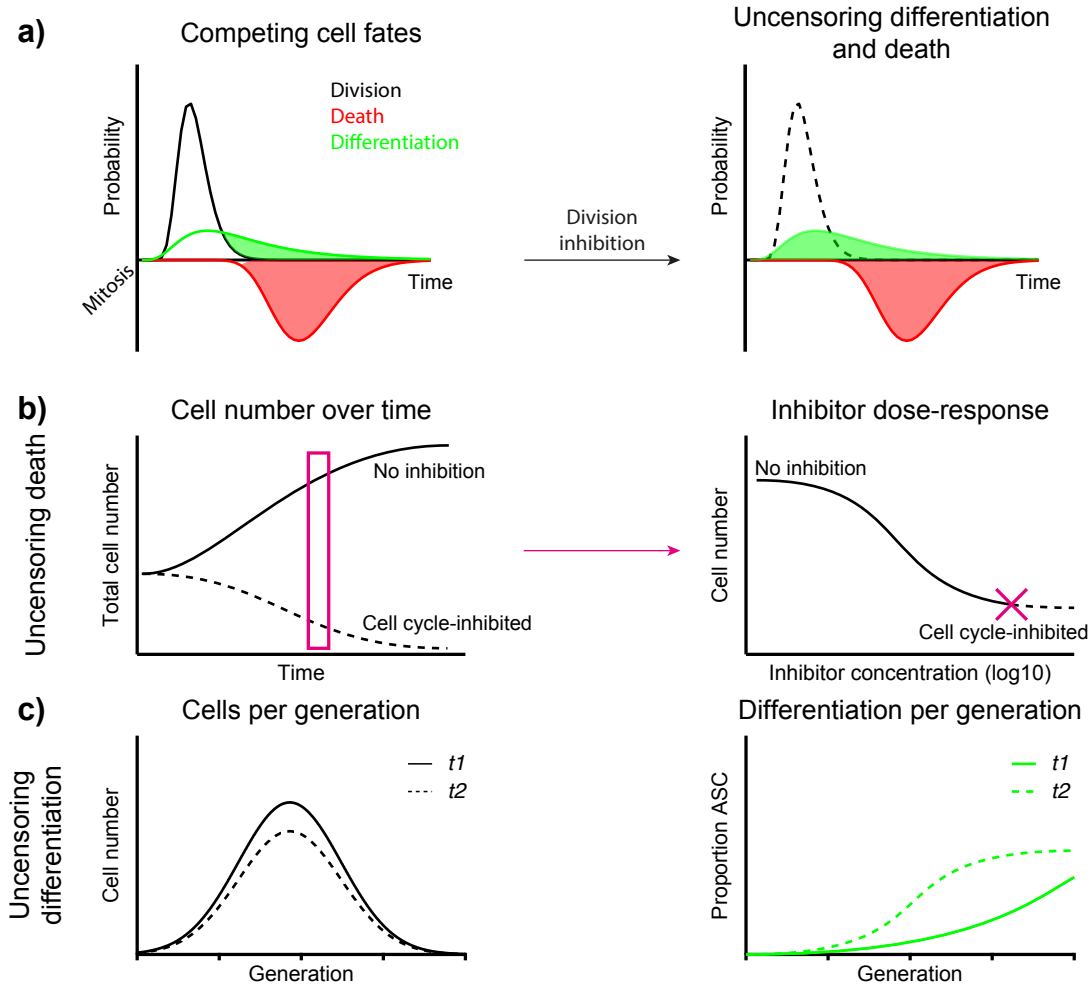

Figure 5.1: Inhibiting division to uncensor cell death and differentiation times.

The model of intracellular fate competition predicts how modifying individual fates can affect the population outcome over time: **a)** Inhibiting cell division will uncensor underlying cell death and differentiation times for the population. **b)** With divisions removed, total cell numbers will not increase over time, but decrease at the rate predicted by the unsynchronised probability distribution for times to die. Cell cycle inhibitory compounds will yield distinctive dose-response curves in total cell numbers, with no change above a concentration where division is completely inhibited. **c)** Without division progression, and hence no mitotic event to censor or redistribute differentiation times, the proportion of cells differentiated to ASC is expected to increase over time. (*t1*, *t2* represent successive time points)

where division censors and restarts differentiation time, as an increased rate of differentiation is an expected outcome of arresting cell division. Given this precedent, the same cell cycle inhibitors – aphidicolin, L-mimosine, nocodazole, and paclitaxel – were assessed here. These compounds were limited in their range of actions and only affected DNA synthesis or mitosis. Thus, to extend the study and include cell cycle inhibition during G_1 phase, compounds affecting cyclin dependent kinases 4 and 6 (CDK4, CDK6), the predominant CDKs driving the cell cycle in B cells [159], were also tested. These and several other inhibitors (Appendix IV) were assessed for their division cessation and uncensoring capabilities.

As the primary targets of the tested compounds are directed at blocking cell division, none of these inhibitors are expected to influence differentiation or cell death pathways directly. Such

an inhibitor would be suitable for testing the hypothesis that inhibiting divisions allows cells additional time to achieve their differentiation threshold, and hence become plasmablasts (**Figure 5.1a**).

The predicted outcomes of an effective division inhibitor are illustrated in **Figure 5.1**. Death of cells will be an automatic consequence of blocking division (**Figure 5.1b**). Notably, the death curve over time for cells that have their division blocked should be the same, irrespective of the inhibitory compound used. By this theory, the death of cells induced by mitotic inhibitors is a product of uncensoring, and not induction of an additional death pathway. Hence, there will be concordance in dose response curves between division cessation and death of cells. Similarly, blocking cell cycle should allow the frequency of cells differentiating in a given generation to increase (**Figure 5.1c**).

The alternative model arising from the last chapter must also be tested, where differentiation timers are dependent on an activation time, and progress irrespective of division events. By this model, a population of division-inhibited cells are expected to continue differentiating at the same rate as untreated cells, as the use of cell cycle inhibitors should not affect activation time and hence will have little effect on plasmablast formation.

The above possibilities are examined in this chapter.

5.2 Results

5.2.1 Efficacy of Cell cycle inhibitors blocking B cell division

A range of cell cycle inhibitors with different biological targets and actions on cell cycle phases were chosen for analysis (Appendix IV). Each inhibitor was first assessed for its efficacy at blocking B cell proliferation to establish an effective dose range and examine the prediction that blocking cell cycle would reveal a consistent death time. Functionally wild type (Blimp-1$^{GFP/+}$ or Fucci Red$^{Tg/+}$/Green$^{Tg/+}$) naïve splenic B cells were cultured with 10 μg/mL anti-CD40 (1C10) and 500 U/mL IL-4. Cells were initially left undisturbed for three days, at which point multiple cell divisions had distributed the population across generations 0-6. At this time cultures were harvested, re-stimulated, and treated with a range of inhibitor concentrations in triplicate 200 μL wells. Division progression was then followed over the subsequent two to four days, by analysing replicate 96-well cultures using flow cytometry with multiple time-points (**Figure 5.2**).

Cells remaining in culture in the absence of the selected compounds continued to proliferate for approximately three further divisions (**Figure 5.2a**), while those affected by inhibitors demonstrated lower total cell numbers over the course of the experiment (**Figure 5.2b**). Total cell numbers were largely dose-dependent (**Figure 5.2c**), and for many but not all of the inhibitors, complete division-inhibiting concentrations could be identified where CTV profiles did not progress over time (**Figure 5.2d**).

Inhibitor dose-response curves showed significant differences in the relation between cell survival and the blocking of division, particularly between cell cycle categories. These patterns are summarised below:

$\underline{G_1}$

Each of the G_1-inhibiting compounds tested effectively blocked cell division (**Figure 2d**), with only the CDK1/2 inhibitor BMS-265246 ('BMS') unable to cause a complete cessation. Higher concentrations of BMS slowed divisions, but did not inhibit them completely when used alone (Section 5.2.4; Figure 5.6). Millipore Cdki and LEE011 were inconclusive, as their addition to the culture media caused the cells to autofluoresce in the CTV channel, thus excluding the use of these compounds for proliferation analyses.

It was notable that, for conditions where division was highly suppressed, most cell cultures progressed for an additional generation before being arrested in the next G_1 phase. This delay of approximately 8 hours, visible in the overlaid CTV profiles (**Figure 5.2d**) was most

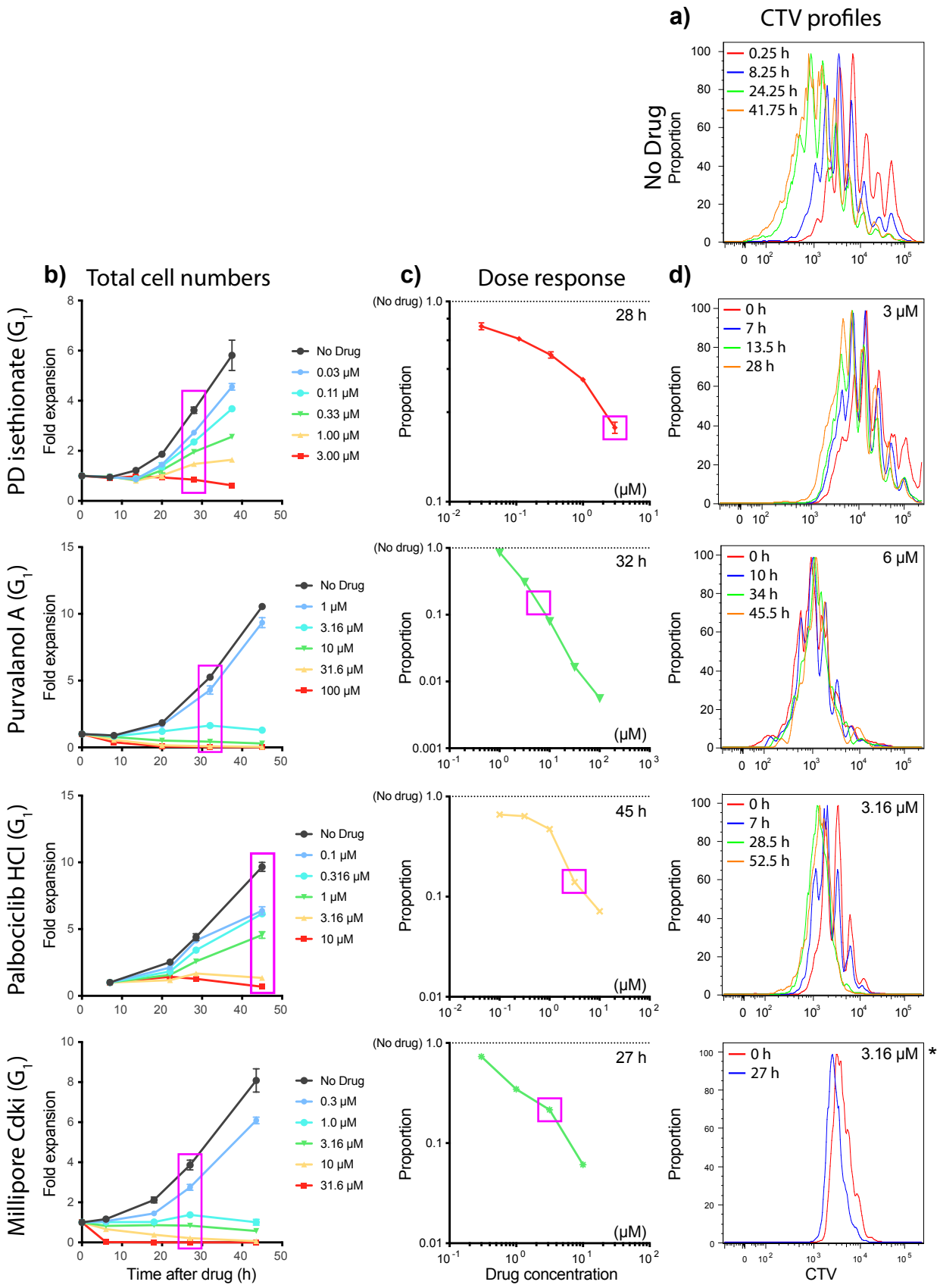
a)
CTV profiles
No Drug
Proportion
0.25 h
8.25 h
24.25 h
41.75 h
b)
Total cell numbers
c)
Dose response
d)
PD isethionate (G1)
Fold expansion
No Drug
0.03 μM
0.11 μM
0.33 μM
1.00 μM
3.00 μM
(No drug) 1.0
28 h
(μM)
Proportion
0 h
7 h
13.5 h
28 h
3 μM
Purvalanol A (G1)
Fold expansion
No Drug
1 μM
3.16 μM
10 μM
31.6 μM
100 μM
(No drug) 1.0
32 h
(μM)
Proportion
0 h
10 h
34 h
45.5 h
6 μM
Palbociclib HCl (G1)
Fold expansion
No Drug
0.1 μM
0.316 μM
1 μM
3.16 μM
10 μM
(No drug) 1.0
45 h
(μM)
Proportion
0 h
7 h
28.5 h
52.5 h
3.16 μM
Millipore Cdki (G1)
Fold expansion
No Drug
0.3 μM
1.0 μM
3.16 μM
10 μM
31.6 μM
(No drug) 1.0
27 h
(μM)
Proportion
0 h
27 h
3.16 μM
*
Time after drug (h)
Drug concentration
CTV

Figure 5.2: Cell cycle inhibitor dose response titrations.

Purified naïve B cells were first stimulated with 10 µg/mL anti-CD40 and 500 U/mL IL-4 for three days. Harvested activated B cells were then re-cultured with fresh stimuli and varying concentrations of the inhibitory drugs indicated. Results from experiments from different days are aggregated. **a)** An example of proliferation progression as indicated by CellTrace Violet fluorescence in the absence of cell cycle inhibitors. **b) T**otal cell numbers over time (mean +/- SEM of triplicate wells) at the indicated inhibitor concentrations. **c)** Dose response curve 1-2 days after treatment with inhibitors (chosen time indicated in magenta rectangle from b). **d)** CTV profiles of selected inhibitor concentrations (magenta box in c), with indicated time points overlaid. Results are representative of 1-3 titrations for each compound. Inhibitory compounds are grouped in sets based on cell cycle inhibitory phase. *Note, for Millipore Cdki and LEE011, compounds were found to interfere with CTV fluorescence and hence prevented proliferation analyses.

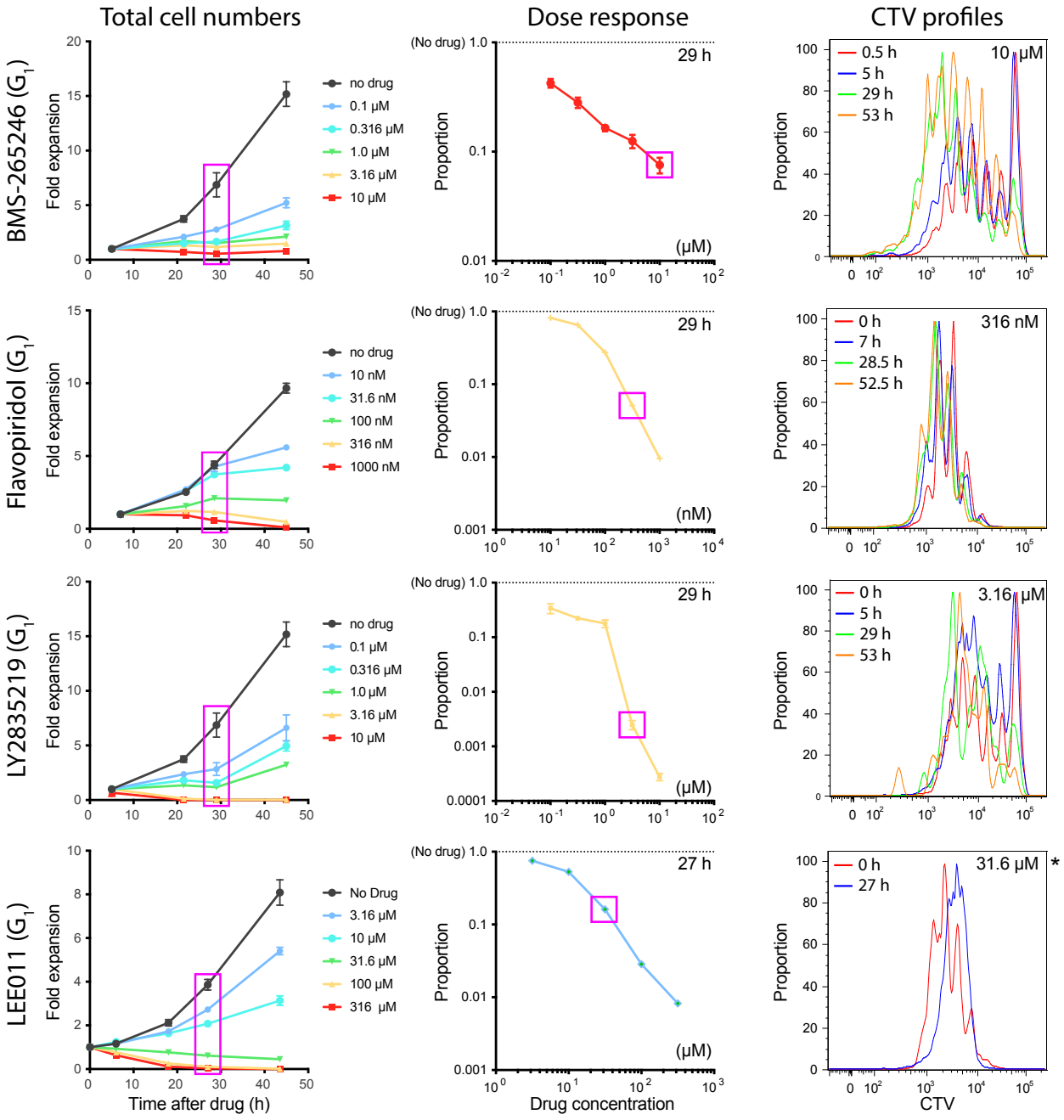

Figure 5.2 continued.

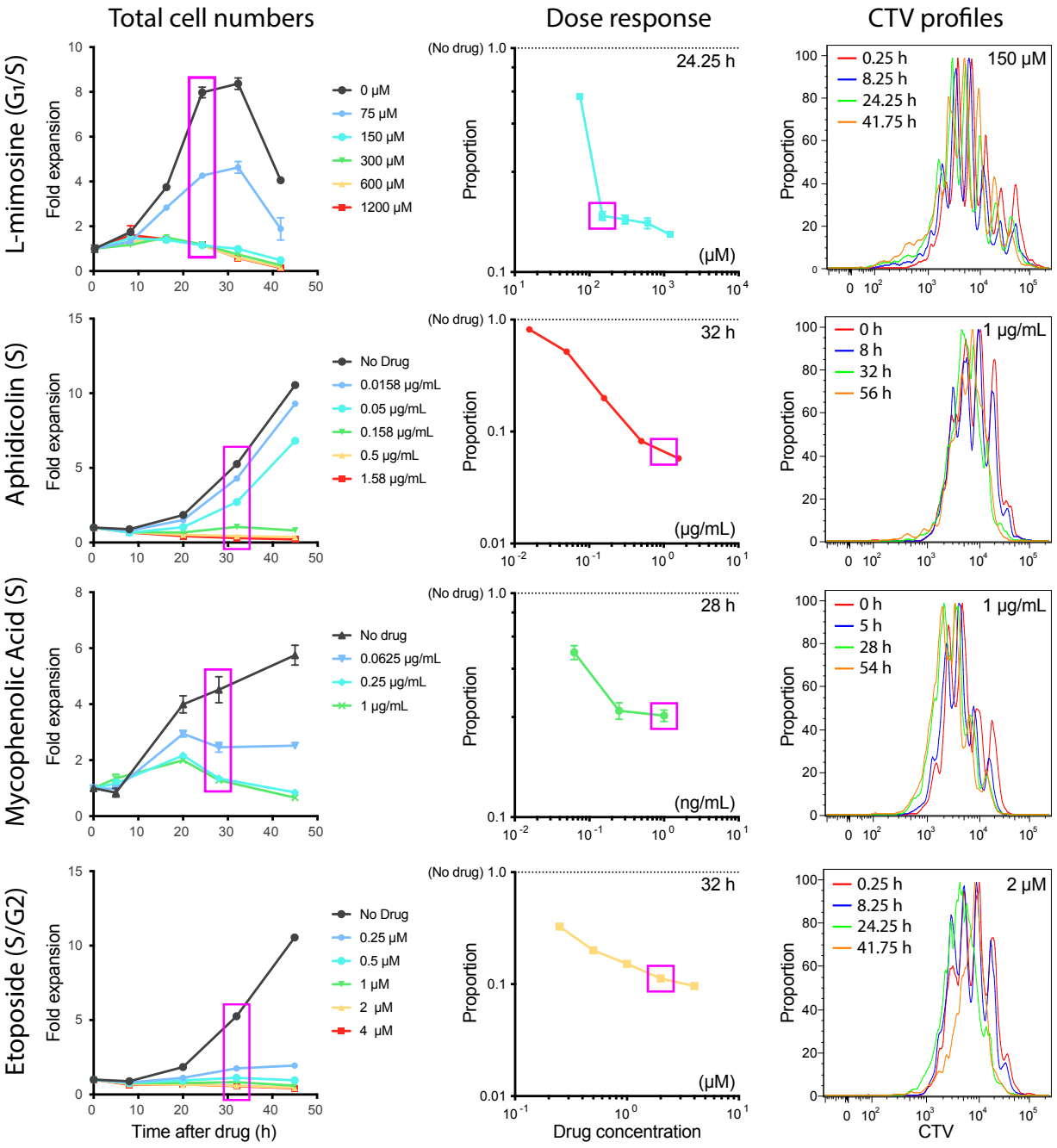

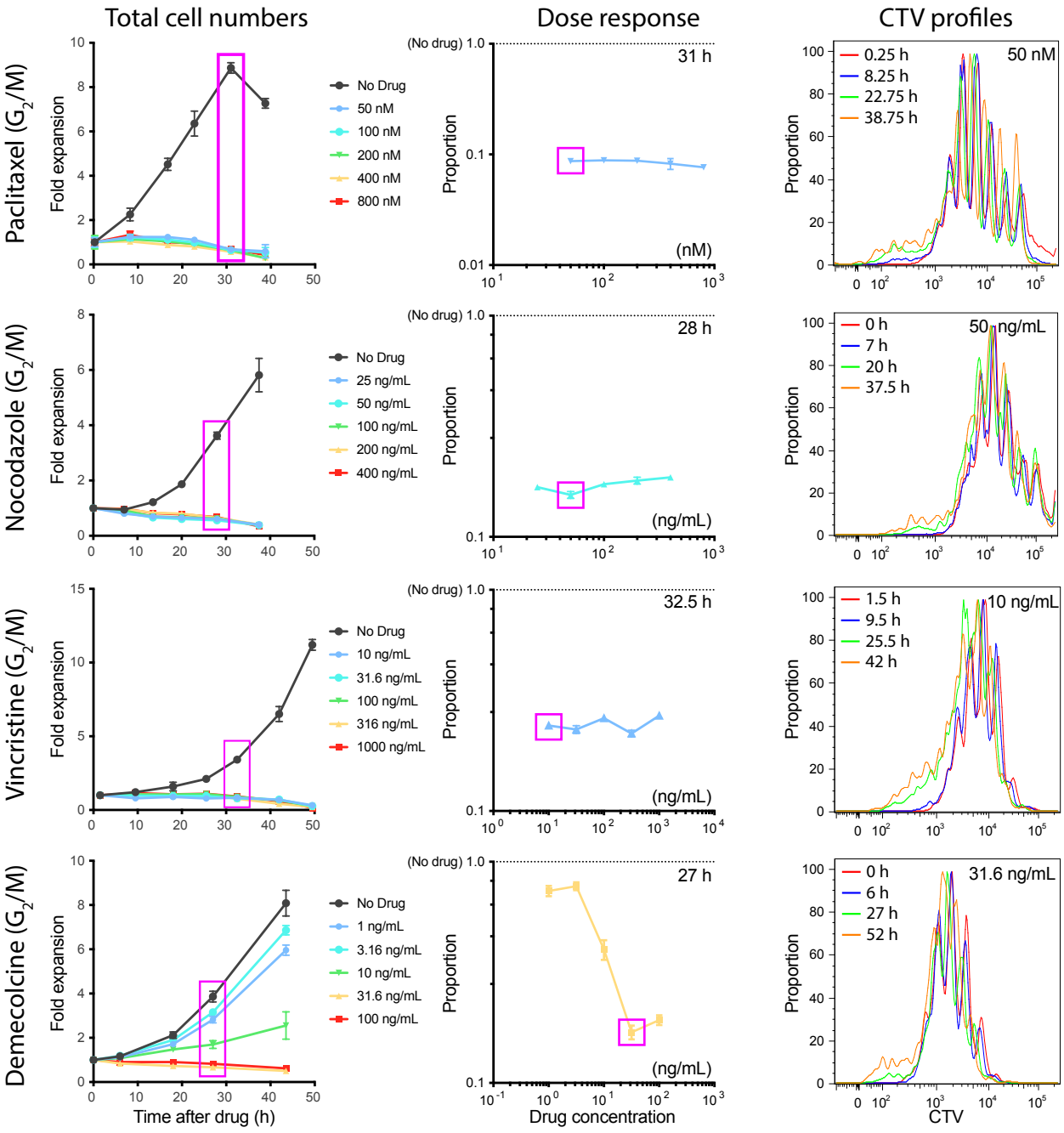
Total cell numbers
Dose response
CTV profiles
Paclitaxel (G2/M)
Nocodazole (G2/M)
Vincristine (G2/M)
Demecolcine (G2/M)
Fold expansion
Time after drug (h)
No Drug
50 nM
100 nM
200 nM
400 nM
800 nM
25 ng/mL
50 ng/mL
100 ng/mL
200 ng/mL
400 ng/mL
10 ng/mL
31.6 ng/mL
100 ng/mL
316 ng/mL
1000 ng/mL
1 ng/mL
3.16 ng/mL
(No drug) 1.0
Proportion
31 h
28 h
32.5 h
27 h
(nM)
(ng/mL)
Drug concentration
0.25 h
8.25 h
22.75 h
38.75 h
0 h
7 h
20 h
37.5 h
1.5 h
9.5 h
25.5 h
42 h
6 h
27 h
52 h
CTV

likely due to those cells transiting through S/G_2/M of the cell cycle at the time inhibitors were added, when they are not regulated by cyclin dependent kinases.

Of particular interest, was the relationship between concentrations that prevented cell division and the coincident reduction in cell numbers due to cell death. For each CDK4/6 inhibitor (Palbociclib HCl, LY2835219), and the pan-CDK inhibitors (Purvalanol A and Flavopiridol), increasing compound concentrations continued to further deplete live cells from culture, beyond the concentrations that arrested cell division, as indicated by their CTV profiles (ie. the magenta box concentrations completely inhibit cell division). Thus, for most G_1 inhibitors there was poor concordance with the prediction of fate competition, that blocking division and the cause of cell death would be coincident. However, this result was in striking contrast to that found for S and M phase inhibitors below.

S phase

L-mimosine has been observed to exhibit a range of effects on both transition from G_1 to S phase and DNA replication [160], in particular its inhibition of Ctf4 binding to chromatin in late G_1, preventing the initiation of S phase and DNA synthesis [161]. Since its mechanism of action more closely resembles that of the other S phase inhibitors, which all interrupt DNA synthesis, rather than progression through G_1, for the purpose of this summary L-mimosine is classed as an S phase inhibitor.

For the S-phase inhibitors tested here – L-mimosine, Aphidicolin, Etoposide, and Mycophenolic Acid – cells responded to the presence of these compounds in a dose-dependent manner. It was striking that at the higher concentrations tested, the effects of each of these inhibitors appeared to reach a limit, where division cessation and the amount of cell death were at maximum effect, such that higher concentrations of drug did not induce any further cell death. This was consistent with the prediction of the uncensoring model where limiting cell division would allow cells to uncensor their pre-determined distribution of death times.

G_2/M

The tested G_2/M drugs primarily inhibit microtubule function, where their assembly and disassembly are normally required for chromosome rearrangement (metaphase and anaphase) and separation of the daughter cells (cytokinesis). Demecolcine responded in a dose-dependent manner, while Paclitaxel, Nocodazole, and Vincristine all completely inhibited cell proliferation at the concentrations tested. As was seen for S phase inhibition, at concentrations above which cell division was inhibited, further increases in concentration did not induce any further cell death within the dose range tested.

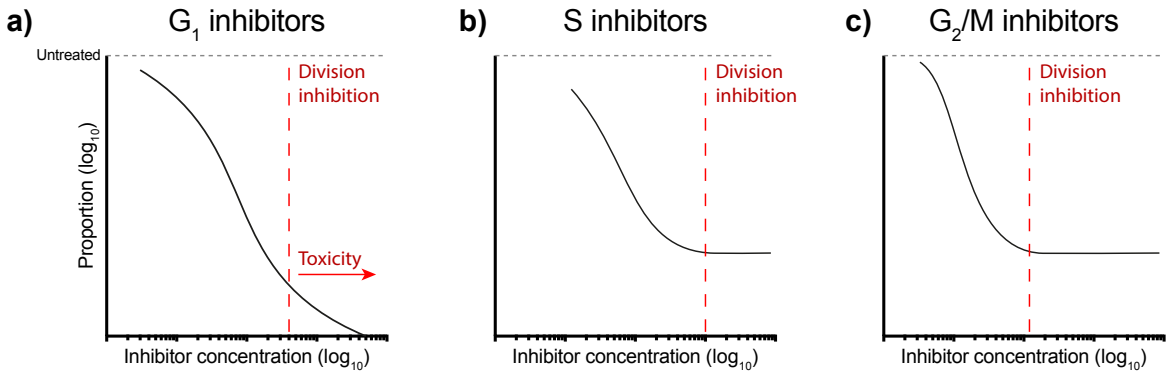

Figure 5.3: Summary of dose-response curves.

Inhibitors affecting different phases of the cell cycle were noted to exhibit distinct traits, as summarised here. Representative diagrams of cell numbers due to cell cycle-inhibition as a proportion of cells in untreated samples, after one day of exposure to inhibitors. **a)** G_1 inhibitors largely produced steep dose-response curves, with increased cell death at higher inhibitor concentrations, irrespective of cell cycle arrest. **b)** Division-inhibiting concentrations of S phase inhibitors were identified, above which total cell numbers plateaued. **c)** G_2/M inhibitors also blocked cell division, with no further death observed at concentrations above which division was inhibited.

The differences in dose response patterns between inhibitors affecting different phases of the cell cycle are summarised and highlighted in **Figure 5.3**.

5.2.2 CDK4/6 inhibitors induce rapid cell death at high concentrations

The above analyses revealed that, in contrast to the S and M phase inhibitory compounds, the G_1 inhibitors tested continued to promote cell death at concentrations beyond those required to inhibit division alone. This result implies these inhibitors are promoting additional pathways to cell death, possibly in an off-target manner. To explore the timing of cell death in relation to cell cycle by one such compound, the CDK4/6 inhibitor PD isethionate, cell imaging was used. We were particularly interested in determining how the time to die coincided with expected cell division times. For this experiment, generation 4 cells sorted three days after stimulation with 20 µg/mL 1C10, 1000 U/mL IL-4, and 5ng/mL IL-5 were seeded in a microscopy chamber slide (Methods 2.9 - 2.11), and imaged for 4 hours prior to the addition of 10 µM PD isethionate or media-only control. This concentration was selected to study how higher concentrations of CDK inhibitors were influencing cell death.

Generation 5 cells were tracked from the previous mitosis until they divided or died (**Figure 5.4**). Cells tracked in the absence of cell cycle inhibitors are illustrated in **Figure 5.4a**. In the presence of PD isethionate (**Figure 5.4b**), 17.2% of cells continued on to divide, with the same distribution of division times as without the drug, and a mean of approximately 9 hours. Death times were notably early in the presence of PD isethionate – approximately 50% of the cells had died 8 hours after their generation in the presence of drugs.

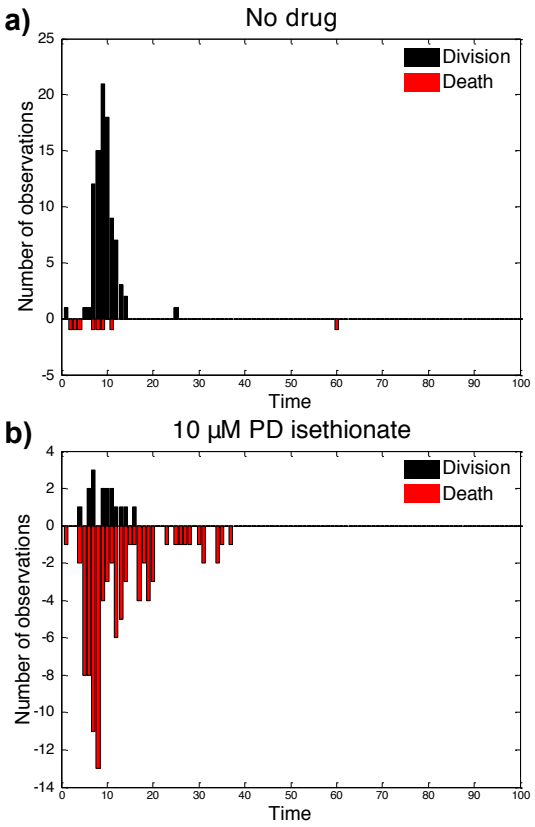

Figure 5.4: Cell fate times were filmed for cells treated with PD isethionate.

Cells stimulated with 10 µg/mL anti-CD40 and 500 U/mL IL-4 were cultured for three days prior to sorting for generation 4 cells and time-lapse imaging. Times from mitosis until subsequent division or death were manually annotated for generation 5 cells. **a)** Times to fates for untreated cells. **b)** Times to fates for cells exposed to 10 µM PD isethionate.

The observed death times here are even earlier than division times in the absence of cell cycle inhibitors, and is indicative of a rapid death triggered by high CDK4/6 inhibitor concentrations causing the cell loss seen with flow cytometry. Curiously, given that the few remaining division times are unchanged, the data highlights a disconnection between division inhibition and promotion of cell death.

5.2.3 Cell cycle inhibitors have the potential to uncensor underlying death times

In contrast to the G_1 inhibitors, increasing concentrations of S phase and G_2/M phase inhibitors did not appear to further deplete cell numbers when used beyond the concentration required to inhibit division, as predicted by the Cyton competition model. When tested in the same experiment, concentrations which completely inhibited division produced very similar survival kinetics, again as predicted by the theory (**Figure 5.5**). This similarity resulted despite the markedly different molecular and cell phase targets for the range of inhibitors used.

The survival curve of cells treated with 6 µM of G_1 inhibitor Purvalanol A also closely resembled that of the S and G_2/M phase inhibitors (one-way ANOVA, no significant difference). At this concentration, divisions are inhibited, and thus the similarity in death times between this and the other drugs is indicative of minimal additional cell toxicity. Taken

together, these times to die are consistent with an underlying distribution of death times that could be revealed by blocking division, as predicted by the competition model.

Drawing upon filming data from the two earlier chapters, estimates of the predicted time to die distributions for CD40 stimulated B cells can be used to compare and evaluate the survival plot of the uncensored death curve shown in **Figure 5.5**. This can be achieved with the following argument.

The time to die plots in **Figure 5.5** are taken from day 3 cultures, with a heterogenous population of cells distributed across multiple cell generations. Imaging from Chapter 3 (Section 3.2.7) and Chapter 4 (Section 4.2.4) revealed that stimulation and division number had little impact on the time to die distribution. Consequently, the uncensored time to die for wild type cells was modelled using the generation 5 death times from Figure 4.10 (fitting log-normal mean = 3.19, standard deviation = 0.32), as an approximation for the average death time for the population, when measured from mitosis. This fitted death times is overlaid in **Figure 5.5** (blue dotted line).

The prediction from filming would be expected if cells were completely cell cycle 'synchronised' by assigning division as time = 0. For the measured data in **Figure 5.5**, however, cells were unsynchronised in their division cycle at the time of exposure to inhibitors; hence, their times to die, once censorship is removed, will involve more variation than the survival curve deduced from filming. Thus, an equation for summarising the net population's survival curve when completely unsynchronised can be used [162], and this calculation is overlaid in

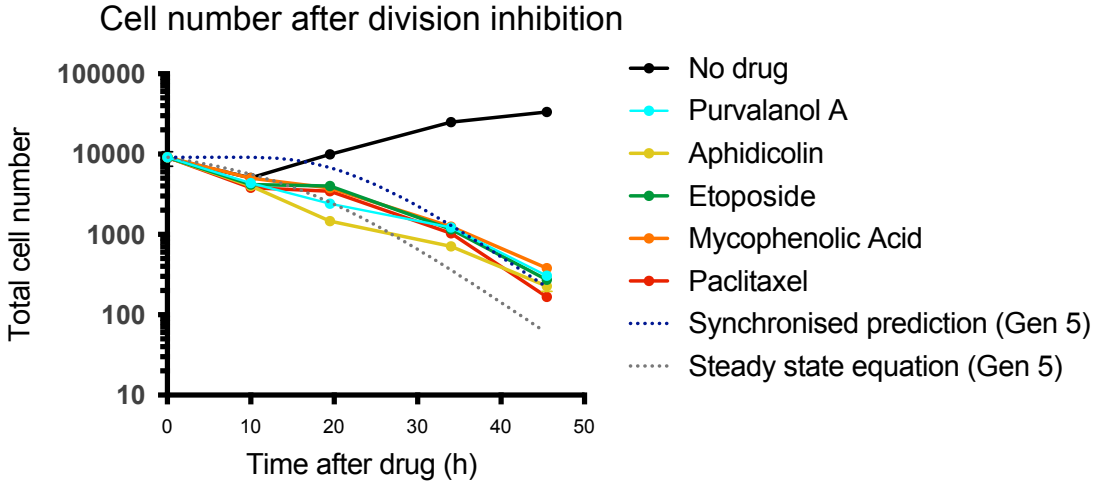

Figure 5.5: Death curves from division-inhibiting concentrations of multiple drugs.

Several S phase and G_2/M inhibitors were used together, with the inclusion of CDK inhibitor Purvalanol A, at concentrations that arrested the cell cycle. Cells stimulated with 10 µg/mL anti-CD40 and 500 U/mL IL-4 were cultured for three days. Division inhibitors were added, and total cell numbers were measured over time. Survival curves in response to cell cycle inhibitors were not significantly different (p=0.998, one-way ANOVA). Predicted death times from filming synchronised cells (1- cumulative lognormal with m = 3.19 and s = 0.323), or the unsynchronised equivalent based on Dowling *et al.* steady state equation [162] (same log-normal parameters) are overlaid (dotted lines).

Figure 5.5 (grey dotted line). In reality, the few hours required for all cells to be arrested by the cell cycle inhibitors should be accounted for, and so a more accurate death curve prediction should sit to the right (later) than Dowling's steady state prediction and to the left (earlier) than the prediction from modelling synchronised cells. The observed survival times are strongly consistent with these uncensoring predictions.

5.2.4 Synergy between G1 inhibitors arrests the cell cycle at reduced concentrations of any one drug alone

For the analysis so far, inhibitors of S and G_2/M phase appeared to successfully uncensor death times, while for the majority of CDK inhibitors tested increasing concentrations always further increased the rate of cell death. Despite this apparent cytotoxicity, targeted G_1 inhibitors with known actions on CDK proteins would be highly valued reagents for fate uncensoring. To further explore the possible use of CDK inhibition, we reasoned induction of cell death might be an off-target effect (ie. unrelated to blocking of CDK) and that combining two of the least cytotoxic compounds might lead to synergistic inhibition, and minimise the putative off-target toxicity. To test this possibility, combinations of two compounds were tested with the prospect of arresting division during G_1, while reducing off-target effects that would induce early apoptosis.

Multiple concentrations of BMS, Purvalanol A, Palbociclib HCl, Flavopiridol, and LY2835219 were first screened in an Alamar Blue assay (Methods 2.16), to obtain a fast readout of a broad, high throughput search for effective combinations. BMS, the CDK1/2 inhibitor, was of particular interest as high concentrations did not appear to harm the cells, however, alone it was unable to completely block cell division. Thus, the inhibitors were combined in chequerboard assays where stimulated cells (10 μg/mL anti-CD40, 500U/mL IL-4 for three days) exposed to each concentration of one inhibitor were simultaneously treated with 6-7 diluting concentrations of a second cell cycle inhibitor. These permutations, or cells in individual inhibitors alone, were cultured for 33 hours prior to the addition of Alamar blue, followed by a further 10 hours for a readout of metabolic activity. Measured fluorescence values were normalised to the no cell and untreated cell controls on the same plate and, compared with Etoposide treated cells (Methods 2.16) as a comparator for the predicted uncensored death at the level of an S phase inhibitor. Relative fluorescence values for representative inhibitor combinations are plotted in **Figure 5.6**, with fluorescence from Etoposide-treated wells marked with a dotted line.

These data were inspected to search for a series of concentration combinations that did not vary in survival effects, but gave cell numbers equivalent to the Etoposide control. When used alone, Purvalanol A, Palbociclib HCl, Flavopiridol, and LY2835219 again induced rapid

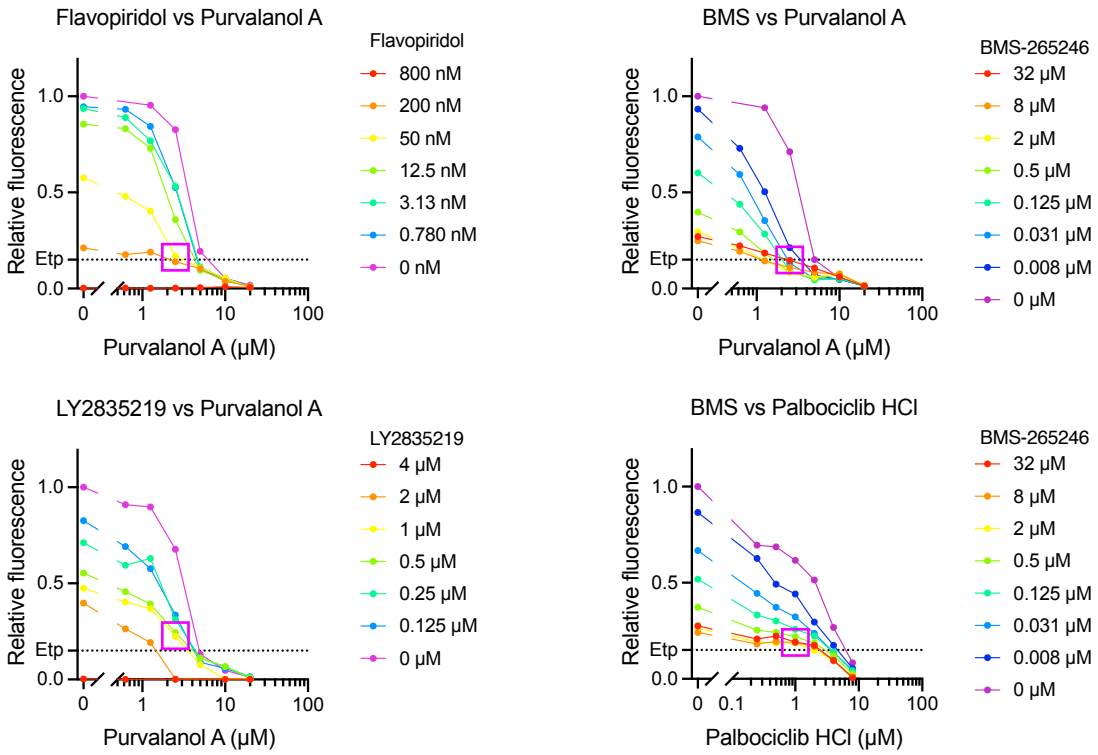

Figure 5.6: Combinations of G1 inhibitors are less cytotoxic.

Cells were cultured in 10 μg/mL anti-CD40 and 500 U/mL IL-4 for three days, before two of Purvalanol A, Flavopiridol, BMS, LY2835219, and Palbociclib HCl were added in combination at the indicated concentrations, in a chequerboard fashion. After 33 hours of exposure to inhibitors, Alamar Blue was added for 10 hours, and fluorescence measured. Fluorescence values were calculated relative to no drug (1.0) and no cells (0.0), and plotted for drug 1 (lines) vs drug 2 (X axis). Fluorescence from Etoposide-treated cells (Etp, dotted line) was included to indicate expected cell numbers as a result of division inhibition. Dose response curves are plotted for four such combinations out of nine tested. Magenta boxes highlight approximate drug concentrations with the potential for further testing. Untreated, no cell, and Etoposide controls were measured from the same plate for each illustrated sample.

sensitivity in cells with increasing inhibitor concentrations. BMS however, was particularly promising when used with Palbociclib HCl, producing several concentrations that were comparable with the use of Etoposide. Having identified a putative optimal combination and dose range with this Alamar blue method, it was important to follow up with CTV profiles to confirm effective cessation of cell division.

Cells stimulated in anti-CD40 and IL-4 were cultured for 3 days, prior to treatment with 0, 0.05, 0.2, 0.8, or 3.2 μM of BMS and 0, 1, 2, or 4 μM Palbociclib HCl. CTV overlays revealed total division progression/cessation in each combination (**Figure 5.7a**), while total cell numbers indicated patterns of cell death (**Figure 5.7b**). Although several combinations had potential, 0.05 μM BMS with 2 μM Palbociclib HCl was selected for further investigation, as it gave the highest cell number return while still blocking division. The combination of the two compounds effectively inhibited division, when neither one could do so alone. In the following section this less cytotoxic G1 combination was included in uncensoring analyses of differentiation along with other inhibitory compounds.

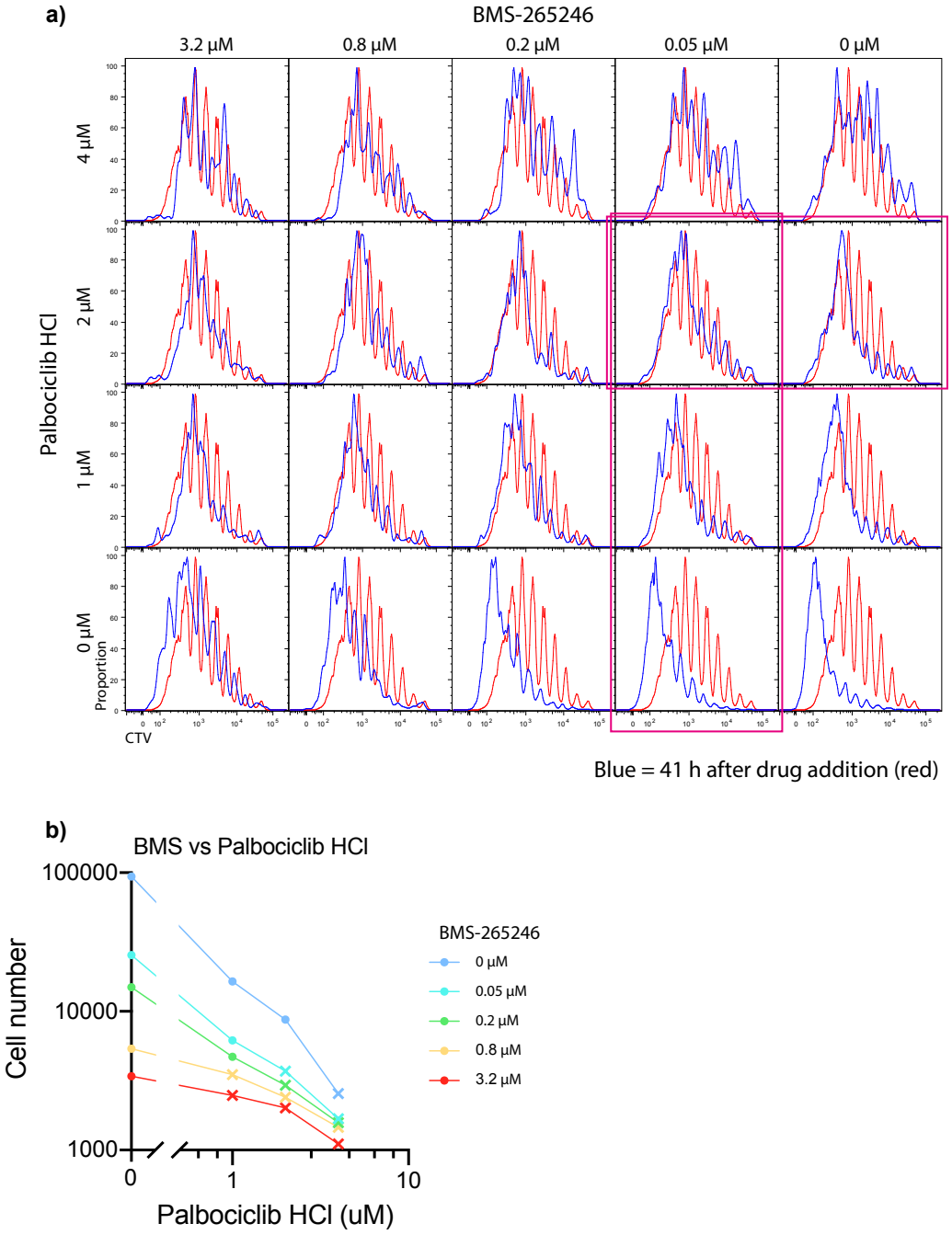

Figure 5.7: CTV progression profiles for BMS-265246 vs Palbociclib HCl.

CTV labelled cells were cultured with anti-CD40 and IL-4 for four days prior to the addition of the indicated concentrations of inhibitors. **a)** Inhibitor-treated cells were analysed 41 hours later, and their histograms overlaid with profiles prior to cell cycle inhibition to compare division progression. Magenta boxes highlight 2 µM Palbociclib HCl and 0.05 µM BMS-265246, neither of which inhibit division alone, but when combined, divisions cease. **b)** Average cell numbers from wells treated with BMS (line) and Palbociclib HCl (X-axis) for 41 h, as in **a**. Crosses mark where divisions are completely inhibited.

5.2.5 Cell cycle inhibition increases the frequency of antibody secreting cells

To test whether differentiation could be uncensored with cell cycle inhibitors, CTV and Blimp-1-GFP were used to compare the development of ASC. Preliminary testing indicated that division-arrested cells often became very large, and as a consequence levels of autofluorescence can increase and interfere with detection of GFP. Hence, it was important to include WT negative controls under identical inhibitory conditions for these experiments. Division-inhibiting concentrations of a short-listed inhibitor panel were tested on Blimp-1-GFP reporter cells. Cells were cultured for three days with 10 μg/mL anti-CD40 and 500 U/mL IL-4, until the population was distributed across generations 0-6. Cell cycle inhibitors were added for 24 hours, before division progression and differentiation were analysed by flow cytometry (**Figure 5.8a**). Proportions of differentiated cells per generation were calculated by subtracting the percentage of cells in the GFP+ gate of the wild type population (see Methods 2.8) from the percentage of cells in the equivalent gate on the Blimp-1-GFP reporter (**Figure 5.8b**).

Filming analyses from the previous chapter (Figure 4.11d) also allowed us to predict the expected differentiation outcome per generation after 24 hours with complete uncensoring (**Figure 5.8c**), and compare with observed data (grey crosses, **Figure 5.8b**). Observed differentiation rates did not meet expectation, however differentiation in division-arrested cells still exceeded the levels measured in untreated cells for each of the inhibitors tested, in particular the G_1 phase inhibitors. A partial repeat using a subset of the shortlisted inhibitor panel produced very similar results (**Figure 5.8d, e**).

With each of the compounds tested, the cells not only continued to differentiate in the 24 hours after cell cycle inhibition, but the level of differentiation exceeded that of the no drug control, where cells continued to cycle through mitotic divisions. The proportion of cells differentiated to ASC became higher for each generation when division-inhibited, and also higher as a total frequency (area under the curve), highlighting the inhibitory effects of cell division on differentiation outcomes. Thus, these data remain consistent with the competition hypothesis, where division events censor differentiation outcomes while resetting the 'timer' in the next generation. The increased population rate of differentiation compared to the no drug control argues against the alternative hypothesis, raised in the previous chapter, of a global timer that counts down differentiation from activation time.

This differentiation outcome was encouraging for the model of competing cell fates; however it was still important to assess whether cells that upregulated Blimp-1-GFP had fully developed into antibody secreting cells, and whether cell cycle arrest perhaps prohibited some cells from fully differentiating.

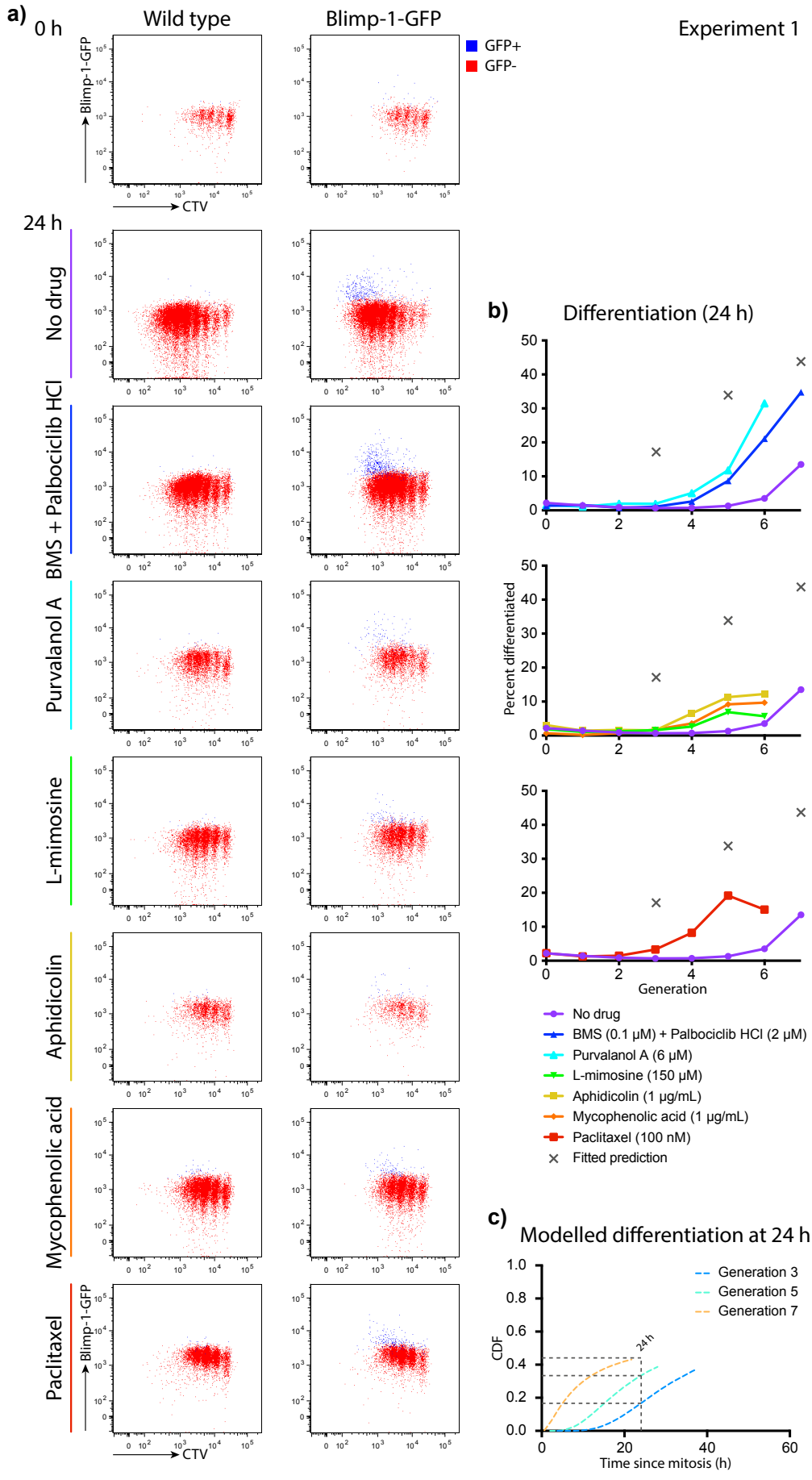
a)
0 h
Wild type
Blimp-1-GFP
Experiment 1
GFP+
GFP-
Blimp-1-GFP
CTV
24 h
No drug
BMS + Palbociclib HCl
Purvalanol A
L-mimosine
Aphidicolin
Mycophenolic acid
Paclitaxel
b)
Differentiation (24 h)
Percent differentiated
Generation
No drug
BMS (0.1 μM) + Palbociclib HCl (2 μM)
Purvalanol A (6 μM)
L-mimosine (150 μM)
Aphidicolin (1 μg/mL)
Mycophenolic acid (1 μg/mL)
Paclitaxel (100 nM)
Fitted prediction
c)
Modelled differentiation at 24 h
Generation 3
Generation 5
Generation 7
CDF
24 h
Time since mitosis (h)

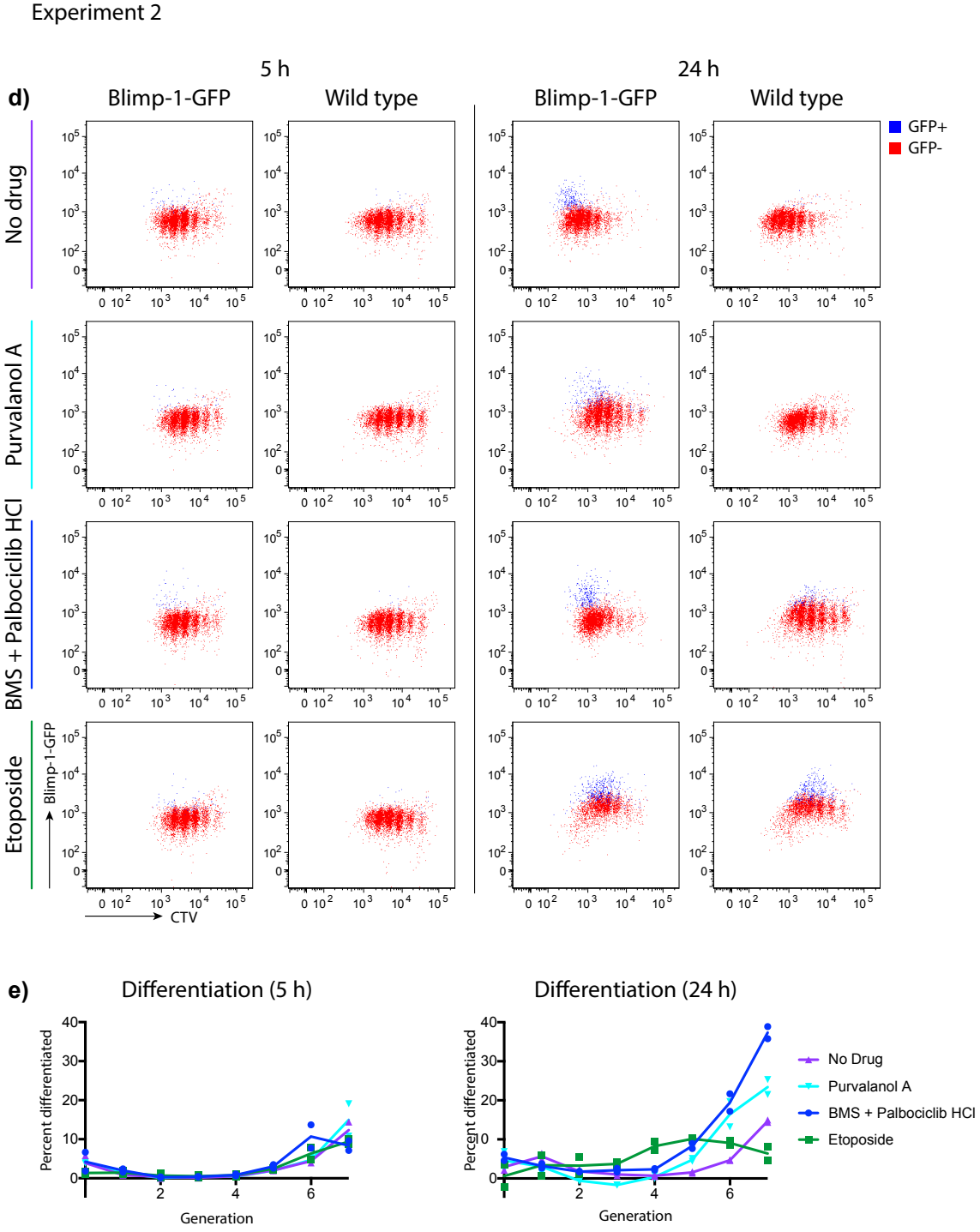

Figure 5.8: Uncensoring division-linked differentiation.

Cells were stimulated with 10 µg/mL anti-CD40 and 500 U/mL IL-4 for three days prior to exposure to the selected panel of inhibitors. **a), d)** Blimp-1-GFP reporter mice were used as an indicator of differentiation to ASC. For GFP+ cells (blue), gating was determined using GFP vs SSC channels to exclude autofluorescence. **b), e)** Proportions of cells differentiated per generation after cell cycle inhibition. The last plotted generation includes all cells in generations 7+. Grey crosses indicate differentiation outcomes predicted from c). **c)** Differentiation times fitted to imaging data from Figure 4.11c predict the amount of differentiation expected at 24 h after last mitosis for cells in generations 3, 5, and 7, when cells were stimulated with 2.5 µg/mL anti-CD40, 500 U/mL IL-4, and 5 ng/mL IL-5.

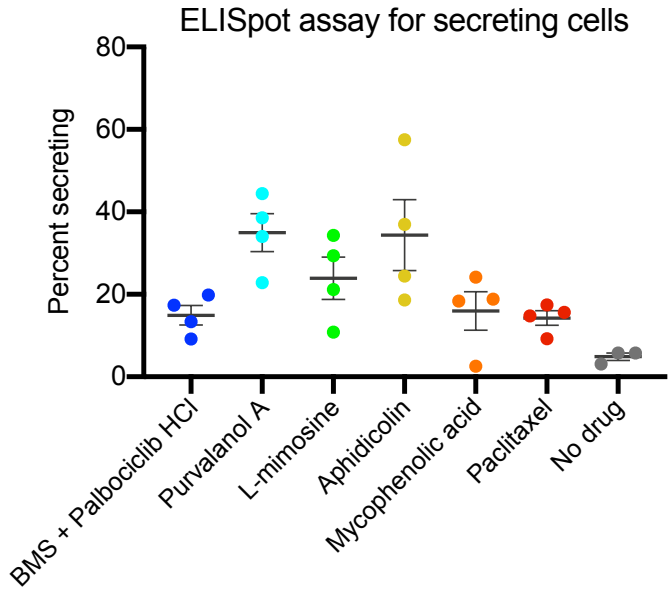

Figure 5.9: ELISpot assays for secreting cells.

Proportion of cells secreting as determined with an ELISpot assay. Cells were cultured for three days in 10 µg/mL anti-CD40 and 500 U/mL IL-4, prior to the addition of cell cycle inhibitors. Secreting cells were measured after 24 hours of exposure to inhibitors. Mean±SEM. The difference between any inhibitor-treated sample and no drug control is statistically significant ($P<0.05$, two-tailed Student's t test).

5.2.6 Blimp-1-GFP-expressing cells produced as a result of inhibiting division secrete antibody

To verify that GFP+ cells generated under the effects of mitotic inhibitors were fully differentiated and hence antibody secreting, ELISpot assays were performed on the treated cells. Cells stimulated for 3 days with 10 µg/mL anti-CD40 and 500 U/mL IL-4 were exposed to cell cycle inhibitors for 24 h, then counted and subjected to an ELISpot secreting assay (Methods 2.17). Plaque-forming cells were counted, and the calculated proportion of cells that were deemed secreting are plotted in **Figure 5.9**. For each of BMS + Palbociclib HCl, Purvalanol A, L-mimosine, Aphidicolin, and mycophenolic acid, a higher proportion of secreting cells were detected than for cells untreated with any inhibitors. The difference between proportions of secreting cells for G_1 (BMS+Palbociclib HCl, Purvalanol A) compared with G_2/M inhibitors (L-mimosine, Aphidicolin, Mycophenolic acid) was not significantly different (Student's t test, $P=0.98$). The proportion of secreting cells under the influence of cell cycle inhibitors, however, were each significantly higher than the proportion detected in the absence of inhibitors (two-tailed Student's t test, $P<0.05$).

Collectively, the data so far indicate that cell cycle inhibitors can effectively uncensor death times, regardless of which phase of the cell cycle division arrest occurs in. Differentiation was also successfully uncensored, producing more antibody-secreting cells than in the absence of cell-cycle inhibitors. The proportion secreting, however, was at lower levels than predicted.

5.3 Discussion

The current Cyton model of cell fate allocation was built around experimental data suggestive of independent, stochastic, and competing intracellular fates. Analyses of observed times to fates can predict the total potential of fate outcomes for a population of cells, as demonstrated in Chapters 3 and 4. For differentiation to ASC, the distribution of potential times to fates is obscured by division and death outcomes, as division events appear to change required differentiation times, while dead cells cannot be observed to differentiate. In this chapter, the potential for cell cycle inhibitors to remove division as competing events, and hence serve as useful tools for dissecting the control of differentiation programs was explored.

For the panel of compounds tested, most appeared to impart their effects on division in a dose-dependent manner. Of the ones that didn't, concentrations tested were initially too high to observe the full dose-response range. Interestingly, for many of the S phase and G_2/M phase inhibitors, a plateau was reached where increased inhibitor concentrations had little to no effect on cell numbers, suggesting that they were able to inhibit division without triggering an additional apoptotic pathway. When tested in parallel at appropriate concentrations for inhibiting cell division, use of the different compounds were found to produce overlapping survival curves. Given that each S phase and G_2/M phase inhibitor was specific for a different target, and yet produced these identical death curves at saturating concentrations for division-inhibition, the notion that those cells died due to various possible off-target effects was unlikely. Rather, the data was consistent with survival estimates from filming in chapter 4, and strongly supports a model where programmed cell death behaves as an independent and competing mechanism to division, and inhibition of the latter left the cells to live out their normal survival times until apoptosis.

Amongst the G_1 phase inhibitors, the majority that targeted CDK prompted cell death at lower concentrations than that required to completely inhibit cell division, and hence these molecules were unable to be used alone for uncensoring differentiation outcomes. PD isethionate, for instance, was found to promote early death times. To circumvent this, CDK inhibitors were combined at lower concentrations to trial division blocking with reduced, potentially off-target, toxic, effects. The synergy between CDK1/2 inhibitor BMS-265246, and CDK4/6 inhibitor Palbociclib HCl was found to be a viable option for inhibiting cell division.

For Purvalanol A, another pan-CDK inhibitor, acceptable concentrations were found for inhibiting cell division, indicating that cells are able to be maintained in G_1 without triggering early cell death or other cell monitoring responses. Unfortunately, when used for microscopy, this molecule appeared not to exhibit its cell cycle-inhibiting properties, perhaps being highly photosensitive [Kim Pham, unpublished], and thus was not useful for imaging experiments.

Further imaging of cells treated with Paclitaxel (a G_2/M inhibitor), performed outside the scope of this project, revealed some unusual properties – the cells would grow and appear to replicate their DNA (cell size and granularity as seen by bright field imaging), as per normal, but after becoming spherical in preparation for mitosis, cells would visibly attempt to undergo cytokinesis without success. This was expected, given the tubulin modulatory effects of Paclitaxel. However, curiously the cells continued to grow, seemingly doubling their DNA again, and attempting to divide into four cells in time with untreated cells. After several rounds of unsuccessful divisions, these multinucleated cells would die. These results corroborate with flow cytometry data from all G_2/M inhibitor treated cells, where forward scatter, correlated with cell size, would increase markedly over time after division inhibition. It is interesting that these cells are still able to differentiate and start producing Blimp-1, suggesting continued gene regulation despite shared internal structures and cycling through subsequent G_1/S/G_2 phases. Differentiation results from the G_2/M inhibitors must then be interpreted with caution, given that cell cycles still proceed, only in the absence of cytokinesis.

Gating of GFP+ cells also needed to be done carefully, particularly of the cell cycle inhibited cells. Over time, the growing cells accumulated autofluorescence, detectable in the GFP and SSC channels, likely due to increasing volumes of cell components and products of metabolism [163, 164]. Nevertheless, including wild type cells proved useful, and all plotted fluorescence values were calculated by deducting measured fluorescence of wild type samples from the equivalent Blimp-1-GFP samples.

For uncensoring of differentiation to ASC, use of the cell cycle inhibitors all increased the proportions of secreting cells in each generation in the absence of cell divisions. These findings were consistent with the hypothesis that blocking division would reveal underlying differentiation times, central to the model of competing cell fates. Further, that the proportion of ASCs accumulated faster in division-inhibited cell populations than in the untreated control led to the rejection of the activation timer hypothesis for differentiation formed in the last chapter. If cells were insensitive to divisions, differentiation would be expected to proceed at the same rate whether cells were division-inhibited or not. Instead, the data is indicative of a suppressive effect of mitosis on differentiation outcomes. When compared with uncensored predictions from imaging, however, these proportions fell short of expectations.

It is possible that traversing through the cell cycle, in particular S phase [165] was a requirement for transcriptional changes resulting in measurable differentiation. It was curious then that cells arrested in G_1 demonstrated a markedly higher level of differentiation to ASC compared to cells arrested in S/G_2/M. This is perhaps indicative of a preference for transcriptional regulation in this first part of the cell cycle [Rhys Allan, in preparation]. When assessed for antibody-forming plaques, however, the number of secreting cells remained similar regardless of which phase cells were arrested in. Together, this would allude to a multi-step

differentiation pathway where signs of differentiation commitment (ie. Blimp-1 upregulation) do not fully coincide with the timing for becoming antibody secreting, in relation to the same cell cycle.

Other possibilities exist for the discrepancy between observed and predicted proportions of ASCs. For example, plasmablasts and lymphoblasts may have different survival requirements [63], and thus plasmablasts could preferentially die in our culture system and evade detection. Additionally, the assumption that blocking cyclins or DNA replication allows other cellular processes to continue unperturbed should not be overlooked. Although there is evidence for independence, interfering with a major cellular process such as division may also delay the progression of other molecular pathways in the cell, and hence the threshold of signals required for differentiation.

Overall, the system of artificially inhibiting the cell cycle tested here was found to be efficient at uncensoring underlying cell death times, otherwise unobservable in the presence of rapid proliferation. For differentiation, cells restrained from completing their cell cycle were observed to differentiate to ASC at an increased rate, and remains consistent with the model of competing cell fates.

CHAPTER 6

General Discussion

The CD40/IL-4 response in B cells has been well characterised as a model for T-dependent B cell regulation [67, 93, 166]. In this thesis, I have utilised this system to observe and model directly how differentiated cells are elicited under different circumstances. My studies tested the assumptions of the Cyton model of independent, stochastic, and competing cell fates [125]. In using this framework of distinct, quantifiable components for the distributions of times to cell fate, I studied the effects of various conditions on cell fate allocation in a systematic way. The relationship between differentiation, division, and death was explored in the context of intracellular competing cell fates, and how their interactions can influence a cell population's overall outcome.

As a starting point for my studies I examined the cause of a curious variation on the well-known feature that the incidence of differentiation to ASC increased with progressive cell divisions [67]. In this variation, low CD40 stimulation increased the likelihood of differentiation to ASC in any given cell generations [70]. By segregating cell fate allocation behaviour into component parameters, the quantitative model of competing cell fates posited several hypotheses by which this could be operating: the propensity for differentiation may have been changing, cells were perhaps differentiating faster, or division times were slowing, and thus allowed cells more time for their differentiation timer to outcompete division. As these alternatives could be distinguished by directly observing and timing cell fate changes using long-term cell imaging, time-lapse microscopy was conducted.

Perhaps surprisingly, the underlying process controlling differentiation outcomes became very clear. The degree of CD40 stimulation did not alter the underlying propensity for differentiating over time at all. Instead, low stimulation slowed average division times, and as a direct consequence of delaying a competing fate, allowed a greater proportion of cells to differentiate in the time before next mitosis.

Using similar methods, the underlying cause for the increase in ASC frequency with division was investigated more closely. Whereas CD40 stimulation did not control differentiation times when measured from mitosis, a further kinetic method of modulating differentiation outcomes was identified here: the number of times a cell had divided since activation directly influenced the average amount of time required for cells to differentiate to ASC. That is, while division times were maintained at a constant, cells that had undergone more divisions would take less time from mitosis to differentiate to ASC.

Taken together, these results portray a B cell response where both strongly and weakly stimulated cells play important roles. When considered in the context of the broader immune response, these data provide insight into why stronger stimulation produces a diminished proportion of effector cells. The level of activation signals received by B cells

when interacting with T cells is determined by the physical properties of the antigen: its avidity to the BCR, the B cell's antigen processing and presentation ability, and the binding efficiency of the MHC complex to TCR. Each of these steps contribute towards the duration of the immunological synapse with helper T cells [81, 90, 167], and hence, ultimately, the strength and longevity of signals received. Given the range of affinities expected in the B cell repertoire, for any given challenge, fewer cells will receive a strong stimulatory signal than a weak signal. Since differentiation to ASC prevents further antibody affinity maturation and isotype switching, suppressing this outcome in the strongly activated cells is necessary to produce a large population of high affinity B cells of specialised Ig classes. These results indicate an automated feature in the system where only after multiplying through several divisions and expanding their number, are these valuable cells permitted to differentiate to ASCs.

In contrast, the majority of activated B cells are likely to be stimulated sub-optimally. My results suggest that, rather than wasting these populations, a default programme to differentiate is triggered to ensure their usefulness in the humoral response. As these cells do not receive a strong impetus to divide and only progress slowly, their differentiation threshold is achieved early, such that many can begin secreting antibody prior to apoptosis. Although of low-affinity and most likely IgM, these secreted antibodies can begin to neutralise, or at least impede their target antigens early in the immune response.

These considerations reveal that the cellular machinery which leads to ASC differentiation may be shared for high and low affinity cells. Thus, rather than evolving to bestow these cells with new instructions, the immune system can take advantage of competing cell fates to achieve the same sophisticated outcome.

The conditions used here emulated a primary immune response, where naïve B cells receive T cell derived stimulation in order to activate, proliferate, and contract once the infection is cleared and those lymphocytes are no longer required. A major feature of the adaptive immune response is its ability to form memory cells. The low-affinity, naïve-like state of memory cells suggest that they form early in the germinal centre [168]. In the imaging experiments, time to die was found to have an extremely long-tailed distribution: not all the cells died, and 2-13% of divided cells survived until the end of imaging, with higher proportions in low stimuli and low generations. Further, the uncensored propensity to differentiate found in Chapter 4 suggested that not all activated cells are programmed to differentiate. The possibility remains that these long-lived, undifferentiated cells may have been the beginnings of memory cell formation, and also arise as a result of heterogeneity in competing times to fates.

It must be noted that a larger proportion of ASCs in a given cell generation does not necessarily mean more secreting cells overall. Populations receiving low CD40 stimulation have slower division kinetics compared to their counterparts receiving higher stimulation, and expand little from their starting population. Moreover, cells receiving high CD40 stimulation multiply rapidly and achieve higher generation numbers, which are subsequently more likely to undergo division-linked differentiation. This brings our findings in line with earlier studies which report that T dependent stimulation drives ASC formation [58, 169]. The strongly activated cells likely correspond to lymphoblasts that remain actively dividing in the germinal centres of lymphatic tissue, where they undergo affinity maturation and multiple rounds of proliferation prior to differentiating into a large nett population of plasmablasts. Mildly activated cells do not expand into such large populations; however, they are consistent with the short-lived plasmablasts found early in the immune response at the periphery of germinal centres [170].

At first, these results appear to contradict the findings of Bolduc *et al.*, where constitutive CD40 signalling in transgenic mice (CD40LBTg) appeared to terminate the germinal centre response [171]. Although hyperproliferation was initially observed, as would be expected from our data, the presence of germinal centre B cells was diminished by 1 week after challenge when compared to wild type, along with reduced antigen-specific IgG_1 cells late in the response. To reconcile with these observations, we must take into consideration both the increased division rates introduced with enhanced CD40 stimulation, and division linked differentiation [67] and isotype switching [92]. By accumulating mitotic events early in the response, these cells are likely driven to differentiate to ASC earlier in the response than normal, and indeed large numbers of ASCs were found in the T cell areas adjacent to germinal centres merely 7 days after immunisation, and marginal zone B cells were found to express increased levels of *prdm1* (Blimp-1) and *irf4*, markers of differentiation [172]. By progressing through their division and differentiation programs much faster than normal, enhanced CD40 signalling would thus lead to early cessation of the germinal centre response, which under normal circumstances is primarily driven by proliferating lymphoblasts [173].

Further, for antibody modifications, the authors reported IgG_1 switching early in the response, but a diminished IgG_1 response later in the experiment. A possible cause for this loss in isotype is the late-stage, division-linked switching to IgE [92] or other immunoglobulin isotypes, which were not measured.

For this project, anti-CD40 and IL-4 were used as a means of focussing on T cell dependent activation. In particular, the effects of varying CD40 were studied; however, CD40 alone is insufficient for activating substantial amounts of B cells [92, 93]. Unlike CD8+ T cells where individual stimulatory signals appear to be additive and a signal of sufficient strength can initiate proliferation [124], B cells require cytokines such as IL-4 as a secondary signal

to promote proliferation and switching [174], perhaps indicative of complementary roles in proliferation kinetics. In filming of the effects of IL-4 concentration on times to fates, preliminary results indicated an increase in the fraction of cells induced to divide each generation, but the effects on death and differentiation were unable to be resolved (data not shown). As such, investigations into this cytokine and others such as IL-5, IL-21, and interferon-γ remain ongoing. It would be of interest to uncover how each of these cytokines control individual parameters in the B cell response; whether they modulate differentiation kinetics in the same or different ways, and whether when used in combination, their effects will add, subtract, synergize, show dominance effects, or perhaps behave with redundancy.

Different methods of modifying differentiation outcomes were observed here. We found direct modulation of differentiation times, as with changing generation numbers. A second mechanism was by controlling division time as a competing cell fate. A third possibility was by modifying the propensity to differentiate, as suggested by the difference in modelled p values between Chapter 3 and 4 imaging experiments.

An alternative method of controlling differentiation was also explored, where the times to fates were determined from activation. This was found to be inconsistent with the cell cycle inhibition data, given that the population's differentiation rate is expected to remain equal regardless of whether the cells divide or not. Instead, differentiation increased markedly in the absence of divisions, indicating some suppressive effects of mitosis on differentiation, in support of the competition hypothesis where fate timers reset upon cell division.

T cell dependent stimulation is not the only method for stimulating B cells. T cell independent stimulation offers unique activation properties, and an opportunity to study the B cell response under an alternate system. Lipopolysaccharide (LPS) is one such option, stimulating B cells through toll-like receptor 4 (TLR-4) as a means of TI activation [56, 70, 175]. This method also produces large amounts of ASCs, however, as for TD stimulation, still induces homotypic adhesion and prevents long-term tracking of individual cells by microscopy. Whether differentiation patterns remain immutable or may be regulated by LPS or other TI activating signals remains unknown, but would be of interest, particularly in the context of competing cell fates.

One common method of activating B cells that avoids homotypic adhesion is stimulation with CpG through TLR-9, however cells do not differentiate to ASC using this method [70, 126]. Earlier filming experiments of CpG stimulated B cells demonstrated a high level of familial concordance between division and death outcomes, similar to that observed with CD40 here. Even cousin cells retained a substantial level of concordance, indicative of a method of pre-programming the number of times cells will divide in progenitors at the time of activation. Mother-daughter cells, however, exhibited very little correlation in times

to divide, and subsequent division times tended to revert to the mean [126]. These trends within cell families could not be interrogated in the CD40 system in the same way, due to upregulation of leukocyte function-associated antigen-1 (LFA-1) and intercellular cell adhesion molecules (ICAM-1 and ICAM-3) [176], causing homotypic adhesion and hence preventing the tracing of large family trees.

A method for circumventing the problem of homotypic adhesion while still obtaining familial differentiation patterns is to sort for single cells using flow cytometry, and increase throughput with multiplexing assays where cells are labelled with unique combinations of division-tracking dyes [177, 178]. Although not a microscopy method and hence lacking temporal information, inheritance data can be inferred from the descendants of individually identifiable founder cells. Undivided cells are labelled with division tracking dyes, sorted into cell culture wells, and left to divide and differentiate freely for several days. Upon analysis, the generation number and phenotypes of all detected descendants may be collected and compared for concordance. Data has been collected in this way for T cells [177, 178]. Similar analyses for B cells are possible and will be informative for differentiation, isotype switching, and changes in other markers detectable using flow cytometry.

The tendency for all members of a family of activated B or T lymphocytes to simultaneously stop proliferating, or reach 'division destiny', can now be attributed to the proto-oncogene Myc [135, 179], a key driver of the metabolic switch to glycolysis after lymphocyte activation. Levels of Myc protein peak in the undivided cell soon after activation, and decline over the subsequent days at the same rate regardless of the number of divisions undergone. Consequently, descendent cells of the same progenitor retain similar levels of Myc protein, and its loss beyond a certain threshold deprives cells of their motivation to divide [135]. Myc is produced by several activation pathways, and its role in integrating CD40 signalling to drive proliferation has been established [135, 180].

These systems all suggest a level of pre-programming in the progenitor cell, where the offspring then behave as related 'automatons' until a subsequent change in their presumably epigenetic coding modifies their behaviour. Indeed, this is consistent with the remarkably high levels of correlations and concordances observed between sibling cell fates in the filming data. Were the mechanisms driving the apparent stochastic cell fates primarily extrinsic to the cells, and created by a microenvironment difference, we would expect greater discrepancies between sibling cell fates. While it could be argued that siblings shared the same paddock and hence an identical microenvironment, there were several instances of sibling pairs that were followed in the same paddock, but still produced non-concordant fates (and these can be accounted for by intracellular competing fates which required very similar times [128]). Similarly, there were a number of cell siblings which initiated in the same well, but escaped their paddocks and traversed across the microgrid, drifting apart. Despite their distance,

these sibling cells would share the same fate at similar times (data not shown). Further, analyses of recorded fate outcomes across each microgrid indicated no relation between paddock location and cell fates (Cameron Wellard, data not shown). Thus, the contribution of differences in the local environment towards population variation is negligible under these circumstances, and likewise, any hypothesis attributing the population's variation to an ongoing, cell autonomous, stochastic process may be eliminated. Examining the level of pre-programming and how susceptible activated cells are to further immune modulation would be valuable for understanding and manipulating the immune response, however the ability to trace complete lineages is currently limited.

When imaging cells for the analyses employed here, individual cells must remain identifiable as they are assessed over time. Following their location, size, trajectory, granularity, fluorescence-intensity and behaviour, however, necessitates a large amount of time, and for a substantial data set, requires many months of tracking, comparing cells' appearances between consecutive frames, as well as across multiple channels. Efforts have been made to build automatic tracking software [181, 182]; while these have been successful with round, and even motile cells, the inherent homotypic adhesion of T cell activated B cells makes cell detection and segregation challenging. These activated B cells climb over each other in 3-dimentional space, form pseudopods and various protrusions that are difficult for software to detect, and the membrane is not always well defined; while visual processing in the human mind is excellent at deducing and completing shapes, even when some edges are not clearly visible, it is difficult to program software to complete the same task. Software that can follow cells by recording their attributes across multiple colour channels and over time would have more information to work with for accurate tracks, though these do not seem to be readily available. An assessment of current tracking algorithms by Ulman et al. [182] found some software to score well in each technical aspect, though none were able to obtain fully correct solutions to the test images. Thus, correcting erroneous tracks from automated detection was found to be more time-consuming for our experimental setup than simply tracking them manually.

A common tool for automated cell tracking is the use of ubiquitously fluorescent cells to aid in cell segregation. Mice ubiquitously expressing DsRed, enhanced cyan fluorescent protein (ECFP), or monomeric red fluorescent protein (mRFP) were obtained for this purpose; however, the difficulty in separating adjacent cells of the same colour remained. Consequently, the additional channel required for imaging these fluorochromes was dispensed of in favour of shorter time intervals between images, particularly in the older (and slower) microscopy system (Zeiss Axiovert 200M). PI was excluded for the same reason, since PI uptake would occur several frames (tens of minutes) after the onset of blebbing. The newer and faster microscopy system (Zeiss Axio Observer.Z1) now offers time for acquisition from additional

channels while maintaining short intervals between images, opening up the possibility of re-including these colours should automated cell tracking become more reliable.

A second method for following individual cells is to physically separate them during image acquisition. The use of microgrids here segregated cells initially as they were seeded, however did not stop them from aggregating after the first division. Micromanipulation at the time of cell division is possible but extremely time consuming. Instead, several groups have developed intricate microfluidic slides, with various designs for single-cell 'catchments' to isolate individual cells even as they divide and develop during imaging [183-185]. These have the potential to be beneficial for following cell family trees in future experiments.

Single cell imaging provided data for calculating uncensored distributions of times to cell fates. The next step was test for these uncensored distributions by directly inhibiting division, while simultaneously testing the competition model. A range of cell cycle inhibitors were assessed for their ability to manipulate cell divisions and influence differentiation to ASC.

For differentiation, the results were consistent with the competition hypothesis in that a greater proportion of ASC was observed overall after 24 hours of cell cycle arrest. The proportion of differentiated cells exceeded even that of the untreated cells when summed by generations, inconsistent with an alternative hypothesis where differentiation is programmed from cell activation. Curiously, these differentiation levels did not meet the proportions predicted from uncensoring analyses of earlier data. There are several possible explanations for this, the first being that cells may need to progress through S phase in order for its transcriptional change to manifest [165]. Alternatively, it's possible that lymphoblasts and plasmablasts possess different proliferation kinetics, an effect that would skew our observations of population data, for instance if plasmablasts have reduced survival under these culture conditions.

As noted by Hasbold *et al.* [67], a common assumption in our calculations is that plasmablasts proliferate at the same rate after differentiation as lymphoblasts, Although they rely on different survival signals to maintain their cell numbers [63], there has been little evidence thus far that they would divide or die at different rates immediately after differentiation (and prior to maturing into plasma cells which then have a slow turnover). Even though cells that differentiate appear to have longer division times, a cause for this correlation is presented in our model where long division times permit more cells to differentiate (Chapter 3; [125]). Despite the two behaviours acting independently, censorship (by division) skews the observed distribution of differentiation times. Whether these differentiated cells then go on to proliferate at different rates in subsequent generations is unknown.

In addition to unveiling differentiation times, the various cell cycle inhibitors appeared to be effective at uncensoring cell death, indicative of an 'always on' death time that progresses

regardless of cell cycle phase. The S and G_2/M phase inhibitors in particular demonstrated independence between division-cessation and survival at the concentrations tested.

Many of the inhibitors tested here are approved chemotherapeutic agents for treating cancer, including Palbociclib, Etoposide, Paclitaxel, and Vincristine (National Cancer Institute, U.S. Department of Health and Human Services). Although these compounds have known targets, a better understanding of their effects on division kinetics would benefit patients with potential personalised treatments, and lowered doses of drugs to reduce ill side-effects while remaining effective at combating cancerous cells. Furthermore, with a Cyton model of quantitative cellular behaviour, it would be possible to investigate how different oncogenic mutations affect proliferation and cell survival, and thus which individual division and apoptotic modulatory agents are most suited to a particular patient.

This Cyton model for quantifying cell division and death outcomes was developed over a number of years from careful, quantitative analyses of flow cytometry data, and more recently, single cell imaging data. These results offer new insights into the kinetics and cellular machinery in operation for interpreting B cell activation signals, and remain consistent with the model of competing intracellular fate outcomes. The finding that simple control of one cell fate can lead to emergent properties at the population level is valuable for understanding B cell response outcomes, with the potential to translate to other cell systems.

References

1. Burnet, F.M., *A modification of Jerne's theory of antibody production using the concept of clonal selection Australian Journal of Science, vol.* ***20****.* 1957.

2. Hodgkin, P.D., Heath, W.R., and Baxter, A.G., *The clonal selection theory: 50 years since the revolution.* Nat Immunol, 2007. **8**(10): p. 1019-26.

3. Pancer, Z., Amemiya, C.T., Ehrhardt, G.R.A., Ceitlin, J., Larry Gartland, G., and Cooper, M.D., *Somatic diversification of variable lymphocyte receptors in the agnathan sea lamprey.* Nature, 2004. **430**(6996): p. 174-180.

4. Miller, J.F. and Mitchell, G.F., *Cell to cell interaction in the immune response. I. Hemolysin-forming cells in neonatally thymectomized mice reconstituted with thymus or thoracic duct lymphocytes.* J Exp Med, 1968. **128**(4): p. 801-20.

5. Mitchell, G.F. and Miller, J.F., *Cell to cell interaction in the immune response. II. The source of hemolysin-forming cells in irradiated mice given bone marrow and thymus or thoracic duct lymphocytes.* J Exp Med, 1968. **128**(4): p. 821-37.

6. Glick, B., Chang, T.S., and Jaap, R.G., *The Bursa of Fabricius and Antibody Production.* Poultry Science, 1956. **35**(1): p. 224-225.

7. Mitchell, G.F. and Miller, J.F., *Immunological activity of thymus and thoracic-duct lymphocytes.* Proceedings of the National Academy of Sciences of the United States of America, 1968. **59**(1): p. 296-303.

8. Miller, Jacques f.a.P. and Sadelain, M., *The Journey from Discoveries in Fundamental Immunology to Cancer Immunotherapy.* Cancer Cell, 2015. **27**(4): p. 439-449.

9. Lopes-Carvalho, T. and Kearney, J.F., *Development and selection of marginal zone B cells.* Immunological Reviews, 2004. **197**(1): p. 192-205.

10. Shapiro-Shelef, M. and Calame, K., *Regulation of plasma-cell development.* Nature Reviews Immunology, 2005. **5**(3): p. 230-242.

11. Fairfax, K.A., Kallies, A., Nutt, S.L., and Tarlinton, D.M., *Plasma cell development: From B-cell subsets to long-term survival niches.* Seminars in Immunology, 2008. **20**(1): p. 49-58.

12. Woof, J.M. and Burton, D.R., *Human antibody–Fc receptor interactions illuminated by crystal structures.* Nature Reviews Immunology, 2004. **4**(2): p. 89-99.

13. Schroeder, H.W. and Cavacini, L., *Structure and function of immunoglobulins.* Journal of Allergy and Clinical Immunology, 2010. **125**(2, Supplement 2): p. S41-S52.

14. Hart, S.P., Smith, J.R., and Dransfield, I., *Phagocytosis of opsonized apoptotic cells: roles for 'old-fashioned' receptors for antibody and complement.* Clin Exp Immunol, 2004. **135**(2): p. 181-5.

15. Zeng, M.Y., Cisalpino, D., Varadarajan, S., Hellman, J., Warren, H.S., Cascalho, M., Inohara, N., and Núñez, G., *Gut Microbiota-Induced Immunoglobulin G Controls Systemic Infection by Symbiotic Bacteria and Pathogens.* Immunity, 2016. **44**(3): p. 647-658.

16. Rose, M.E., *Evaluating and managing hypogammaglobulinemia.* Cleveland Clinic journal of medicine, 2006. **73**(2): p. 133.

17. Wall, S.D. and Jones, B., *Gastrointestinal tract in the immunocompromised host: opportunistic infections and other complications.* Radiology, 1992. **185**(2): p. 327-335.

18. Shaffer, A., Lin, K.-I., Kuo, T.C., Yu, X., Hurt, E.M., Rosenwald, A., Giltnane, J.M., Yang, L., Zhao, H., and Calame, K., *Blimp-1 orchestrates plasma cell differentiation by extinguishing the mature B cell gene expression program.* Immunity, 2002. **17**(1): p. 51-62.

19. Manz, R.A., Hauser, A.E., Hiepe, F., and Radbruch, A., *Maintenance of serum antibody levels.* Annual Review of Immunology, 2005. **23**(1): p. 367-386.

20. Belnoue, E., Tougne, C., Rochat, A.-F., Lambert, P.-H., Pinschewer, D.D., and Siegrist, C.-A., *Homing and adhesion patterns determine the cellular composition of the bone marrow plasma cell niche.* The Journal of Immunology, 2012. **188**(3): p. 1283-1291.

21. Chu, V.T. and Berek, C., *The establishment of the plasma cell survival niche in the bone marrow.* Immunological Reviews, 2013. **251**(1): p. 177-188.

22. Corcoran, L.M. and Tarlinton, D.M., *Regulation of germinal center responses, memory B cells and plasma cell formation—an update.* Current Opinion in Immunology, 2016. **39**: p. 59-67.

23. Hardy, R.R. and Hayakawa, K., *B Cell Development Pathways.* Annual Review of Immunology, 2001. **19**(1): p. 595-621.

24. Halliley, J.L., Tipton, C.M., Liesveld, J., Rosenberg, A.F., Darce, J., Gregoretti, I.V., Popova, L., Kaminiski, D., Fucile, C.F., and Albizua, I., *Long-lived plasma cells are contained within the CD19− CD38hiCD138+ subset in human bone marrow.* Immunity, 2015. **43**(1): p. 132-145.

25. Corbett, S.J., Tomlinson, I.M., Sonnhammer, E.L.L., Buck, D., and Winter, G., *Sequence of the human immunoglobulin diversity (D) segment locus: a systematic analysis provides no evidence for the use of DIR segments, inverted D segments, "minor" D segments or D-D recombination11Edited By J. Karn.* Journal of Molecular Biology, 1997. **270**(4): p. 587-597.

26. Ravetch, J.V., Siebenlist, U., Korsmeyer, S., Waldmann, T., and Leder, P., *Structure of the human immunoglobulin μ locus: Characterization of embryonic and rearranged J and D genes.* Cell, 1981. **27**(3, Part 2): p. 583-591.

27. Cook, G.P. and Tomlinson, I.M., *The human immunoglobulin VH repertoire.* Immunology Today, 1995. **16**(5): p. 237-242.

28. Kurosawa, Y. and Tonegawa, S., *Organization, structure, and assembly of immunoglobulin heavy chain diversity DNA segments.* The Journal of Experimental Medicine, 1982. **155**(1): p. 201-218.

29. Trepel, F., *Number and distribution of lymphocytes in man. A critical analysis.* Klinische Wochenschrift, 1974. **52**(11): p. 511-515.

30. Perelson, A.S. and Oster, G.F., *Theoretical studies of clonal selection: Minimal antibody repertoire size and reliability of self-non-self discrimination.* Journal of Theoretical Biology, 1979. **81**(4): p. 645-670.

31. Coleclough, C., Perry, R.P., Karjalainen, K., and Weigert, M., *Aberrant rearrangements contribute significantly to the allelic exclusion of immunoglobulin gene expression.* Nature, 1981. **290**(5805): p. 372-378.

32. Edwards, B.M., Barash, S.C., Main, S.H., Choi, G.H., Minter, R., Ullrich, S., Williams, E., Du Fou, L., Wilton, J., Albert, V.R., Ruben, S.M., and Vaughan, T.J., *The Remarkable Flexibility of the Human Antibody Repertoire; Isolation of Over One Thousand Different Antibodies to a Single Protein, BLyS.* Journal of Molecular Biology, 2003. **334**(1): p. 103-118.

33. Hieter, P.A., Maizel, J., and Leder, P., *Evolution of human immunoglobulin kappa J region genes.* Journal of Biological Chemistry, 1982. **257**(3): p. 1516-1522.

34. Gay, D., Saunders, T., Camper, S., and Weigert, M., *Receptor editing: an approach by autoreactive B cells to escape tolerance.* The Journal of Experimental Medicine, 1993. **177**(4): p. 999-1008.

35. Levine, M.H., Haberman, A.M., Sant'angelo, D.B., Hannum, L.G., Cancro, M.P., Janeway, C.A., and Shlomchik, M.J., *A B-cell receptor-specific selection step governs immature to mature B cell differentiation.* Proceedings of the National Academy of Sciences, 2000. **97**(6): p. 2743-2748.

36. Goodnow, C.C., Crosbie, J., Jorgensen, H., Brink, R.A., and Basten, A., *Induction of self-tolerance in mature peripheral B lymphocytes.* Nature, 1989. **342**(6248): p. 385-391.

37. Nemazee, D., Russell, D., Arnold, B., Hahmmerling, G., Allison, J., Miller, J.F.a.P., Morahan, G., and Buerki, K., *Clonal Deletion of Autospecific B Lymphocytes.* Immunological Reviews, 1991. **122**(1): p. 117-132.

38. Goodnow, C.C., Cyster, J.G., Hartley, S.B., Bell, S.E., Cooke, M.P., Healy, J.I., Akkaraju, S., Rathmell, J.C., Pogue, S.L., and Shokat, K.P., *Self-Tolerance Checkpoints in B Lymphocyte Development*, in *Advances in Immunology*, F.J. Dixon, Editor. 1995, Academic Press. p. 279-368.

39. Kurd, N. and Robey, E.A., *T-cell selection in the thymus: a spatial and temporal perspective.* Immunological Reviews, 2016. **271**(1): p. 114-126.

40. Palmer, E., *Cell death and immunity: Negative selection—clearing out the bad apples from the T-cell repertoire.* Nature Reviews Immunology, 2003. **3**(5): p. 383.

41. Sprent, J. and Kishimoto, H., *The thymus and negative selection.* Immunological reviews, 2002. **185**(1): p. 126-135.

42. Zinkernagel, R.M. and Doherty, P.C., *MHC-restricted cytotoxic T cells: studies on the biological role of polymorphic major transplantation antigens determining T-cell restriction-specificity, function, and responsiveness*, in *Advances in immunology*. 1979, Elsevier. p. 51-177.

43. Morris, P.J., Wood, K.J., Sprent, J., and Kishimoto, H., *The thymus and central tolerance.* Philosophical Transactions of the Royal Society of London. Series B: Biological Sciences, 2001. **356**(1409): p. 609-616.

44. Croft, N.P., Smith, S.A., Pickering, J., Sidney, J., Peters, B., Faridi, P., Witney, M.J., Sebastian, P., Flesch, I.E., and Heading, S.L., *Most viral peptides displayed by class I MHC on infected cells are immunogenic.* Proceedings of the National Academy of Sciences, 2019. **116**(8): p. 3112-3117.

45. Cresswell, P., *Assembly, transport, and function of MHC class II molecules.* Annual review of immunology, 1994. **12**(1): p. 259-291.

46. Chan, S.H., Cosgrove, D., Waltzinger, C., Benoist, C., and Mathis, D., *Another view of the selective model of thymocyte selection.* Cell, 1993. **73**(2): p. 225-236.

47. Davis, C.B., Killeen, N., Crooks, M.E.C., Raulet, D., and Littman, D.R., *Evidence for a stochastic mechanism in the differentiation of mature subsets of T lymphocytes.* Cell, 1993. **73**(2): p. 237-247.

48. Lanzavecchia, A., *Antigen-specific interaction between T and B cells.* Nature, 1985. **314**(6011): p. 537-539.

49. Maclennan, I.C., Toellner, K.M., Cunningham, A.F., Serre, K., Sze, D.M., Zuniga, E., Cook, M.C., and Vinuesa, C.G., *Extrafollicular antibody responses.* Immunol Rev, 2003. **194**: p. 8-18.

50. Jenkins, M.R., Kedzierska, K., Doherty, P.C., and Turner, S.J., *Heterogeneity of Effector Phenotype for Acute Phase and Memory Influenza A Virus-Specific CTL.* The Journal of Immunology, 2007. **179**(1): p. 64-70.

51. Sallusto, F., Geginat, J., and Lanzavecchia, A., *Central Memory and Effector Memory T Cell Subsets: Function, Generation, and Maintenance.* Annual Review of Immunology, 2004. **22**(1): p. 745-763.

52. Kalia, V., Sarkar, S., Gourley, T.S., Rouse, B.T., and Ahmed, R., *Differentiation of memory B and T cells.* Current Opinion in Immunology, 2006. **18**(3): p. 255-264.

53. Stemberger, C., Huster, K.M., Koffler, M., Anderl, F., Schiemann, M., Wagner, H., and Busch, D.H., *A Single Naive CD8+ T Cell Precursor Can Develop into Diverse Effector and Memory Subsets.* Immunity, 2007. **27**(6): p. 985-997.

54. Armitage, R.J., Fanslow, W.C., Strockbine, L., Sato, T.A., Clifford, K.N., Macduff, B.M., Anderson, D.M., Gimpel, S.D., Davis-Smith, T., Maliszewski, C.R., Clark, E.A., Smith, C.A., Grabstein, K.H., Cosman, D., and Spriggs, M.K., *Molecular and biological characterization of a murine ligand for CD40.* Nature, 1992. **357**(6373): p. 80-82.

55. Noelle, R.J., Roy, M., Shepherd, D.M., Stamenkovic, I., Ledbetter, J.A., and Aruffo, A., *A 39-kDa protein on activated helper T cells binds CD40 and transduces the signal for cognate activation of B cells.* Proceedings of the National Academy of Sciences, 1992. **89**(14): p. 6550-6554.

56. Coutinho, A., Gronowicz, E., Bullock, W.W., and Möller, G., *Mechanism of thymus-independent immunocyte triggering: mitogenic activation of B cells results in specific immune responses.* Journal of Experimental Medicine, 1974. **139**(1): p. 74-92.

57. Kearney, J.F., Klein, J., Bockman, D.E., Cooper, M.D., and Lawton, A.R., *B Cell Differentiation Induced by Lipopolysaccharide.* V. Suppression of Plasma Cell Maturation by anti-μ: Mode of Action and Characteristics of Suppressed Cells, 1978. **120**(1): p. 158-166.

58. Phan, T.G., Paus, D., Chan, T.D., Turner, M.L., Nutt, S.L., Basten, A., and Brink, R., *High affinity germinal center B cells are actively selected into the plasma cell compartment.* The Journal of Experimental Medicine, 2006. **203**(11): p. 2419-2424.

59. Zotos, D. and Tarlinton, D.M., *Determining germinal centre B cell fate.* Trends in Immunology, 2012. **33**(6): p. 281-288.

60. Berek, C., Berger, A., and Apel, M., *Maturation of the immune response in germinal centers.* Cell, 1991. **67**(6): p. 1121-1129.

61. Roco, J.A., Mesin, L., Binder, S.C., Nefzger, C., Gonzalez-Figueroa, P., Canete, P.F., Ellyard, J., Shen, Q., Robert, P.A., Cappello, J., Vohra, H., Zhang, Y., Nowosad, C.R., Schiepers, A., Corcoran, L.M., Toellner, K.-M., Polo, J.M., Meyer-Hermann, M., Victora, G.D., and Vinuesa, C.G., *Class-Switch Recombination Occurs Infrequently in Germinal Centers.* Immunity, 2019. **51**(2): p. 337-350.e7.

62. Noia, J.M.D. and Neuberger, M.S., *Molecular Mechanisms of Antibody Somatic Hypermutation.* Annual Review of Biochemistry, 2007. **76**(1): p. 1-22.

63. Tangye, S.G., *Staying alive: regulation of plasma cell survival.* Trends in Immunology, 2011. **32**(12): p. 595-602.

64. Moser, K., Tokoyoda, K., Radbruch, A., Maclennan, I., and Manz, R.A., *Stromal niches, plasma cell differentiation and survival.* Current Opinion in Immunology, 2006. **18**(3): p. 265-270.

65. Peperzak, V., Vikström, I., Walker, J., Glaser, S.P., Lepage, M., Coquery, C.M., Erickson, L.D., Fairfax, K., Mackay, F., Strasser, A., Nutt, S.L., and Tarlinton, D.M., *Mcl-1 is essential for the survival of plasma cells.* Nature Immunology, 2013. **14**(3): p. 290-297.

66. Tangye, S.G., Avery, D.T., and Hodgkin, P.D., *A division-linked mechanism for the rapid generation of Ig-secreting cells from human memory B cells.* J Immunol, 2003. **170**(1): p. 261-9.

67. Hasbold, J., Corcoran, L.M., Tarlinton, D.M., Tangye, S.G., and Hodgkin, P.D., *Evidence from the generation of immunoglobulin G-secreting cells that stochastic mechanisms regulate lymphocyte differentiation.* Nat Immunol, 2004. **5**(1): p. 55-63.

68. Takeuchi, O. and Akira, S., *Pattern Recognition Receptors and Inflammation.* Cell, 2010. **140**(6): p. 805-820.

69. Medzhitov, R. and Janeway Jr, C.A., *Innate immune recognition and control of adaptive immune responses.* Seminars in Immunology, 1998. **10**(5): p. 351-353.

70. Hawkins, E.D., Turner, M.L., Wellard, C.J., Zhou, J.H.S., Dowling, M.R., and Hodgkin, P.D., *Quantal and graded stimulation of B lymphocytes as alternative strategies for regulating adaptive immune responses.* Nat Commun, 2013. **4**: p. 2406.

71. Pasare, C. and Medzhitov, R., *Toll-like receptors: linking innate and adaptive immunity.* Microbes and Infection, 2004. **6**(15): p. 1382-1387.

72. Akira, S. and Hemmi, H., *Recognition of pathogen-associated molecular patterns by TLR family.* Immunology Letters, 2003. **85**(2): p. 85-95.

73. Turner, M.L., Hawkins, E.D., and Hodgkin, P.D., *Quantitative Regulation of B Cell Division Destiny by Signal Strength.* The Journal of Immunology, 2008. **181**(1): p. 374-382.

74. Nürnberger, T. and Brunner, F., *Innate immunity in plants and animals: emerging parallels between the recognition of general elicitors and pathogen-associated molecular patterns.* Current Opinion in Plant Biology, 2002. **5**(4): p. 318-324.

75. Chaturvedi, A., Dorward, D., and Pierce, S.K., *The B Cell Receptor Governs the Subcellular Location of Toll-like Receptor 9 Leading to Hyperresponses to DNA-Containing Antigens.* Immunity, 2008. **28**(6): p. 799-809.

76. Cyster, J.G., Hartley, S.B., and Goodnow, C.C., *Competition for follicular niches excludes self-reactive cells from the recirculating B-cell repertoire.* Nature, 1994. **371**(6496): p. 389-395.

77. Cook, M.C., Basten, A., and Groth, B.F.D.S., *Outer Periarteriolar Lymphoid Sheath Arrest and Subsequent Differentiation of Both Naive and Tolerant Immunoglobulin Transgenic B Cells Is Determined by B Cell Receptor Occupancy.* The Journal of Experimental Medicine, 1997. **186**(5): p. 631-643.

78. Hay, J.B., Cahill, R.N.P., and Trnka, Z., *The kinetics of antigen-reactive cells during lymphocyte recruitment.* Cellular Immunology, 1974. **10**(1): p. 145-153.

79. Neefjes, J.J., Stollorz, V., Peters, P.J., Geuze, H.J., and Ploegh, H.L., *The biosynthetic pathway of MHC class II but not class I molecules intersects the endocytic route.* Cell, 1990. **61**(1): p. 171-183.

80. Peters, P.J., Neefjes, J.J., Oorschot, V., Ploegh, H.L., and Geuze, H.J., *Segregation of MHC class II molecules from MHC class I molecules in the Golgi complex for transport to lysosomal compartments.* Nature, 1991. **349**(6311): p. 669-676.

81. Carrasco, Y.R., Fleire, S.J., Cameron, T., Dustin, M.L., and Batista, F.D., *LFA-1/ICAM-1 Interaction Lowers the Threshold of B Cell Activation by Facilitating B Cell Adhesion and Synapse Formation.* Immunity, 2004. **20**(5): p. 589-599.

82. Lee, F., Yokota, T., Otsuka, T., Meyerson, P., Villaret, D., Coffman, R., Mosmann, T., Rennick, D., Roehm, N., and Smith, C., *Isolation and characterization of a mouse interleukin cDNA clone that expresses B-cell stimulatory factor 1 activities and T-cell- and mast-cell-stimulating activities.* Proceedings of the National Academy of Sciences, 1986. **83**(7): p. 2061-2065.

83. Yokota, T., Otsuka, T., Mosmann, T., Banchereau, J., Defrance, T., Blanchard, D., De Vries, J.E., Lee, F., and Arai, K., *Isolation and characterization of a human interleukin cDNA clone, homologous to mouse B-cell stimulatory factor 1, that expresses B-cell- and T-cell-stimulating activities.* Proceedings of the National Academy of Sciences, 1986. **83**(16): p. 5894-5898.

84. Rousset, F., Garcia, E., Defrance, T., Péronne, C., Vezzio, N., Hsu, D.H., Kastelein, R., Moore, K.W., and Banchereau, J., *Interleukin 10 is a potent growth and differentiation factor for activated human B lymphocytes.* Proceedings of the National Academy of Sciences, 1992. **89**(5): p. 1890-1893.

85. Zotos, D., Coquet, J.M., Zhang, Y., Light, A., D'costa, K., Kallies, A., Corcoran, L.M., Godfrey, D.I., Toellner, K.-M., Smyth, M.J., Nutt, S.L., and Tarlinton, D.M., *IL-21 regulates germinal center B cell differentiation and proliferation through a B cell–intrinsic mechanism.* The Journal of Experimental Medicine, 2010. **207**(2): p. 365-378.

86. Coffman, R.L., Seymour, B.W., Lebman, D.A., Hiraki, D.D., Christiansen, J.A., Shrader, B., Cherwinski, H.M., Savelkoul, H.F., Finkelman, F.D., Bond, M.W., and Et Al., *The role of helper T cell products in mouse B cell differentiation and isotype regulation.* Immunol Rev, 1988. **102**: p. 5-28.

87. Lebman, D.A. and Coffman, R.L., *Interleukin 4 causes isotype switching to IgE in T cell-stimulated clonal B cell cultures.* The Journal of Experimental Medicine, 1988. **168**(3): p. 853-862.

88. Lundgren, M., Persson, U., Larsson, P., Magnusson, C., Smith, C.I.E., Hammarström, L., and Severinson, E., *Interleukin 4 induces synthesis of IgE and IgG4 in human B cells.* European Journal of Immunology, 1989. **19**(7): p. 1311-1315.

89. Tolar, P., Sohn, H.W., and Pierce, S.K., *The initiation of antigen-induced B cell antigen receptor signaling viewed in living cells by fluorescence resonance energy transfer.* Nature Immunology, 2005. **6**(11): p. 1168-1176.

90. Batista, F.D. and Neuberger, M.S., *Affinity Dependence of the B Cell Response to Antigen: A Threshold, a Ceiling, and the Importance of Off-Rate.* Immunity, 1998. **8**(6): p. 751-759.

91. Kehry, M.R. and Hodgkin, P.D., *B-Cell Activation by Helper T-Cell Membranes.* 1994. **14**(3-4): p. 221-238.

92. Hasbold, J., Lyons, A.B., Kehry, M.R., and Hodgkin, P.D., *Cell division number regulates IgG1 and IgE switching of B cells following stimulation by CD40 ligand and IL-4.* European Journal of Immunology, 1998. **28**(3): p. 1040-1051.

93. Rush, J.S. and Hodgkin, P.D., *B cells activated via CD40 and IL-4 undergo a division burst but require continued stimulation to maintain division, survival and differentiation.* European Journal of Immunology, 2001. **31**(4): p. 1150-1159.

94. Hawkins, E.D., Hommel, M., Turner, M.L., Battye, F.L., Markham, J.F., and Hodgkin, P.D., *Measuring lymphocyte proliferation, survival and differentiation using CFSE time-series data.* Nat Protoc, 2007. **2**(9): p. 2057-67.

95. Heath, A.W., Wu, W.W., and Howard, M.C., *Monoclonal antibodies to murine CD40 define two distinct functional epitopes.* European Journal of Immunology, 1994. **24**(8): p. 1828-1834.

96. Moon, H., Severinson, E., Heusser, C., Johansson, S., Möller, G., and Persson, U., *Regulation of IgG1 and IgE synthesis by interleukin 4 in mouse B cells.* Scandinavian journal of immunology, 1989. **30**(3): p. 355-361.

97. Snapper, C. and Paul, W., *Interferon-gamma and B cell stimulatory factor-1 reciprocally regulate Ig isotype production.* Science, 1987. **236**(4804): p. 944-947.

98. Lyons, A.B. and Parish, C.R., *Determination of lymphocyte division by flow cytometry.* J Immunol Methods, 1994. **171**(1): p. 131-7.

99. Quah, B.J.C., Warren, H.S., and Parish, C.R., *Monitoring lymphocyte proliferation in vitro and in vivo with the intracellular fluorescent dye carboxyfluorescein diacetate succinimidyl ester.* Nature Protocols, 2007. **2**(9): p. 2049-2056.

100. Quah, B.J.C. and Parish, C.R., *New and improved methods for measuring lymphocyte proliferation in vitro and in vivo using CFSE-like fluorescent dyes.* Journal of Immunological Methods, 2012. **379**(1): p. 1-14.

101. Tempany, J.C., Zhou, J.H.S., Hodgkin, P.D., and Bryant, V.L., *Superior properties of CellTrace Yellow™ as a division tracking dye for human and murine lymphocytes.* Immunology & Cell Biology, 2018. **96**(2): p. 149-159.

102. Hodgkin, P.D., Lee, J.H., and Lyons, A.B., *B cell differentiation and isotype switching is related to division cycle number.* The Journal of Experimental Medicine, 1996. **184**(1): p. 277-281.

103. Deenick, E.K., Hasbold, J., and Hodgkin, P.D., *Switching to IgG3, IgG2b, and IgA is division linked and independent, revealing a stochastic framework for describing differentiation.* J Immunol, 1999. **163**(9): p. 4707-14.

104. Tangye, S.G., Ferguson, A., Avery, D.T., Ma, C.S., and Hodgkin, P.D., *Isotype switching by human B cells is division-associated and regulated by cytokines.* J Immunol, 2002. **169**(8): p. 4298-306.

105. Mandler, R., Finkelman, F.D., Levine, A.D., and Snapper, C.M., *IL-4 induction of IgE class switching by lipopolysaccharide-activated murine B cells occurs predominantly through sequential switching.* The Journal of Immunology, 1993. **150**(2): p. 407-418.

106. Nutt, S.L., Heavey, B., Rolink, A.G., and Busslinger, M., *Commitment to the B-lymphoid lineage depends on the transcription factor Pax5.* Nature, 1999. **401**(6753): p. 556-562.

107. Revilla-I-Domingo, R., Bilic, I., Vilagos, B., Tagoh, H., Ebert, A., Tamir, I.M., Smeenk, L., Trupke, J., Sommer, A., Jaritz, M., and Busslinger, M., *The B-cell identity factor Pax5 regulates distinct transcriptional programmes in early and late B lymphopoiesis.* The EMBO Journal, 2012. **31**(14): p. 3130-3146.

108. Schebesta, A., Mcmanus, S., Salvagiotto, G., Delogu, A., Busslinger, G.A., and Busslinger, M., *Transcription Factor Pax5 Activates the Chromatin of Key Genes Involved in B Cell Signaling, Adhesion, Migration, and Immune Function.* Immunity, 2007. **27**(1): p. 49-63.

109. Pridans, C., Holmes, M.L., Polli, M., Wettenhall, J.M., Dakic, A., Corcoran, L.M., Smyth, G.K., and Nutt, S.L., *Identification of Pax5 Target Genes in Early B Cell Differentiation.* The Journal of Immunology, 2008. **180**(3): p. 1719-1728.

110. Nera, K.-P., Kohonen, P., Narvi, E., Peippo, A., Mustonen, L., Terho, P., Koskela, K., Buerstedde, J.-M., and Lassila, O., *Loss of Pax5 Promotes Plasma Cell Differentiation.* Immunity, 2006. **24**(3): p. 283-293.

111. Angelin-Duclos, C., Cattoretti, G., Lin, K.-I., and Calame, K., *Commitment of B Lymphocytes to a Plasma Cell Fate Is Associated with Blimp-1 Expression In Vivo.* The Journal of Immunology, 2000. **165**(10): p. 5462-5471.

112. Kallies, A., Hawkins, E.D., Belz, G.T., Metcalf, D., Hommel, M., Corcoran, L.M., Hodgkin, P.D., and Nutt, S.L., *Transcriptional repressor Blimp-1 is essential for T cell homeostasis and self-tolerance.* Nature Immunology, 2006. **7**(5): p. 466-474.

113. Nutt, S.L., Fairfax, K.A., and Kallies, A., *BLIMP1 guides the fate of effector B and T cells.* Nature Reviews Immunology, 2007. **7**(12): p. 923-927.

114. Kallies, A., Hasbold, J., Tarlinton, D.M., Dietrich, W., Corcoran, L.M., Hodgkin, P.D., and Nutt, S.L., *Plasma cell ontogeny defined by quantitative changes in blimp-1 expression.* J Exp Med, 2004. **200**(8): p. 967-77.

115. Vincent, S.D., Dunn, N.R., Sciammas, R., Shapiro-Shalef, M., Davis, M.M., Calame, K., Bikoff, E.K., and Robertson, E.J., *The zinc finger transcriptional repressor Blimp1/Prdm1 is dispensable for early axis formation but is required for specification of primordial germ cells in the mouse.* Development, 2005. **132**(6): p. 1315-1325.

116. Sanderson, R.D., Lalor, P., and Bernfield, M., *B lymphocytes express and lose syndecan at specific stages of differentiation.* Cell Regulation, 1989. **1**(1): p. 27-35.

117. Barwick, B.G., Scharer, C.D., Bally, A.P.R., and Boss, J.M., *Plasma cell differentiation is coupled to division-dependent DNA hypomethylation and gene regulation.* Nature Immunology, 2016. **17**(10): p. 1216-1225.

118. Knödel, M., Kuss, A.W., Berberich, I., and Schimpl, A., *Blimp-1 over-expression abrogates IL-4- and CD40-mediated suppression of terminal B cell differentiation but arrests isotype switching.* European Journal of Immunology, 2001. **31**(7): p. 1972-1980.

119. Rush, J.S., Liu, M., Odegard, V.H., Unniraman, S., and Schatz, D.G., *Expression of activation-induced cytidine deaminase is regulated by cell division, providing a mechanistic basis for division-linked class switch recombination.* Proceedings of the National Academy of Sciences of the United States of America, 2005. **102**(37): p. 13242-13247.

120. Hawkins, E.D., Turner, M.L., Dowling, M.R., Van Gend, C., and Hodgkin, P.D., *A model of immune regulation as a consequence of randomized lymphocyte division and death times.* Proc Natl Acad Sci U S A, 2007. **104**(12): p. 5032-7.

121. Gett, A.V. and Hodgkin, P.D., *A cellular calculus for signal integration by T cells.* Nat Immunol, 2000. **1**(3): p. 239-44.

122. De Boer, R.J., Ganusov, V.V., Milutinovic, D., Hodgkin, P.D., and Perelson, A.S., *Estimating lymphocyte division and death rates from CFSE data.* Bull Math Biol, 2006. **68**(5): p. 1011-31.

123. Hommel, M. and Hodgkin, P.D., *TCR Affinity Promotes CD8⁺ T Cell Expansion by Regulating Survival.* The Journal of Immunology, 2007. **179**(4): p. 2250-2260.

124. Marchingo, J.M., Kan, A., Sutherland, R.M., Duffy, K.R., Wellard, C.J., Belz, G.T., Lew, A.M., Dowling, M.R., Heinzel, S., and Hodgkin, P.D., *Antigen affinity, costimulation, and cytokine inputs sum linearly to amplify T cell expansion.* Science, 2014. **346**(6213): p. 1123-1127.

125. Duffy, K.R. and Hodgkin, P.D., *Intracellular competition for fates in the immune system.* Trends Cell Biol, 2012. **22**(9): p. 457-64.

126. Hawkins, E.D., Markham, J.F., Mcguinness, L.P., and Hodgkin, P.D., *A single-cell pedigree analysis of alternative stochastic lymphocyte fates.* Proc Natl Acad Sci U S A, 2009. **106**(32): p. 13457-62.

127. Mitchell, S., Roy, K., Zangle, T.A., and Hoffmann, A., *Nongenetic origins of cell-to-cell variability in B lymphocyte proliferation.* Proceedings of the National Academy of Sciences, 2018. **115**(12): p. E2888-E2897.

128. Duffy, K.R., Wellard, C.J., Markham, J.F., Zhou, J.H.S., Holmberg, R., Hawkins, E.D., Hasbold, J., Dowling, M.R., and Hodgkin, P.D., *Activation-induced B cell fates are selected by intracellular stochastic competition.* Science, 2012. **335**(6066): p. 338-41.

129. Day, D., Pham, K., Ludford-Menting, M.J., Oliaro, J., Izon, D., Russell, S.M., and Gu, M., *A method for prolonged imaging of motile lymphocytes.* Immunology & Cell Biology, 2009. **87**(2): p. 154-158.

130. Markham, J.F., Wellard, C.J., Hawkins, E.D., Duffy, K.R., and Hodgkin, P.D., *A minimum of two distinct heritable factors are required to explain correlation structures in proliferating lymphocytes.* J R Soc Interface, 2010. **7**(48): p. 1049-59.

131. Buchholz, V.R., Flossdorf, M., Hensel, I., Kretschmer, L., Weissbrich, B., Gräf, P., Verschoor, A., Schiemann, M., Höfer, T., and Busch, D.H., *Disparate Individual Fates Compose Robust CD8⁺ T Cell Immunity.* Science, 2013. **340**(6132): p. 630-635.

132. Gerlach, C., Rohr, J.C., Perié, L., Van Rooij, N., Van Heijst, J.W.J., Velds, A., Urbanus, J., Naik, S.H., Jacobs, H., Beltman, J.B., De Boer, R.J., and Schumacher, T.N.M., *Heterogeneous Differentiation Patterns of Individual CD8⁺ T Cells.* Science, 2013. **340**(6132): p. 635-639.

133. Hodgkin, P.D., *A probabilistic view of immunology: Drawing parallels with physics.* Immunology & Cell Biology, 2007. **85**(4): p. 295-299.

134. Hodgkin, P.D., *Modifying clonal selection theory with a probabilistic cell.* Immunological Reviews, 2018. **285**(1): p. 249-262.

135. Heinzel, S., Binh Giang, T., Kan, A., Marchingo, J.M., Lye, B.K., Corcoran, L.M., and Hodgkin, P.D., *A Myc-dependent division timer complements a cell-death timer to regulate T cell and B cell responses.* Nature Immunology, 2017. **18**(1): p. 96-103.

136. Egle, A., Harris, A.W., Bath, M.L., O'reilly, L., and Cory, S., *VavP-Bcl2 transgenic mice develop follicular lymphoma preceded by germinal center hyperplasia.* Blood, 2004. **103**(6): p. 2276-83.

137. Sakaue-Sawano, A., Kurokawa, H., Morimura, T., Hanyu, A., Hama, H., Osawa, H., Kashiwagi, S., Fukami, K., Miyata, T., Miyoshi, H., Imamura, T., Ogawa, M., Masai, H., and Miyawaki, A., *Visualizing Spatiotemporal Dynamics of Multicellular Cell-Cycle Progression.* Cell, 2008. **132**(3): p. 487-498.

138. Clark, L.B., Foy, T.M., and Noelle, R.J., *CD40 and its ligand.* Adv Immunol, 1996. **63**: p. 43-78.

139. Sze, D.M., Toellner, K.M., Garcia De Vinuesa, C., Taylor, D.R., and Maclennan, I.C., *Intrinsic constraint on plasmablast growth and extrinsic limits of plasma cell survival.* J Exp Med, 2000. **192**(6): p. 813-21.

140. Chan, T.D., Gatto, D., Wood, K., Camidge, T., Basten, A., and Brink, R., *Antigen affinity controls rapid T-dependent antibody production by driving the expansion rather than the differentiation or extrafollicular migration of early plasmablasts.* J Immunol, 2009. **183**(5): p. 3139-49.

141. Zhou, J.H.S., Markham, J.F., Duffy, K.R., and Hodgkin, P.D., *Stochastically Timed Competition Between Division and Differentiation Fates Regulates the Transition From B Lymphoblast to Plasma Cell.* Frontiers in Immunology, 2018. **9**(2053).

142. Vaux, D.L., Cory, S., and Adams, J.M., *Bcl-2 gene promotes haemopoietic cell survival and cooperates with c-myc to immortalize pre-B cells.* Nature, 1988. **335**(6189): p. 440-2.

143. Cory, S., *Regulation of lymphocyte survival by the bcl-2 gene family.* Annu Rev Immunol, 1995. **13**: p. 513-43.

144. Carrington, E.M., Tarlinton, D.M., Gray, D.H., Huntington, N.D., Zhan, Y., and Lew, A.M., *The life and death of immune cell types: the role of BCL-2 anti-apoptotic molecules.* Immunol Cell Biol, 2017. **95**(10): p. 870-877.

145. Hanahan, D. and Weinberg, R.A., *The hallmarks of cancer.* Cell, 2000. **100**(1): p. 57-70.

146. Ogilvy, S., Metcalf, D., Print, C.G., Bath, M.L., Harris, A.W., and Adams, J.M., *Constitutive Bcl-2 expression throughout the hematopoietic compartment affects multiple lineages and enhances progenitor cell survival.* Proc Natl Acad Sci U S A, 1999. **96**(26): p. 14943-8.

147. O'reilly, L.A., Huang, D.C., and Strasser, A., *The cell death inhibitor Bcl-2 and its homologues influence control of cell cycle entry.* EMBO J, 1996. **15**(24): p. 6979-90.

148. Greider, C., Chattopadhyay, A., Parkhurst, C., and Yang, E., *BCL-x(L) and BCL2 delay Myc-induced cell cycle entry through elevation of p27 and inhibition of G1 cyclin-dependent kinases.* Oncogene, 2002. **21**(51): p. 7765-75.

149. De Mesquita, B.B., *Risk, Power Distributions, and the Likelihood of War.* International Studies Quarterly, 1981. **25**(4): p. 541-568.

150. Hueber, A.O. and Evan, G.I., *Traps to catch unwary oncogenes.* Trends Genet, 1998. **14**(9): p. 364-7.

151. O'reilly, L.A., Harris, A.W., Tarlinton, D.M., Corcoran, L.M., and Strasser, A., *Expression of a bcl-2 transgene reduces proliferation and slows turnover of developing B lymphocytes in vivo.* J Immunol, 1997. **159**(5): p. 2301-11.

152. O'reilly, L.A., Harris, A.W., and Strasser, A., *bcl-2 transgene expression promotes survival and reduces proliferation of CD3-CD4-CD8- T cell progenitors.* Int Immunol, 1997. **9**(9): p. 1291-301.

153. Huang, D.C., O'reilly, L.A., Strasser, A., and Cory, S., *The anti-apoptosis function of Bcl-2 can be genetically separated from its inhibitory effect on cell cycle entry.* EMBO J, 1997. **16**(15): p. 4628-38.

154. Vairo, G., Innes, K.M., and Adams, J.M., *Bcl-2 has a cell cycle inhibitory function separable from its enhancement of cell survival.* Oncogene, 1996. **13**(7): p. 1511-9.

155. Usui, T., Wakatsuki, Y., Matsunaga, Y., Kaneko, S., Koseki, H., Kita, T., and Kosek, H., *Overexpression of B cell-specific activator protein (BSAP/Pax-5) in a late B cell is sufficient to suppress differentiation to an Ig high producer cell with plasma cell phenotype.* The Journal of Immunology, 1997. **158**(7): p. 3197-3204.

156. Tarlinton, D.M. and Smith, K.G.C., *Dissecting affinity maturation: a model explaining selection of antibody-forming cells and memory B cells in the germinal centre.* Immunology Today, 2000. **21**(9): p. 436-441.

157. Smith, K.G.C., Weiss, U., Rajewsky, K., Nossal, G.J.V., and Tarlinton, D.M., *Bcl-2 increases memory B cell recruitment but does not perturb selection in germinal centers.* Immunity, 1994. **1**(9): p. 803-813.

158. Richter, A., Lohning, M., and Radbruch, A., *Instruction for cytokine expression in T helper lymphocytes in relation to proliferation and cell cycle progression.* J Exp Med, 1999. **190**(10): p. 1439-50.

159. Fink, J.R. and Lebien, T.W., *Novel expression of cyclin-dependent kinase inhibitors in human B-cell precursors.* Exp Hematol, 2001. **29**(4): p. 490-8.

160. Perry, C., Sastry, R., Nasrallah, I.M., and Stover, P.J., *Mimosine Attenuates Serine Hydroxymethyltransferase Transcription by Chelating Zinc IMPLICATIONS FOR INHIBITION OF DNA REPLICATION.* Journal of Biological Chemistry, 2005. **280**(1): p. 396-400.

161. Park, S.Y., Im, J.S., Park, S.R., Kim, S.E., Wang, H.J., and Lee, J.K., *Mimosine arrests the cell cycle prior to the onset of DNA replication by preventing the binding of human Ctf4/And-1 to chromatin via Hif-1alpha activation in HeLa cells.* Cell Cycle, 2012. **11**(4): p. 761-6.

162. Dowling, M.R., Milutinović, D., and Hodgkin, P.D., *Modelling cell lifespan and proliferation: is likelihood to die or to divide independent of age?* Journal of The Royal Society Interface, 2005. **2**(5): p. 517-526.

163. Aubin, J.E., *Autofluorescence of viable cultured mammalian cells.* Journal of Histochemistry & Cytochemistry, 1979. **27**(1): p. 36-43.

164. Wagnieres, G.A., Star, W.M., and Wilson, B.C., *In Vivo Fluorescence Spectroscopy and Imaging for Oncological Applications.* Photochemistry and Photobiology, 1998. **68**(5): p. 603-632.

165. Caron, G., Hussein, M., Kulis, M., Delaloy, C., Chatonnet, F., Pignarre, A., Avner, S., Lemarié, M., Mahé, Elise a., Verdaguer-Dot, N., Queirós, Ana c., Tarte, K., Martín-Subero, José i., Salbert, G., and Fest, T., *Cell-Cycle-Dependent Reconfiguration of the DNA Methylome during Terminal Differentiation of Human B Cells into Plasma Cells.* Cell Reports, 2015. **13**(5): p. 1059-1071.

166. Kawabe, T., Naka, T., Yoshida, K., Tanaka, T., Fujiwara, H., Suematsu, S., Yoshida, N., Kishimoto, T., and Kikutani, H., *The immune responses in CD40-deficient mice: impaired immunoglobulin class switching and germinal center formation.* Immunity, 1994. **1**(3): p. 167-78.

167. Huppa, J.B., Gleimer, M., Sumen, C., and Davis, M.M., *Continuous T cell receptor signaling required for synapse maintenance and full effector potential.* Nature Immunology, 2003. **4**(8): p. 749-755.

168. Blink, E.J., Light, A., Kallies, A., Nutt, S.L., Hodgkin, P.D., and Tarlinton, D.M., *Early appearance of germinal center–derived memory B cells and plasma cells in blood after primary immunization.* The Journal of Experimental Medicine, 2005. **201**(4): p. 545-554.

169. Pérez-Melgosa, M., Hollenbaugh, D., and Wilson, C.B., *Cutting Edge: CD40 Ligand Is a Limiting Factor in the Humoral Response to T Cell-Dependent Antigens.* The Journal of Immunology, 1999. **163**(3): p. 1123-1127.

170. Paus, D., Phan, T.G., Chan, T.D., Gardam, S., Basten, A., and Brink, R., *Antigen recognition strength regulates the choice between extrafollicular plasma cell and germinal center B cell differentiation.* The Journal of Experimental Medicine, 2006. **203**(4): p. 1081-1091.

171. Bolduc, A., Long, E., Stapler, D., Cascalho, M., Tsubata, T., Koni, P.A., and Shimoda, M., *Constitutive CD40L expression on B cells prematurely terminates germinal center response and leads to augmented plasma cell production in T cell areas.* J Immunol, 2010. **185**(1): p. 220-30.

172. Klein, U., Casola, S., Cattoretti, G., Shen, Q., Lia, M., Mo, T., Ludwig, T., Rajewsky, K., and Dalla-Favera, R., *Transcription factor IRF4 controls plasma cell differentiation and class-switch recombination.* Nature Immunology, 2006. **7**(7): p. 773-782.

173. Jacob, J., Kelsoe, G., Rajewsky, K., and Weiss, U., *Intraclonal generation of antibody mutants in germinal centres.* Nature, 1991. **354**(6352): p. 389.

174. Clark, E.A. and Ledbetter, J.A., *How B and T cells talk to each other.* Nature, 1994. **367**(6462): p. 425-428.

175. Coffman, R.L., Lebman, D.A., and Shrader, B., *Transforming growth factor beta specifically enhances IgA production by lipopolysaccharide-stimulated murine B lymphocytes.* The Journal of Experimental Medicine, 1989. **170**(3): p. 1039-1044.

176. Zapata, J., Campanero, M., Marazuela, M., Sanchez-Madrid, F., and De Landazuri, M., *B-cell homotypic adhesion through exon-A restricted epitopes of CD45 involves LFA-1/ICAM-1, ICAM-3 interactions, and induces coclustering of CD45 and LFA-1.* Blood, 1995. **86**(5): p. 1861-1872.

177. Marchingo, J.M., Prevedello, G., Kan, A., Heinzel, S., Hodgkin, P.D., and Duffy, K.R., *T-cell stimuli independently sum to regulate an inherited clonal division fate.* Nature Communications, 2016. **7**(1): p. 13540.

178. Horton, M.B., Prevedello, G., Marchingo, J.M., Zhou, J.H.S., Duffy, K.R., Heinzel, S., and Hodgkin, P.D., *Multiplexed Division Tracking Dyes for Proliferation-Based Clonal Lineage Tracing.* The Journal of Immunology, 2018. **201**(3): p. 1097-1103.

179. Vervoorts, J., Lüscher-Firzlaff, J., and Lüscher, B., *The Ins and Outs of MYC Regulation by Posttranslational Mechanisms.* Journal of Biological Chemistry, 2006. **281**(46): p. 34725-34729.

180. Finkin, S., Hartweger, H., Oliveira, T.Y., Kara, E.E., and Nussenzweig, M.C., *Protein Amounts of the MYC Transcription Factor Determine Germinal Center B Cell Division Capacity.* Immunity, 2019. **51**(2): p. 324-336.e5.

181. Chakravorty, R., Rawlinson, D., Zhang, A., Markham, J., Dowling, M.R., Wellard, C., Zhou, J.H.S., and Hodgkin, P.D., *Labour-efficient in vitro lymphocyte population tracking and fate prediction using automation and manual review.* PLoS One, 2014. **9**(1): p. e83251.

182. Ulman, V., Maška, M., Magnusson, K.E.G., Ronneberger, O., Haubold, C., Harder, N., Matula, P., Matula, P., Svoboda, D., Radojevic, M., Smal, I., Rohr, K., Jaldén, J., Blau, H.M., Dzyubachyk, O., Lelieveldt, B., Xiao, P., Li, Y., Cho, S.-Y., Dufour, A.C., Olivo-Marin, J.-C., Reyes-Aldasoro, C.C., Solis-Lemus, J.A., Bensch, R., Brox, T., Stegmaier, J., Mikut, R., Wolf, S., Hamprecht, F.A., Esteves, T., Quelhas, P., Demirel, Ö., Malmström, L., Jug, F., Tomancak, P., Meijering, E., Muñoz-Barrutia, A., Kozubek, M., and Ortiz-De-Solorzano, C., *An objective comparison of cell-tracking algorithms.* Nature Methods, 2017. **14**(12): p. 1141-1152.

183. Kim, M.J., Lee, S.C., Pal, S., Han, E., and Song, J.M., *High-content screening of drug-induced cardiotoxicity using quantitative single cell imaging cytometry on microfluidic device.* Lab on a Chip, 2011. **11**(1): p. 104-114.

184. Mazutis, L., Gilbert, J., Ung, W.L., Weitz, D.A., Griffiths, A.D., and Heyman, J.A., *Single-cell analysis and sorting using droplet-based microfluidics.* Nature Protocols, 2013. **8**: p. 870+.

185. Yin, H. and Marshall, D., *Microfluidics for single cell analysis.* Current Opinion in Biotechnology, 2012. **23**(1): p. 110-119.

Appendices

APPENDIX I – Recipes

I-I Advanced B cell medium (AdvBCM) recipe

Concentration	Ingredient
Base medium	Advanced RPMI 1640, GIBCO, cat# 12633-012 For imaging: Custom made Advanced RPMI 1640, no phenol red
10mM	HEPES, GIBCO, cat# 15630-130
2mM	GlutaMAX, GIBCO, cat# 35050-061
100U/mL penicillin, 100ug/mL streptomycin	Penicillin/Streptomycin, GIBCO, cat# 15140-148
50µM	2-mercaptoethanol (2-ME), Sigma-Aldrich, cat# M7522
5%	Foetal Calf Serum (FCS), GIBCO, cat# 10099-141, Australian origin

I-II MACS buffer

Concentration	Ingredient
Base medium	Mouse tenacity phosphate buffered saline (MTPBS), WEHI Media kitchen
2mM	Ethylenediaminetetraacetic acid (EDTA), Sigma-Aldrich, cat# E6758
0.5%	Bovine serum albumin (BSA), Sigma-Aldrich, cat# A3294

I-III FACS buffer

Concentration	Ingredient
Base medium	Mouse tenacity phosphate buffered saline (MTPBS), WEHI Media kitchen
0.1%	Bovine serum albumin (BSA), Sigma-Aldrich, cat# A3294
0.1%	Sodium azide, Sigma-Aldrich

Appendix II – Reagents

II-I B cell preparation

Reagent	Source
Red blood cell lysis buffer	WEHI Media kitchen
Foetal calf serum	Gibco
RPMI 1640	Gibco, cat# 11875-093
'100%' Percoll	Percoll: GE Healthcare, cat# 17-0891-01 +10% 10x MTPBS (mouse tenacity PBS, WEHI Media kitchen)
50, 65, 80% Percoll	Mix '100% Percoll' with Dulbecco's phosphate buffered saline: Gibco cat# 14190-144
B cell isolation kit	Miltenyi Biotec, cat# 130-090-862
CellTrace Violet (CTV)	Invitrogen, cat# C34557
PBS/0.1%BSA	Dulbecco's phosphate buffered saline: Gibco cat# 14190-144 Bovine serum albumin: Sigma-Aldrich, cat# A3294
Flow Check Rhodamine Low-Brite Beads	Polysciences, cat# 24257-5
Sphero Rainbow Calibration Particles (6 peaks), 6.0 - 6.4 µm	BD Biosciences, cat# 556288
Propidium iodide (PI)	Sigma-Aldrich, cat# P4170
AlamarBlue	AbD Serotec, subsequently Bio-Rad, cat# BUF012B
Goat anti-mouse Ig-unlabelled	Southern Biotech, cat# 1010-01
Goat anti-mouse kappa-biotin	Southern Biotech, cat# 1050-08
BCIP/NBT	Mabtech, cat#3650-10

II-II Stimuli for B cell activation

Stimulus	Source
αCD40 monoclonal antibody (1C10)	WEHI antibody facility, prepared from original hybridoma
Recombinant mouse IL-4	Dialysed at WEHI from Sf21 supernatant
Recombinant mouse IL-5	R&D Systems, cat #405-ML-025

Appendix III – Flow cytometry

III-I Fluorochrome-conjugated antibodies

Target molecule	Conjugate	Clone	Stock concentration	Dilution	Source
IgG1	APC	x56	0.2 mg/mL	1/500	BD Pharmaceuticals, cat# 550874
CD138/Syndecan-1	PE	281-2	0.2 mg/mL	1/400	BD Pharmaceuticals, cat# 553714
CD138/Syndecan-1	Biotin	281-2	0.5 mg/mL	1/1000	BD Pharmaceuticals, cat# 553713
B220	APC	RA3-6B2	0.2 mg/mL	1/1000	BD Pharmaceuticals, cat# 553092
B220	PE	RA3-6B2	0.2 mg/mL	1/1000	BD Pharmaceuticals, cat# 553089
CD19	FITC	1D3	0.5 mg/mL	1/300	BD Pharmaceuticals, cat# 553785
IgM	PE-Cy7	R6-60.2	0.2mg/mL	1/100	BD Pharmingen, cat# 552867
IgD	PerCP/ Cy5.5	11-26c.2a	0.2mg/mL	1/100	BioLegend, Cat# 405710

III-II Streptavidin

Conjugate	Stock concentration	Dilution	Source
PE.Cy7	0.15 mg/mL	1/100	Caltag Laboratories, cat# SA1012

III-III Flow cytometer configurations

Fluorochrome	Excitation (nm)	Filter/bandpass (nm)
CellTrace Violet (CTV) Rhodamine beads	Violet 405	450/50
Propidium iodide (PI)	Blue 488 (Canto) Yellow Green 561 (Fortessa)	670 longpass (Canto) 610/20 (Fortessa)
Green fluorescent protein (GFP) Fluorescein isothiocyanate (FITC)	Blue 488	530/30 (Canto) 525/50 (Fortessa)
Allophycocyanin (APC)	Red 635	660/20 (Canto) 670/30 (Fortessa)
Phycoerythrin (PE)	Blue 488 (Canto) Yellow Green 561 (Fortessa)	585/42 (Canto) 586/15 (Fortessa)
PE.Cy7	Blue 488 (Canto) Yellow Green 561 (Fortessa)	780/60
PerCP-Cy5.5	Blue 488	670 longpass (Canto) 695/40 (Fortessa)

Data acquired on BD Canto II or BD Fortessa X20

Appendix IV – Cell cycle inhibitors

Compound	Mode of action	Source
Aphidicolin • Stock: 1 mg/mL in ethanol • Use 1 µg/mL on naïve B cells	Specifically inhibits DNA Polymerase-alpha (DNA replication), but not beta or gamma (RNA and protein synthesis).	Sigma Aldrich #A0781
BMS-265246 • Stock: 10 mM in DMSO • 1-10 µM very similar but doesn't inhibit B cell division	Potent and selective CDK1/2 inhibitor.	SelleckChem #S2014
Demecolcine • (aka. Colcemid) • Stock: 10 µg/mL in HBSS • Use 32 ng/mL on naïve B cells	Depolarizes microtubules and inactivates spindle fibre formation, arresting cells in metaphase.	Sigma-Aldrich #D1925
Etoposide • Stock: 50 mM in DMSO • Use 2 µM on naïve B cells	Complexes with topoisomerase II and DNA to enhance double-strand and single-strand cleavage of DNA.	Sigma-Aldrich #E1383
Flavopiridol HCl • Stock: 10 mM in DMSO • Use ~500 nM on naïve B cells	Pan CDK inhibitor. Competes with ATP to inhibit CDKs including CDK1, CDK2, CDK4 and CDK6.	SelleckChem #S2679
LEE011 • Stock: 15 mM in DMSO • Autofluorescent	Highly specific CDK4/CDK6 inhibitor.	Selleckchem.com #S7440
L-mimosine • Stock: 60 mM, 75 mM in 10% $NaHCO_3$ • Use 150 µM on naïve B cells	Late G1-phase inhibitor, reversible. Seems to have multiple effects: inhibits eukaryote initiation factor 5-A, Ctf4, deoxyribonucleotide metabolism (arrests DNA synthesis), is also an iron chelator, may activate a CDKI	Sigma Aldrich #M0253
LY2835219 • Stock: 10 mM in DMSO • Toxic before it inhibits divisions	Potent and selective inhibitor of CDK4 and CDK6.	SelleckChem #S7158

Compound	Mode of action	Source
Mycophenolic Acid • Stock: 16 mg/mL in methanol • Use 1 µg/mL on naïve B cells	Selective inhibitor of inosine monophosphate dehydrogenase, preventing DNA synthesis in lymphocytes.	Sigma-Aldrich #M3536
Nocodazole • Stock: 5 mg/mL in DMSO • Use <25 ng/mL in naïve B cells	Interferes with the structure and function of microtubules. Disrupts cell cycle during interphase and mitosis. Thought to bind directly to tubulin.	Sigma Aldrich #M1404
Paclitaxel • Stock: 1 mM in ethanol • Use 100 nM in naïve B cells	Lowers the critical concentration for tubulin polymerization. Reversibly binds to tubulin, prohibiting depolymerization during mitosis.	MP Biomedicals # 0219353201
Palbociclib HCl • (aka PD-0332991 HCl) • Stock: 5 mM in DMSO • Use 3.16 µM on B cells	Highly selective inhibitor of CDK4/6. It shows no activity against CDK1/2/5, EGFR, FGFR, PDGFR, InsR.	SelleckChem #S1116
PD 0332991 isethionate • (aka. Palbociclib) • Stock: 10 mM in H_2O • Use ~3 µM on naïve B cells	Potent selective inhibitor of CDK4 and CDK6.	Sigma Aldrich #PZ0199
Purvalanol A • Stock: 50 mM in DMSO • Use 6 µM on naïve B cells	Potent, cell-permeable pan cyclin-dependent protein kinase (CDK) inhibitor.	Sigma Aldrich #P4484
Vincristine • Stock: 1 mg/mL in methanol • Use ≤10 ng/mL	Inhibits microtubule assembly by binding tubulin and inducing coiled spiral aggregate formation. Arrests in G2/M-phase by blocking mitotic spindle formation.	Sigma-Aldrich #V8879
2-Bromo-12,13-dihydro-5H-indolo[2,3-a]pyrrolo[3,4-c] carbazole-5,7(6H)-dione • (Referred to here as 'Millipore Cdki') • Stock: 10 mM in DMSO • Autofluorescent	Potent, selective, reversible and ATP-competitive inhibitor of Cdk4/D1. Inhibits the activity of other CDKs only at much higher concentrations.	illipore CalBiochem #219476